Escola de Camins
Escola Tècnica Superior d'Enginyeria de Camins, Canals i Ports
UPC BARCELONATECH

# Quantitative analysis for more informed data collection and wave-mangrove modelling.

MASTER FINAL THESIS


Final thesis developed by:
**Tian Ning Lim**

Supervised by:
**Dr. Allen Bateman**

Mentored by:
**Dr. Bregje van Wesenbeeck (Deltares)**

IHE-Delft Examiner:
**Dr. Hans van der Kwast**


Master of Science in:
**Flood Risk Management**

Barcelona, September 2022

*Erasmus Mundus Program in Flood Risk Management*

# Abstract

The study of mangroves as a coastal protection measure has become a topic of great research interest in the last two decades in light of the consequences that climate change could bring and the wave attenuating abilities that these forests have. The main analytical models used to study the wave attenuation capacity of mangroves originates from Dalrymple et al., (1984), where trees are represented as individual cylinders. Further modifications by Mendez & Losada, (2004) and Suzuki et al., (2012) have made it possible to implement the model for irregular waves and introduce variations in vegetation properties along the water column. This thesis seeks to provide insights into how we can more efficiently advance our understanding of mangroves as a coastal flood protection measure with quantitative information. This is done by performing quantitative analyses with the extended version of the model by Dalrymple et al., (1984) to study the contributions of different (vertical) components of mangrove trees to short-wave attenuation during storm surges.

In this study, quantitative analyses focusing on the mangrove, Rhizophora *sp.* (R *sp.*), have been conducted to understand the 1) effect of the choice of bulk drag coefficient, $C_D$, on the wave attenuation results, 2) sensitivity of the wave attenuation model to the complex root system of R *sp.* at various water levels, and 3) contribution analyses of the root, trunk, and canopy of R *sp.* tree to wave dampening.

At the scale of a laboratory experiment, it is shown that given the same physical conditions, $C_D$ is not transferable between numerical models of the same physical vegetation model. At the forest scale, results indicate that the magnitudes of error can be high when $C_D$ is approximated to 1 for short cross-shore distance (forest width < 350m). For larger forests (forest width > 350m), error is insignificant if the actual $C_D$ values is greater than 1. $C_D$ is likely to be greater than or close to 1 if the surge does not flow through much of the canopy layer. On the other hand, depending on how much smaller the actual $C_D$ value is from 1, error produced by the model where $C_D$=1 can still be significant for large forests.

The sensitivity analysis of the root model shows that the complex roots of R *sp.* do contribute significantly to wave attenuation even at extremely high water levels ($h_0$=10m). At low water levels, the wave attenuation model is sensitive to the errors due to the resolution and (lack of) accuracy in the total frontal area in the root models. At water levels significantly higher than the root layer, the resolution of the vegetation model has almost no influence over the results of wave attenuation.

Lastly, the contribution analysis of R *sp.* forest shows that the canopy can contribute to wave attenuation more than the root layer in certain high water conditions. A maximum contribution of 23% by the canopy layer is observed in this study. This value may vary depending on the height of the trees and how the frontal area of the canopy is calculated and distributed along the trunk.

The results of these analyses are then used to craft recommendations that can guide future research.



**Keywords**: short-wave attenuation, mangrove, Rhizophora, sensitivity analysis, storm, extreme conditions, bulk drag coefficient, canopy, root

# Acknowledgements

This thesis journey was made possible by the patience and generosity of many people who have helped me through these six months.

First from Delft, to Bregje, my mentor, I would like to thank you for believing in my capacity to complete this work and for making time to provide feedback throughout this journey even though you are always extremely busy. Next, I would love to give a big thank you to Alejandra and Su for teaching me the relevant technical knowledge, double-checking the implementation of my code with me, and providing constructive feedbacks on analysis and writing. Your help made this thesis so much less daunting and more manageable. I would also like to thank Robyn for introducing me to Bregje and Deltares, helping me to jump-start my coding journey in Python, and for always being so encouraging.

Second, from Singapore, I would love to extend my thanks to Shawn Lum and Sylvia Tan for answering my questions regarding the mangroves across time zones and helping me with data collection. Your help provided key insights into the modelling of mangroves and I hope that there will be opportunities beyond this thesis to apply this knowledge into studying mangroves as coastal defences.

Next, from Barcelona, I would like to thank Allen – my supervisor – for our discussion on the topic of $C_D$ and the pointers you gave during our meeting.

Finally, beyond the people who contributed directly to this thesis, I would love to thank my partner, family, and friends for providing the much-needed moral support all this time. I am grateful to have you, wonderful people, in my life.

# Contents

**List of Tables**

**List of Figures**

**Nomenclature (abbreviations and symbols)**

| | |
|---|---|
| a | wave amplitude |
| α | ratio of the height of a submerged vegetation layer to the total depth of the water column |
| $b_v$ | diameter of the vegetation model, where the plant is represented by a single or layers of cylinders |
| c | phase speed; $c = \frac{\lambda}{T}$ |
| $c_g$ | group velocity |
| $C_D$ | bulk drag coefficient |
| $C_{canopy}$ | Contribution, in percentage, to wave attenuation by the canopy layer |
| $C_{trunk}$ | Contribution, in percentage, to wave attenuation by the trunk layer |
| $C_{root}$ | Contribution, in percentage, to wave attenuation by the root layer |
| DBH | diameter at breast height |
| E | wave energy per unit area; $E = \frac{1}{2}\rho a^2$ |
| ε | time-averaged rate of energy dissipation per unit horizontal area due in the vegetation field |
| Error | $Error = k_{t,model} - k_{t,benchmark}$, where $k_{t,model}$ refers to the kt values generated by the model of interest, and $k_{t,benchmark}$ refers to the $k_t$ values generated by the most accurate model |
| $Error_{rel}$ | $Error_{rel} = \frac{Error}{k_{t,benchmark}}$ |
| $Error_{abs}$ | $Error_{abs} = \lvert Error \rvert$ |
| FA | Frontal area |
| g | gravitational acceleration |
| h | water level |
| H | wave height |
| $H_s$ | significant wave height |
| $H_{rms}$ | root mean square wave height |
| k | wave number; $k = \frac{2\pi}{\lambda}$ |
| $k_p$ | wave number associated with the peak period of an irregular wave; $k = \frac{2\pi}{\lambda_p}$ |
| $k_t$ | wave transmission; $k_t = \frac{H_x}{H_i}$, where $H_x$ is the wave height at point x, and $H_i$ is the initial wave height |
| KC | Keulegan-Carpenter number |
| η | wave profile |
| $N_v$ | vegetation density |
| R | Wave height reduction in terms of $k_t$; $R = (1 - k_t) \times 100\%$ |
| Re | Reynold's number |
| s | cross-shore slope |
| T | wave period |
| $T_p$ | peak wave period of an irregular wave |
| u | horizontal particle velocity |
| ω | $\omega = \frac{2\pi}{T}$ |
| x | point along the cross-shore direction |
| xVeg | cross-shore width of mangrove forest |
| z | point along the water column, where 0 is the water surface |
| λ | wave length |

# 1. Introduction

Coastal flooding threatens hundreds of million people and multi-billion dollars' worth of assets globally (Kirezci et al., 2020; Kulp & Strauss, 2019). This exposure is projected to increase with rising sea levels, and the frequency and severity of storms as a result of climate change (Kirezci et al., 2020; Kulp & Strauss, 2019). Global vulnerability to coastal flooding is also expected to increase with rapid population growth and urbanization along the coastlines, especially in the tropics (Neumann et al., 2015). Mangroves have the capacity to reduce the impact of waves and winds during storm events and provide co-benefits that contribute to the United Nations Sustainable Development Goals (SDGs). Thus, these forests are promoted globally as coastal protection measures (Gijsman et al., 2021; van Wesenbeeck et al., 2022). As a consequence, the study of mangroves as a coastal protection measure has become a topic of great research interest in the last two decades. Studies that investigated the coastal protection functions of mangroves against storms tend to focus on the surge and wave attenuation capacity of mangroves (e.g., Montgomery et al., 2018; Suzuki et al., 2012; Wang et al., 2022; Zhang et al., 2012), integration of mangroves into coastal protection measures (van Zelst et al., 2021), and the ability of mangroves to resist (Doyle et al., 2009; Krauss & Osland, 2019; Paling et al., 2008; Swales et al., 2015) and recover (Cahoon et al., 2003; Steinke & Ward, 1989; Vogt et al., 2012) from extreme events and adapt to sea level rise (Furukawa & Wolanski, 1996; S. Li et al., 2015; Mogensen et al., 2018).

Studies showed that immensely large areas of mangrove forests are required for surge reduction (Krauss et al., 2009; Montgomery et al., 2018; Montgomery et al., 2019; Zhang et al., 2012). Depending on the absence or presence of channels and creeks within the forest, field studies suggest that surges can be attenuated at a rate of 4cm to 50cm per km of mangrove forests (Krauss et al., 2009; Mclvor, Spencer, et al., 2012; Montgomery et al., 2018). Channels and creeks would reduce the surge attenuation effect of mangroves (Montgomery et al., 2018). Hence, mangroves are limitedly effective for surge attenuation.

Mangroves have been observed to be effective in short-wave attenuation (Mclvor, Möller, et al., 2012). Although mangroves alone are unable to lower inundation levels due to surges, these forests can reduce flood damage by reducing the incoming wave energy. More importantly, mangroves have been found to reduce the cost of flood protection when they are implemented in combination with dikes (van Zelst et al., 2021). In such mangrove-dike systems, forests are situated in front of the dikes and wave attenuation function of mangroves reduces wave impact and run-up (van Zelst, 2018; van Zelst et al., 2021). Consequently, this limits the required freeboard of the dike, thereby lowering the cost of construction and maintenance (van Zelst et al., 2021). The implementation of such systems requires quantitative information on the short-wave attenuation function of mangroves at high water levels.

Studies of wave-mangrove interactions involve the collection of field measurements (eg., Brinkman, 2006; Quang Bao, 2011; Quartel et al., 2007; etc.), laboratory experiments (e.g., Maza et al., 2019; van Wesenbeeck et al., 2022; Wang et al., 2022; etc), and analytical, empirical and numerical modelling (e.g., Dalrymple et al., 1984; Mendez & Losada, 2004; Suzuki et al., 2012, 2019; van Wesenbeeck et al., 2022; Wang et al., 2022). Data collected in the field and laboratory complement the development of models (Wang et al., 2022). Numerical models are becoming increasingly valuable tools in the study of wave attenuation by mangroves (Suzuki et al., 2019), but systematic evaluation of models, modelling parameters and collection of in situ data on mangrove characteristics is lacking behind. Observational and experimental data collection can be very resource intensive. This is even more so for study of storm conditions where their occurrences are much fewer and less predictable (Marois & Mitsch, 2015), and their conditions are more expensive to recreate in laboratories. The accuracy and

reliability of modelling results, depend strongly on the representation of mangrove characteristics in the models and calibration and validation during the modelling process (Wang et al., 2022). It is, thus, valuable for future research to know which components of the model require more information, and which areas require less. This allows more efficient allocation of resources for data collection and modelling.

## 1.1 Research Framework

The objective of this study is to provide insights into how we can more efficiently advance our understanding of mangroves as a coastal flood protection measure with quantitative information. The output of this thesis should inform future studies on the relevant knowledge gaps in short wave-mangrove interaction research for storm surge conditions. More specifically, this thesis aims to understand the influence of the individual vertical components of a mangrove on the modelling of wave attenuation, especially for high water conditions. To this end, the following research questions are being explored in this study.

### Main research question

- What are the contributions of different (vertical) components of a mangrove tree to wave attenuation during storm surges?

### Sub questions

- Is short-wave attenuation sensitive to the root system at high water levels? Above what water levels are the effects of wave attenuation by the root system negligible?
- How sensitive is modelled short-wave attenuation to the complexity of the schematized root system?
- How much uncertainty does the choice of bulk drag coefficient, $C_D$, contribute to wave attenuation results?
- How much do canopies contribute to wave attenuation during high water levels?

### General approach

A widely used wave-mangrove interaction model was adapted for the purpose of this study. The model is an extension of model developed by Dalrymple et al., (1984) by Mendez & Losada, (2004) and Suzuki et al., (2012) (Chapter 2.2). The model is implemented using Python, and validated with existing studies by van Wesenbeeck et al., (2022) and Wang et al., (2022). The effect of different $C_D$ values on the results of wave attenuation modelling is also explored using these papers. Finally, a hypothetical model – with parameter values informed by global data, current literature, and expert interviews – is built for exploring the sensitivity of mangrove-wave attenuation model to various input parameters, and estimating the contribution of various tree components to wave attenuation in the context of storm surges.

# 2 Literature Review

## 2.1 Mangrove and Storms

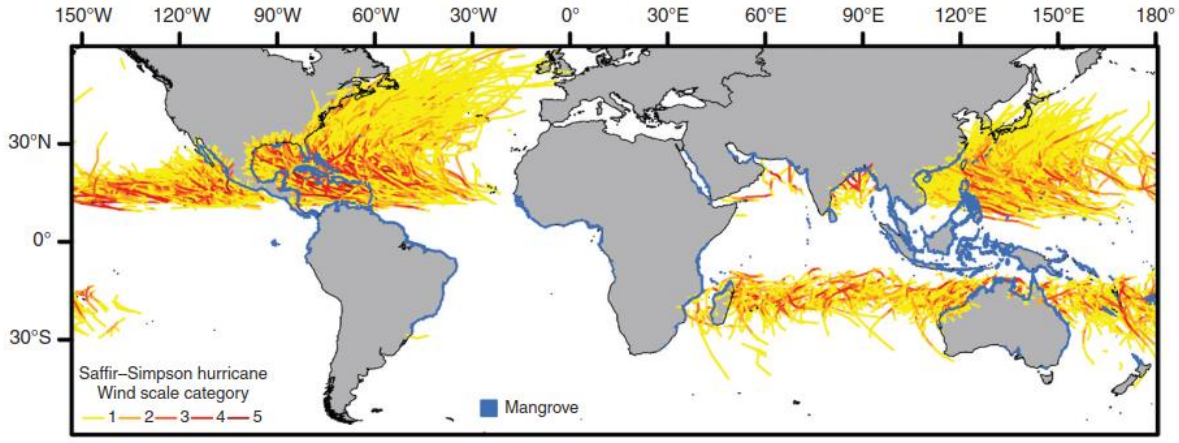


*Figure 2.1 Map of mangrove and storm tracks from Krauss & Osland, 2019 based on data from Giri et al., 2011 and Knapp et al., 2010*

Mangroves are a group of halophytic, temperature sensitive tree and shrub species that are found along the coastlines within 32° north and 38° south of the Equator (Figure 2.1) (Krauss et al., 2008). Being situated in the intertidal zones, mangrove forests serve as barriers between the open water bodies and the settlements behind them. Depending on their location, mangrove forests are exposed to ocean waves of different periods, from gravity to trans-tidal waves (Bosboom & Stive, 2021; Gijsman et al., 2021) (Figure 2.2). Mangroves located outside 5° north and south of the Equator – such as the forests in Australia, Mexico, Myanmar, the Philippines, Bangladesh, the Bahamas, Guadeloupe – may be influenced by tropical storms which can result in storm surges (Krauss & Osland, 2019) (Figure 2.1).

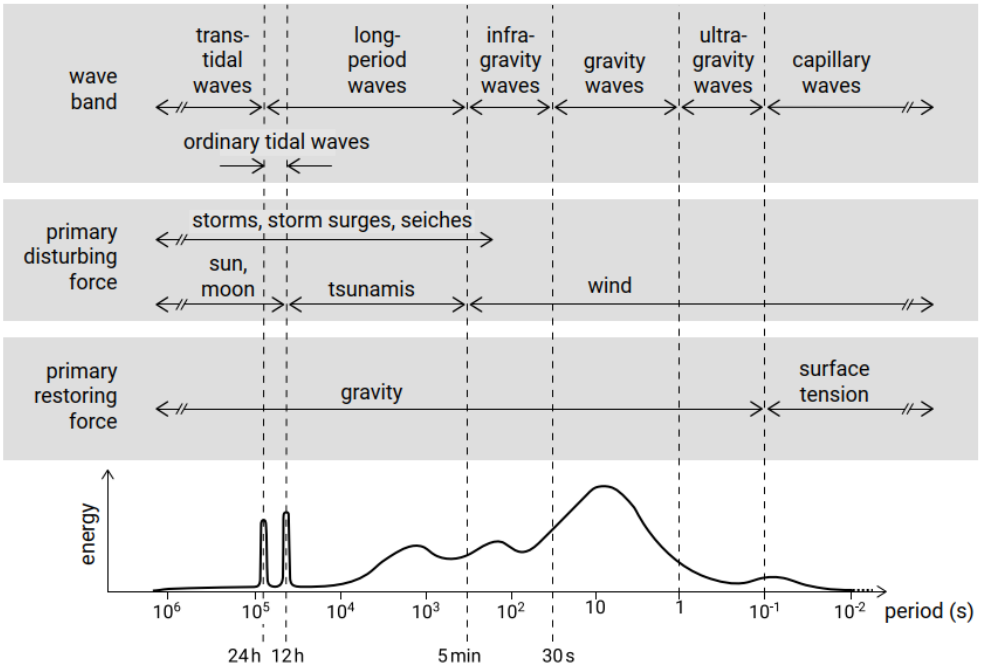


*Figure 2.2 A classification of ocean waves based on the wave periods and the respective relative amounts of energy (Bosboom & Stive, 2021 after Munk (1950) and Kinsman (1965)).*

Mangroves attenuate waves by directly providing additional drag against the incoming flow through their root systems, trunks, and – during high water levels – the canopies (Mazda et al., 2006). As such, the tree species, root structure, stem density, stem diameter, and tree height of mangroves are important factors that determine the amount of wave attenuation (Gijsman et al., 2021). Mangrove species largely influence wave dissipation because different species can have vastly different root systems, pneumatophores, trunks, and canopies. Other than the characteristics of mangrove trees, growing literature in wave-mangrove interaction indicate that the functionality of a mangrove forest for wave attenuation depends on the combination of various hydrodynamic and physical factors. These factors include inundation depth, wave height, wave period, flow velocity, intertidal topography, the forest cross-shore width, and the presence of drainage channels within the forests (Gijsman et al., 2021). Field measurements at mangrove forests in Thailand, Vietnam, Japan, and Australia, for low water conditions have reported wave attenuation rates between $0.0001m^{-1}$ and $0.017m^{-1}$ (Table 2.1) (Horstman et al., 2014).

| **Location-mangrove type (publication)** | **Vegetation** | **Reduction** |
|---|---|---|
| Tong King Delta, Vietnam – Fringing mangroves (Mazda et al., 1997a) | Sparse Kandelia candel seedlings to dense Kandelia candel, up to 1 m high | 0.01 – 0.22 per 100m |
| Vinh Quang, Vietnam – Fringing mangroves (Mazda et al., 2006) | Sonneratia *sp.* | $0.002\text{-}0.006m^{-1}$ |
| Do Son, Vietnam – Fringing mangroves (Quartel et al., 2007) | Kandelia candel bushes and small trees | $0.004\text{-}0.012m^{-1}$ |
| Red River Delta, Vietnam – Fringing (?) mangroves (Bao, 2011) | Mixed vegetation | $0.0055 – 0.01\ m^{-1}$ |
| Can Gio, Vietnam – Fringing (?) mangroves (Bao, 2011) | Mixed vegetation | $0.017m^{-1}$ |
| Trang Province, Thailand – fringing mangroves (Horstman et al., 2014) | Front Avicennia and Sonneratia (sparse)<br>Back Rhizophora (dense) | $0.002m^{-1}$<br>$0.012m_{-1}$ |

*Table 2.1 Wave height reduction per unit length reported by various studies. (Adapted from Horstman et al., 2014).*

### 2.1.1 Hydrodynamic conditions during storms

Storm surges happen due to low atmospheric pressures and strong winds (Wells, 1997). A storm surge can be understood as a combination of two components: a temporary increase in still sea water level (SWL) – the surge – and stronger wind-generated waves, which can propagate further landwards due to the larger water depths (Bosboom & Stive, 2021; Lowe et al., 2001). Increase in SWL due to reduced atmospheric pressure can last between hours to days (Bosboom & Stive, 2021; Marois & Mitsch, 2015) (Figure 2.2). On the other hand, waves generated by strong winds have a period up to 5 minutes (Bosboom & Stive, 2021)(Figure 2.2). The severity of a storm surge depends on the timing of the storm occurrence relative to tidal cycles, direction and strength of the wind, and shape of the coastline (Bosboom & Stive, 2021).

Estimated peak water levels during storm surge events for areas around mangroves have been reported to be up to 9m (Dasgupta et al., 2017; Krauss et al., 2009; Montgomery et al., 2019; K. Zhang

et al., 2012). Most wind-driven wave height measurements are made during normal conditions, or during high tide conditions at best. The ranges of these wave heights are between 0.2m and 0.7m (Brinkman, 2006; Quang Bao, 2011; Vo-Luong & Massel, 2008). The only reported wind-driven wave height that is recorded during a typhoon event is 0.4m by Mazda et al., (2006) at Vinh Quang in Northern Vietnam.

### 2.1.2 Mangrove

There are 45 species of mangrove trees found globally (The Ocean Portal Team, 2018), with nine principal genera – Avicennia, Laguncularia, Lumnitzera, Nypa, Bruguiera, Ceriops, Kandelia, Rhizophora, and Sonneratia (Tomlinson, 1986). These trees have developed coping mechanisms to adapt to the harsh environment of the intertidal zone – such as high temperatures, low relative air humidity, high and changing salt concentrations, and hypoxia – where they are found (Srikanth et al., 2016).

Mangrove forests can exhibit clear zonation based on a combination of factors including salinity, soil conditions, tidal inundation levels, and interspecific competition (Ng & Sivasothi, 2001). For example, it is noted that in Southeast Asia, monospecific zonation parallel to the coastline can be observed in relatively undisturbed forests. Avicennia and Sonneratia are commonly found to occupy the seaward edge of the forests, followed by Rhizophora further inland. Bruguiera and Ceriops are found in the most inland part of the forests (Ng & Sivasothi, 2001). On the other hand, it was found that Rhizophora dominated the coastal fringes while Avicennia and Laguncularia were found further inland of Calabash Cay, Belize (Piou et al., 2006). In disturbed forests, however, such zonation may not be noticeable (Ng & Sivasothi, 2001). Furthermore, reforested or afforested areas may consist of only single species of mangroves (e.g. Villamayor et al., 2016).

At the global scale, the height distribution of mangroves depends on three main factors: temperature, precipitation, and the frequency of storm events (Figure 2.3a) (Simard et al., 2019). The tallest mangroves are found within ±10° of the equator where temperature and precipitation rates (Figure 2.3b, blue lines) are generally high, while the frequency of cyclones are low (Figure 2.3, grey bars). Over latitudes where the frequencies of cyclones are relatively high i.e. 10° to 30° north and south of the equator, the 95$^{th}$ percentile of maximum mangrove canopy heights range from around 7m to 17.5m (Figure 2.3a).

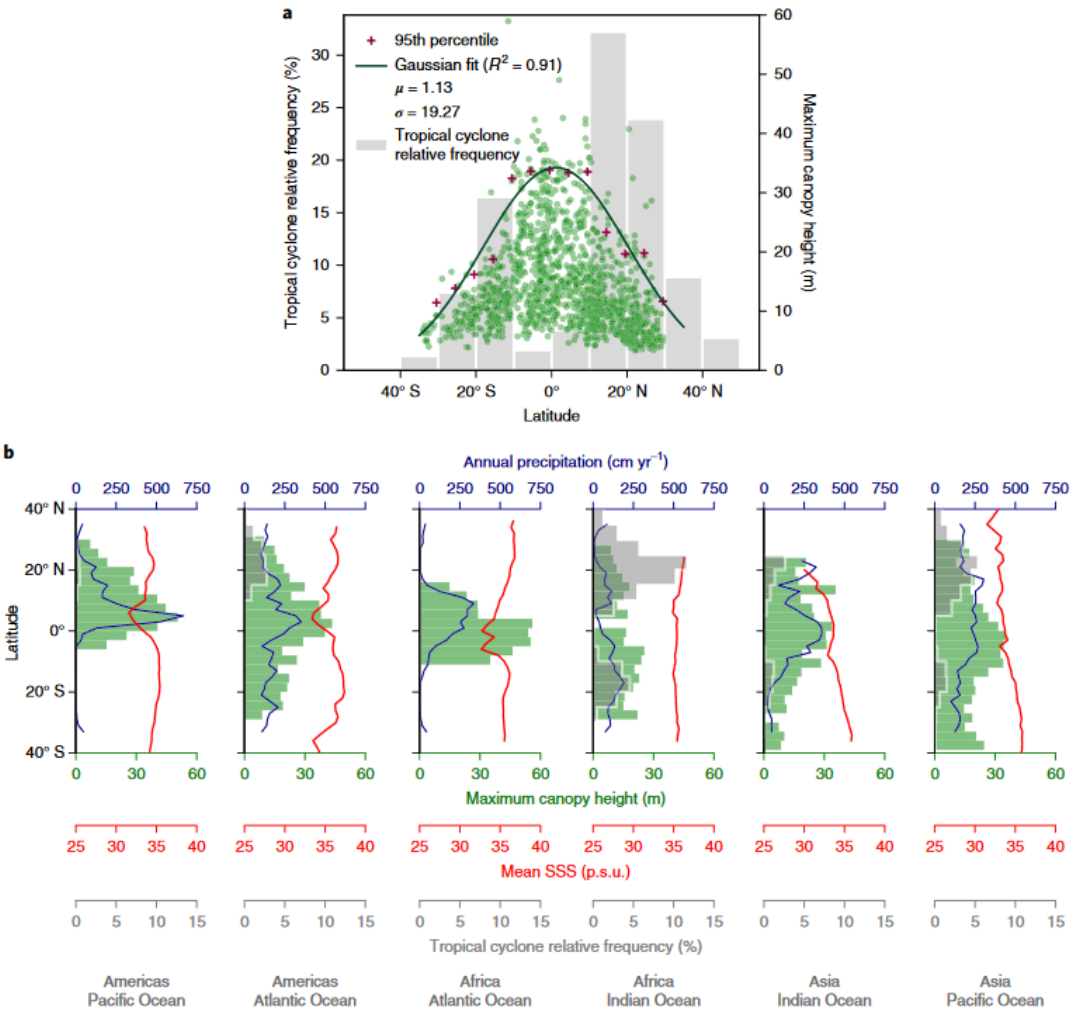


*Figure 2.3 a) Black line: distribution of maximum canopy height (green dots) against latitude calculated based on the 95th percentile of the maximum canopy heights in every 5° latitude (red dots). Grey histogram: frequency of tropical cyclones. b) Latitudinal trends of precipitation (blue lines), sea surface salinity (red lines), cyclone frequency (grey bars), and maximum mangrove canopy height (green bars) for various regions around the world.*

In the context of wave attenuation, Rhizophora is one of the better studied genera of mangroves. As such, Rhizophora will be the focus of this thesis. There are 8 species of Rhizophora: R. *apiculata*, R. *lamarckii*, R. *mangle*, R. *mucronata*, R. *racemosa*, R. *samoensis*, and R. *stylosa*. R. mangle is found in the Americas, while R. *apiculata,* R. *mucronate,* and R. *stylosa* are common in Asia, Africa, and Australia (Tomlinson, 1986). When the species of Rhizophora is not identifiable, or if data of a Rhizophora forest is conflated, the species is referred to as R. *sp* (Tomlinson, 1986).

| Publication | Location | Reported Nv (trees/m$^2$) | DBH (cm) |
|---|---|---|---|
| Ong et al., 1995<br>Clough et al., 1997 | Matang Matang Forest Reserve, Malaysia | 0.3 | 15 |
| Mazda et al., 1997 | Nakama Gawa, Japan<br>Coral Creek, Australia | 1.0<br>0.8 | 5.7<br>8.6 |
| Tanaka et al., 2007 | Sri Lanka & Thailand (various locations) | 0.25-1 | 10-15 |
| Alongi et al., 2008 | Mekong Delta, Vietnam | 0.04 – 2 | 2.2 – 24.3 |
| Narayan 2009 | Various sources | 0.5 - 1.7 | 15 – 40 |
| Tusinski 2012 | Various sources | 0.3 - 0.35 | 15 – 70 |
| Horstman et al. 2014 | Trang Province, Thailand | 0.06 - 0.15 | -* |

*Table 2.2 Summary on R sp. forest density and DBH from past studies. *The number of elements (i.e. trunk+roots) and average diameter at different heights above the ground were provided instead of the average DBH.*

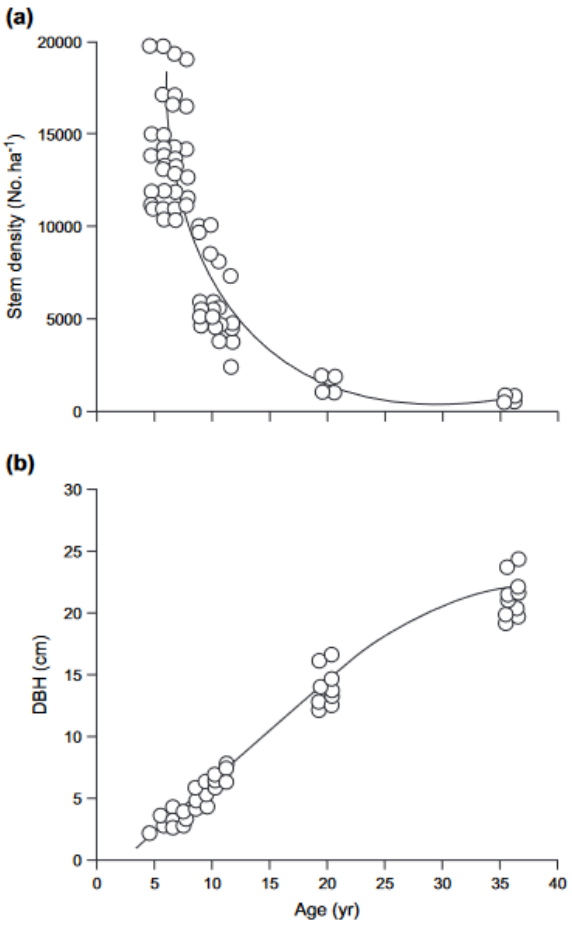


*Figure 2.4 Relationship between forest density and diameter at breast height with age of R sp. forest in the Mekong Delta, Vietnam (Alongi, 2008).*

Depending on the type (e.g. managed, pristine, disturbed, reforested) and age of mangrove forests, the forest densities ($N_v$) and diameter at breast heights (DBH) of the trees can differ. Table 2.2 shows the values of $N_v$ and DBH for R *sp.* forests from past studies.

There have been papers that reported the inverse relationship in $N_v$ and DBH among mangrove forests (Alongi, 2008; Rovai et al., 2021; Tanaka et al., 2007). In general, $N_v$ and DBH of a forest evolve over time due to processes such as thinning, where some trees are naturally or artificially removed to allow the growth of other trees. As such, as the trees in a forest grow larger over time, the density of the forest itself reduces. Figure 2.4 shows how $N_v$ and density of R *sp.* forest in the Mekong delta evolve with age (Alongi, 2008).

### Vertical structure of mangroves

Mangroves have vertical layering which segments the tree into three different sections: the root system, trunks, and canopy. The aerial roots that are developed to cope with the unstable, soft soils and hypoxic environment of the intertidal zone contribute to the wave attenuation function of mangroves, especially at shallow waters (Srikanth et al., 2016). There are many types of specialized roots among mangroves: buttress roots, fly buttresses, surface roots, prop roots, stilt roots, spreading roots, cable roots with pneumatophores, knee roots, pencil roots, and cone roots (Srikanth et al., 2016). At shallow waters,

the different geometries, size, and flexibility of these roots and pneumatophores can influence wave attenuation significantly (Wang et al., 2022).

R *sp.* trees have prop roots (Figure 2.5). Field studies have been carried out in various sites around the globe to quantify various morphological parameters of the R. *sp* root system. Mazda et al., (1997), in their attempt to quantify drag force on tidal currents in mangrove swamps, took measurements of R. *stylosa* in Nakama-Gawa, Japan and Coral Creek, Australia (Figure 2.5). Ohira et al., (2013) collected morphological data of a mix of R. *apiculata* and R. *mucronata*. In addition to the parameters that were measured by Mazda et al., (1997), Ohira et al., (2013) measured the angle between the root and shoot point, and the distance between the trunk and the edge of the root. Lastly, on top of the parameters shown in Figure 2.5, X. Zhang, (2014) applied the Strahler ordering scheme to the root system of R. *stylosa* in Berlayer Creek, Singapore; the diameter of stilt roots from different orders were measured. He also found that the bending strength of the prop roots to be approximately 83 MPa and concluded that the roots behave like "massive and rigid structures".

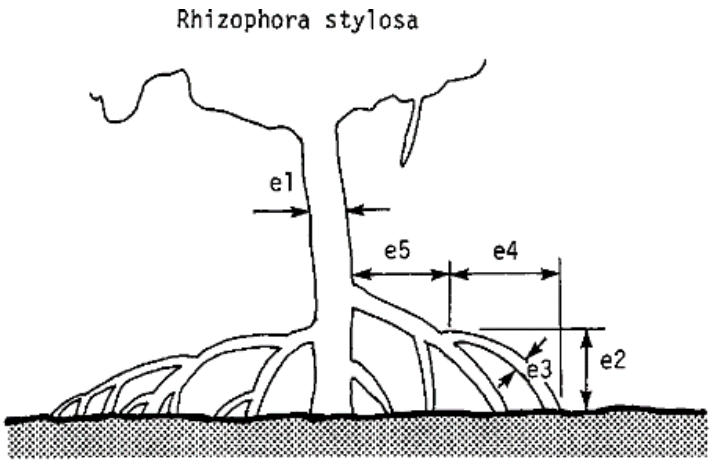


*Figure 2.5 Morphological parameters of R. stylosa collected in Nakama-Gawa, Japan and Coral Creek, Australia. e1: diameter at breast height (DBH), e2: height of root, e3: diameter of root, e4: spread of secondary root, e5: distance of secondary root from the trunk*

Trunks are also crucial wave attenuating elements, especially at higher water levels (Wang et al., 2022). The shape, diameter, and height of trunks are some physical characteristics that are known to significantly affect wave dissipation (Vo-Luong & Massel, 2008).

Finally, at extremely high water levels, currents and waves may go through the canopy of mangrove forests. The crown form – shapes and sizes of canopies – of R *sp.* trees can show significant differences (Tomlinson, 1986). For example, due to the availability of light, trees in (matured) closed canopy forest are likely to be tall and have narrow crowns, while trees in open mudflats are likely to be shorter and have broader crowns. More extreme variations in crown shape can also result from injury e.g. broken branches. The significant plasticity in form of R *sp.* trees is due to reiteration. Reiteration is the most usual response of a mangrove tree to environmental stresses and perturbation, where the tree partially or fully repeats the architecture of the trees (Tomlinson, 1986). In R *sp.* this comes in the form of reorienting its axis such that an existing branch now grows to become the "new" crown on the side of the tree (Figure 2.6). This process is, however, only prominent in the sapling stage of the trees. All in all, the crown shape of R *sp.* is a "result of deterministic and opportunistic processes".

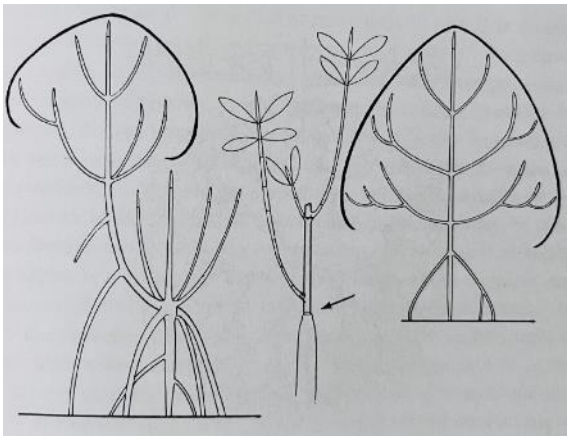

*Figure 2.6 Image illustrating the reiteration process of reorientation in Rhizophora. Right: Normal conditions where tree conforms its architectural model. Left: Reorientation of existing branch in response to external environmental changes to form a reiterated crown. (Tomlinson, 1986)*

In the context of wave attenuation, the height at which the canopy begins is an important parameter for developing the vegetation model. However, limited publications regarding the start-height of the canopy has been found. Only two publications by J.-E. Ong et al., (1995) and B. Clough et al., (1997), based on the systematically managed Matang Matang Forest Reserve, provided some information.

The age of the R. *apiculata* stand at the forest reserve at the time of data collection were estimated to be 20 and 22 years old by J.-E. Ong et al., (1995) and B. Clough et al., (1997) respectively. J.-E. Ong et al., (1995) reported that no leaves were found below 10m depth from the top of the 21m high canopy. On the other hand, B. Clough et al., (1997) measured the leaf area index (LAI) of four 0.25m x 0.25m quadrats from a 22m tall tower (Figure 2.7). Based on their results, it seems that the canopy of trees within a closed forest usually starts at a depth of 6m from the top of the forest, and with some branches found as low as 14m from the top (Figure 2.7).

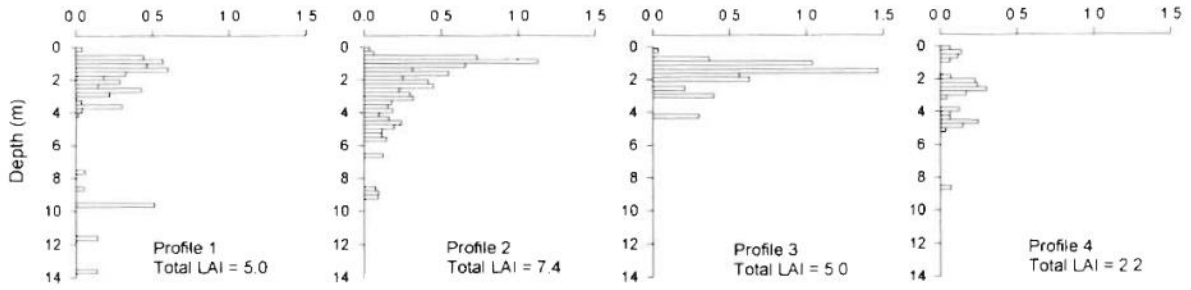


*Figure 2.7 Vertical profile of leaf area index (LAI) for four 0.25m x 0.25m quadrats taken down through the canopy from the top of a 22m tall tower (Clough et al., 1997)*

Even though most studies do not account for wave dissipation through the canopy, it is believed that canopies can efficiently attenuate waves due to the high density of branches and leaves (Burger, 2005).

## 2.2 Wave-Mangrove Interaction Models

Numerical wave-vegetation interaction models are increasingly valuable to the understanding and estimation of wave propagation through coastal wetlands (Borsje et al., 2011; Suzuki et al., 2012, 2019). Earlier models accounted for wave dissipation by vegetation as added bottom friction in the energy conservation equation e.g., Hasselmann, 1968; Möller et al., 1999 (Suzuki et al., 2019). Dalrymple et al. (1984) represented vegetation as rigid vertical cylinders, and attributed the attenuation of regular waves to the drag force exerted by the vegetation cylinders on the flow, expressed in terms of the Morison equation (Morison et al., 1950). The schematization of vegetation

as cylinders has since been adopted and implemented in most wave-vegetation interaction models. Based on the controlling physical equation, these models can be categorized into two groups: energy conservation models and momentum conservation models (Table 2.3) (Suzuki et al., 2019).

| Source | Control Equation | Vegetation schematization |
|---|---|---|
| Dalrymple et al., 1984; Losada et al., 2016; Mendez & Losada, 2004 | Energy conservation equation | Rigid vertical cylinders |
| Suzuki et al., 2012 | Spectral action balance equation | Rigid vertical cylinders |
| Cao et al., 2015; Tang et al., 2015 | Mild slope equation | Rigid vertical cylinders |
| Augustin et al., 2009; Huang et al., 2011; Iimura & Tanaka, 2012; Karambas et al., 2016; Yang et al., 2018 | Boussineq equations | Rigid vertical cylinders |
| Li & Yan, 2007; Ma et al., 2013; Maza et al., 2013, 2016 | RANS equations | Rigid vertical cylinders |
| Kobayashi et al., 1993; Liu et al., 2015; Mei et al., 2011; Suzuki et al., 2019 | Shallow water equations | Rigid vertical and horizontal cylinders |

*Table 2.3 Numerical models for wave attenuation (Suzuki et al., 2019)*

In energy-conservation models, wave-vegetation interaction is modelled as work done by the waves against vegetation. These include the original model by Dalrymple et al. (1984), and the extended versions of it presented by Mendez & Losada (2004) and Losada et al. (2016), where irregular waves, wave breaking, and wave-current interactions are accounted for. The effect of vegetation on wave attenuation were also modelled by a spectral-action balance equation model (Suzuki et al., 2012) and mild-slope equation models (Cao et al., 2015; Tang et al., 2015).

On the other hand, momentum-conservation models of wave-vegetation interaction quantify wave attenuation by calculating the loss of momentum in the flow due to vegetation (Suzuki et al., 2019). These models use equations such as the shallow water, Boussineq-type, and Reynolds-averaged Navier Stokes (RANS) equations, which are based on momentum conservation (Suzuki et al., 2019) (Table 2.3). In exchange for higher computational time compared to energy-conservation models, momentum-conservation models provide information on velocity structure with intra-wave resolutions on top of wave-field information (Suzuki et al., 2019). This additional information is essential for interpreting wave propagation and sediment transport within wetlands (Suzuki et al., 2019).

Of the existing models, two models with varying complexity in the schematization of mangrove structure have been identified for the purpose of this research. These are the extended models of Dalrymple et al. (1984) by Mendez & Losada, (2004) and Suzuki et al. (2019), which will be referred to as the Dalrymple model from hereon. In this study, energy-conservation models will be used for the analysis of wave attenuation.

### 2.2.1 Quantification of Energy Dissipation by Vegetation

The force acting on vegetation, $F_V$, can be described by the Morison equation (Eq. 1). This equation is one of the key cornerstones to studying wave attenuation by mangroves.

$$F_v = \frac{1}{2(\eta+h)} C_D \int_{-h}^{\eta} u|u| dA(z) + \frac{1}{(\eta+h)} C_M \int_{-h}^{\eta} \frac{\partial u}{\partial t} dV(z) \quad \text{(Eq. 1)}$$

*where $\eta$ is the free surface elevation, $h$ the water depth, $u$ the horizontal wave orbital velocity, $C_M$ is the inertia coefficient, $A(z)$ and $V(z)$ the vertical variation of frontal area and submerged volume of mangroves.*

The model by Dalrymple et al. (1984) has been applied in numerous studies of wave-vegetation interaction, and this includes the study of mangrove on wave attenuation (e.g., He et al., 2019; Kelty et al., 2022; Suzuki et al., 2012; van Wesenbeeck et al., 2022; Wang et al., 2022). In this model, vegetation is represented as rigid vertical cylinders with a diameter of $b_v$. Energy dissipation by a vegetation field is calculated by integrating the work done by the drag forces over a wave period, for a vegetation field with density $N_v$ with the assumption of the linear wave theory. This was expressed in Mendez & Losada, (2004) in the following form.

$$\varepsilon_v = \frac{2}{3\pi}\rho C_D b_v N_v \left(\frac{gk}{2\sigma}\right)^3 \frac{\sinh^3 k\alpha h + 3\sinh k\alpha h}{3k\cosh^3 kh} H^3 \quad \text{(Eq. 2)}$$

*where $\varepsilon_v$ is the time-averaged rate of energy dissipation per unit horizontal area by vegetation, k is the wave number, $b_v$ is the diameter of a vegetation cylinder, $N_v$ is the number of vegetation cylinders per unit area, g is the gravitational acceleration, σ is the wave angular velocity, and H is the wave height.*

By introducing Equation 2 into the energy balance equation (Eq. 3). Wave height decay through the vegetation field was then obtained by solving the energy balance equation (Eq. 3) while assuming the linear wave theory and that the effect of vegetation on the surrounding flow field is negligible (Dalrymple et al., 1984; Mendez & Losada, 2004). This results in an exponential wave decay function (Eq. 4), which depends on a wave damping factor, $\beta$, given by Equation 5:

$$\frac{\partial(Ec_g)}{\partial x} = -\varepsilon_v \quad \text{(Eq. 3)}$$

*where $E = \frac{1}{2}\rho a^2$ is the wave energy per unit area, and $c_g$ is the wave group velocity.*

$$H = \frac{1}{1+\beta x} H_0 \quad \text{(Eq. 4)}$$

$$\text{where } \beta = \frac{A_0 H_0}{2} = \frac{4}{9\pi} C_D b_v N H_0 k \frac{\sinh^3 k\alpha h + 3\sinh k\alpha h}{(\sinh 2kh + 2kh)\sinh kh} \quad \text{(Eq. 5)}$$

*where $H_0$ is the wave height at x=0, h is the water depth, and α is the ratio of the height of the (submerged part) of the vegetation to h, the height of the water.*

Equation 2 was also modified by Mendez and Losada (2004) for the estimation of wave height decay of a narrow band of random waves (Eq. 6).

$$< \varepsilon_v > = \frac{1}{2\pi}\rho \tilde{C}_D b_v N \left(\frac{gk_p}{2\sigma_p}\right)^3 \frac{\sinh^3 k_p\alpha h + 3\sinh k_p\alpha h}{3k_p\cosh^3 k_p h} {H_{rms}}^3 \quad \text{(Eq. 6)}$$

*where $< \varepsilon_v >$ is the time time-averaged rate of energy dissipation per unit horizontal area of an random waves with a Rayleigh distribution, and $\tilde{C}_D$ is the calibrated drag coefficient. The subscript p refers to values associated with the peak period. $H_{rms}$ is the root-mean-square height of the irregular waves.*

Subsequently, Suzuki et al., (2012) adapted Equations 2 and 6 to model vertical differences in vegetation characteristics (Figure 2.8). Equation 7 calculates the total energy dissipated individual layers for regular waves, while Equation 8 considers irregular waves

$$< \varepsilon_{v,i} > = \frac{2}{3\pi}\rho_i C_D b_{v,i} N_i \left(\frac{gk}{2\sigma}\right)^3 \frac{(\sinh^3 k\alpha_i h - \sinh^3 k\alpha_{i-1} h) + (3\sinh k\alpha_i h - 3\sinh k\alpha_{i-1} h)}{3k\cosh^3 kh} H^3 \quad \text{(Eq. 7)}$$

$$< \varepsilon_{v,i} > = \frac{1}{2\pi}\rho_i C_D b_{v,i} N_i \left(\frac{gk_p}{2\sigma_p}\right)^3 \frac{(\sinh^3 k_p\alpha_i h - \sinh^3 k_p\alpha_{i-1} h) + (3\sinh k_p\alpha_i h - 3\sinh k_p\alpha_{i-1} h)}{3k_p\cosh^3 k_p h} {H_{rms}}^3 \quad \text{(Eq. 8)}$$

*Where i refers to the horizontal layers in the model, $\alpha_i$ refer to the ratio of the top of the layer, and $\alpha_{i-1}$ refers to bottom of layer i (*Figure 2.8*).*

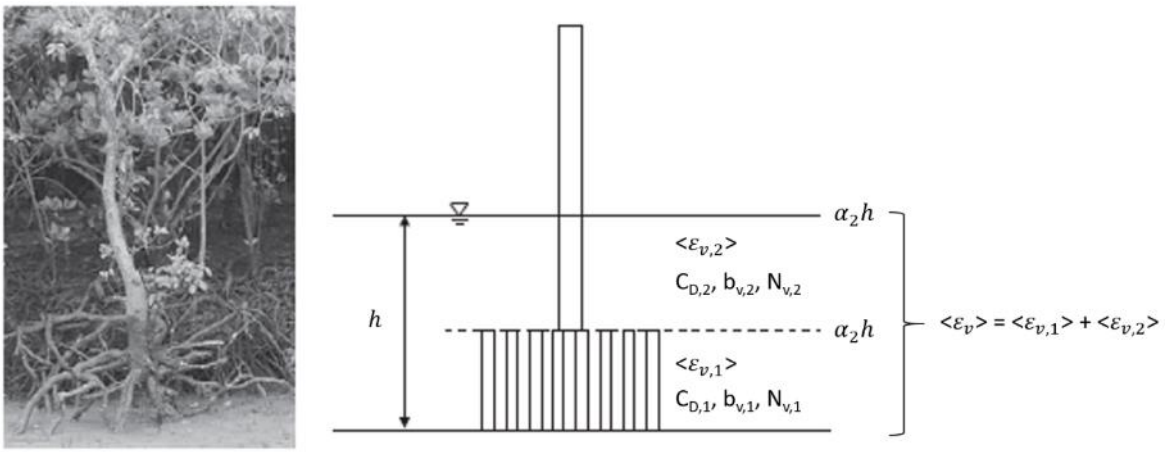


*Figure 2.8 Schematization of mangrove tree using cylinders in a common modelling software, SWAN (adapted from Suzuki et al., 2012)*

### 2.2.2 Modelling approach and limitations

The energy dissipation models described in section 2.2.1 have been applied in many mainstream wave models such as SWAN and xBeach. In the study of wave energy dissipation by vegetation, such models are used to calculate the wave height along the defined cross-shore direction by propagating the wave energy, defined by offshore boundary conditions, inland (e.g. Suzuki et al., 2012; van Wesenbeeck et al., 2022; Vuik et al., 2016). The application of the Dalrymple model (Eq. 4-6) and its extensions (Eq. 7 - 8) require knowledge of the bulk drag coefficient, $C_D$. $C_D$ can be understood as the bulk parameter for quantifying the mean drag force asserted on the flow by the vegetation field (Ozeren et al., 2014; Wang et al., 2022). These models implicitly assumes $C_D$ as the only calibration parameter to account for the assumptions made (Jacobsen et al., 2019; Wang et al., 2022). Calibration is often done using field or experimental measurements of wave heights (e.g. Ozeren et al., 2014; van Wesenbeeck et al., 2022; Wang et al., 2022).

Aside from calibrating the $C_D$ values directly with measurements, many studies also proposed using empirical formulas to derive $C_D$. The goal is to have a universally applicable formular for $C_D$ so that the accuracy of wave-attenuation models is not as sensitive to data availability, alleviating the data dependency in this area of study. Two main parameters – the Reynold's number (Re) and Keulegan-Carpenter number (KC) – are used to predict $C_D$ (van Wesenbeeck et al., 2022; Wang et al., 2022). Published empirical formulas are usually in the form of Equation (9) and Equation (10). As of now, there is still a lack of agreement in these derived formulas (Wang et al., 2022).

$$C_D = (\frac{m}{Re})^k + n \quad \text{(Eq. 9)}$$

$$C_D = (\frac{m}{KC})^k + n \quad \text{(Eq. 10)}$$

*where m, n, and k are fitted parameters*

## 2.3 Applications of the Dalrymple model

### 2.3.1 Mild Conditions

The study of wave attenuation by mangroves is usually conducted for mild water conditions. The papers that apply the Dalrymple model in their study include include field (S. V. et al., 2019; Y. Zhang et al., 2020), laboratory experiments (Maza et al., 2019; Wang et al., 2022), and numerical modelling studies (Burger, 2005; Cao et al., 2015). Field studies have been conducted in forests with mixed mangrove species such that the structure of the forest is spatially variable. With collected field measurements used to validate the results of the Dalrymple model, S. V. et al., (2019) aimed to quantify the amount of attenuation off the coast of Mumbai, India. Y. Zhang et al., (2020) focused on studying the non-linear behaviour of wave attenuation across vegetation structure and time. The laboratory experiments by Wang et al., (2022) and Maza et al., (2019) seek to understand the wave attenuation effect of the R *sp.* complex root better. In both studies, scaled-down R *sp.* root models – which was empirically developed by Ohira et al., (2013) – were applied in the experiments. The results of these studies show that calculations of drag forces and wave attenuation from the analytical model compare well with measurements from the experiments. The thesis by Burger, (2005), attempted to model wave attenuation by mangrove forests using the Dalrymple model for different wave and tidal boundary conditions. Cao et al., (2015) used the work by Mendez and Losada (2004) and SWAN to validate their implementation of the vegetation-induced wave dissipation component in a numerical wave model based on the extended mild-slope equation.

*Scaled down flume experiment with R sp. root models*

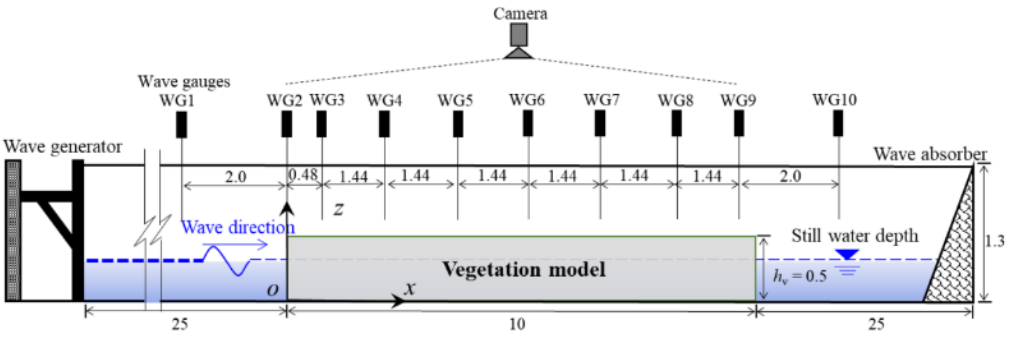


*Figure 2.9 Flume experiment set up in (Wang et al., 2022)*

Wang et al., 2022 carried out a series of laboratory experiments to explore wave-attenuation by mangrove roots under various water levels. 1:20 models of Rhizophora sp. roots and stems, as proposed by Ohira et al., (2013), were positioned in staggered arrangements along a wave flume for this study. The wave flume has a dimension of 60.0m x 1.2m x 1.3m. Aside from the complex models of R. *sp* roots, experiments were also carried out with uniform cylinders. The results from these experiments were compared to study the contribution of complex roots to wave attenuation.

For each experiment, the mangrove models were placed along 10m of the flume, 25m away from the wave generator (Figure 2.9). 10 wave gauges, with sampling rates of 50Hz, were placed near and long these tree models.

The wave measurements were then fitted to the model by Dalrymple et al., (1984), where β from Equation 5 is calibrated. This indirectly calibrates for $C_d$. Within this analytical model, the submerged part of the vegetation model is represented by a uniform cylinder of representative diameter d*. This means that the total frontal area of the uniform cylinder is the same as that of the complex root model.

The results of this study show that the complex roots contribute significantly to wave attenuation, and that representing the R *sp.* root-trunk system with only a single cylinder would introduce considerable error into the wave attenuation model. A new $C_D$ formula was also introduced, where $KC_{rv}$ – the KC parameter calculated using the average pore velocity and vegetation-related hydraulic radius – was used to correlate with $C_D$ instead of the KC or Re. It was, however, noted that only a small range of conditions were used to derive this formula and more data will be required to improve the parameter space.

### 2.3.2 Storm Conditions

As of now, only a few publications were found to directly tackle the topic of storm surge attenuation, most of which were on the study of surge height reduction (Krauss et al., 2008; Montgomery et al., 2018, 2019; Xu et al., 2010; K. Zhang et al., 2012). On the other hand, there were no field studies found on short-wave attenuation. Other than a few small-scale experiments (e.g., He et al., 2019; Maza et al., 2019), the only relevant large-scale experiment of wave attenuation at extreme water levels with aquatic trees was by van Wesenbeeck et al., (2022), where wave attenuation by willows were measured for high water levels of 3.0m to 4.5m. The analytical model used to study short-wave attenuation during storm surges (He et al., 2019; Maza et al., 2019; van Wesenbeeck et al., 2022) are the same as those used to study mild conditions.

*Large scale flume experiment with willow trees*

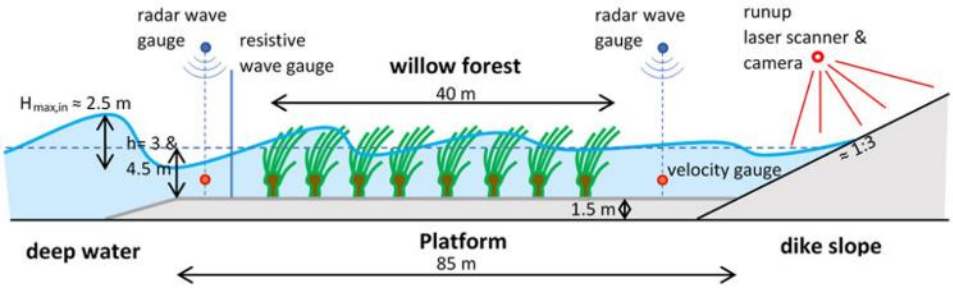


*Figure 2.10 Flume experiment set up in (van Wesenbeeck et al., 2022)*

Van Wesenbeeck et al., (2022) conducted experiments with 15 years old willows in a 330m long, 5.0m, and 9.5m deep flume to study the effect of wave attenuation and reduction in dike run-up by willows in storm surge conditions. A total of 32 willow trees were arranged in 16 rows of 2 along the flume to make up the willow forest (Figure 2.10). Three sets of trees with differing canopy density were used in various runs of the experiment. Water depths of 3m and 4.5m, and irregular waves of Hs = 0.2m to 1.5m and steepness of 0.02 to 0.06 were applied in this study. The dike runup, and wave height in front and behind of the willow forest were measured to study the energy dissipation effect of the willows.

The wave measurements were used to calibrate the SWAN model. In the model, the willow trees were represented by the total frontal area per unit volume per vertical elevation, dFA (Kalloe et al., 2022; van Wesenbeeck et al., 2022). Comparing to the equations in Chapter 2.2.1, dFA of the canopy layer is equivalent to the multiplication of the average branch diameter and density of branches in a tree, $b_vN_v$. The model of the willow trees – developed by Kalloe et al., (2022) – was based on a single representative willow tree, where all the branches at breast height that were greater than 3mm were counted and measured. The final model was derived after applying a branching model to the measurements (Figure 2.11).

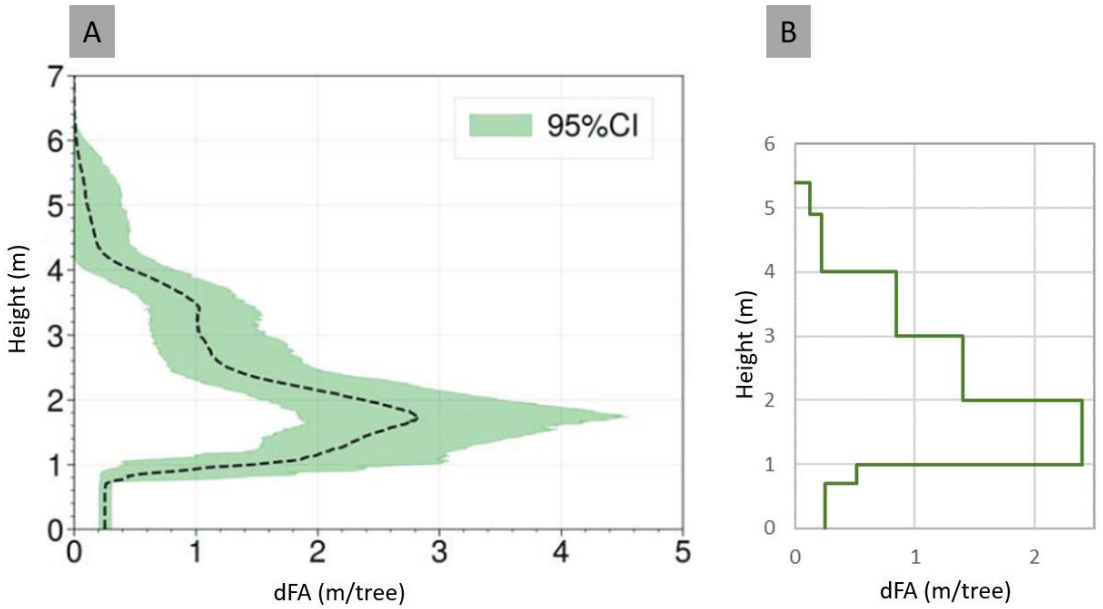


*Figure 2.11 Frontal area of a willow tree developed by Kalloe et al., (2022). A) Measured frontal area of sample willow tree with 95% confidence interval. B) Willow tree model with lower vertical resolution developed using data from A.*

The calibrated $C_D$ values were found to fit well with the relationship between $C_D$ and KC proposed by Keulegan & Carpenter, (1958) (Figure 2.12). KC is defined as in Equation 11 below.

$$KC = \frac{u_s T_p}{b_v} \qquad \text{(Eq. 11)}$$

*where $T_p$ is the peak period, $b_v$ is the diameter of the stem, and $u_s = \frac{H_s}{2}\frac{2\pi}{T_p}\frac{cosh(k_p \alpha h)}{sinh(k_p h)}$ is the maximum horizontal velocity of the oscillation*

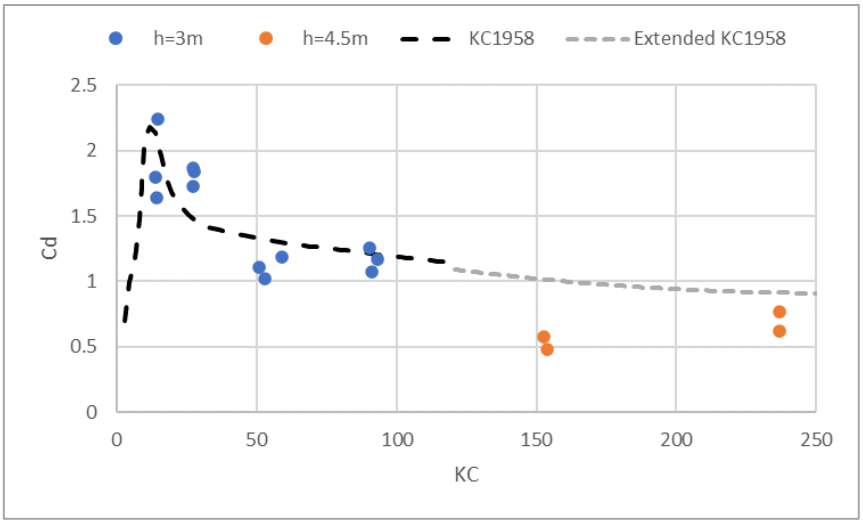


*Figure 2.12 Observed relationship between KC and $C_D$ (van Wesenbeeck et al., 2022)*

Overall, this large-scale study found that short wave attenuation for high water levels are around 22% over a distance of 40m for a canopy with leaves and 20% for canopy without leaves. Wave attenuation was observed to be 5% to 7% less when the canopy density was reduced.

## 2.4 Mangrove tree modelling: Rhizophora *sp.*

Information of mangrove morphology that are relevant wave attenuation modelling are limited. Among the 45 true mangrove species, Rhizophora *sp*. is one of the better studied species. Much attention has been given to this family of mangroves especially since the 2004 Indian Ocean Tsunami, when the studies of tsunami damage behind R *sp.* forests brought to light the possible wave attenuation effect of these forests (Ohira et al., 2013). As of now, most research that looks at the modelling of R sp. for studying wave attenuation focuses primarily on the stilt roots of this trees (Maza et al., 2013, 2019; Ohira et al., 2013; Wang et al., 2022). Results of these studies are based on measurements of real R *sp.* trees. On the other hand, few attempts have been made to model the canopy of R *sp.* data (Janssen, 2016; Narayan, 2009). The developed canopy models from these studies, however, are largely based on arbitrary assumptions of a typical mangrove tree due to the lack of data (Janssen, 2016; Narayan, 2009).

Aside from coastal engineering researches that look at the characterization of the morphology of mangroves for wave attenuation modelling, ecological studies on allometric relationships in mangroves also provide insights for developing the vegetation models. Allometric equations are tools that are used for estimating total above-ground biomass of trees. These equations, which are usually species specific, statistically relate the above-ground biomass to various dendrometric variables such as tree height and diameter at breast height (DBH)(Daba & Soromessa, 2019). Allometric equations for estimating the total biomass and biomass of specific components (i.e. root, trunk, canopy etc.) of R sp. various species have been developed (Clough & Scott, 1989; Cole et al., 1999; Gevana & Im, 2016; Ong et al., 1995).

### 2.4.1 Rhizophora *sp.* root

Ohira et al., (2013) developed an empirical model of roots of the R *sp.* based on a total of 18 R *apiculata* and R *mucronata* trees from Muang Kluang and Thung Maphrap mangrove forest, Thailand. Field measurements of DBH, root height, number of roots, root diameter, the angle of root at the shoot point, and the spread of the root from the trunk were taken. The final root model consists of a combination of allometric equations that were developed to relate the various root morphological factors of the primary roots to DBH.

Maza et al., (2019) adapted the model by Ohira et al., (2013) to build a 1:6 physical model of a R *sp.* root. This model was designed considering a mature R *sp.* tree, with a DBH of 0.20m. Based on this physical model, the frontal area of the root is calculated (Figure 2.13)

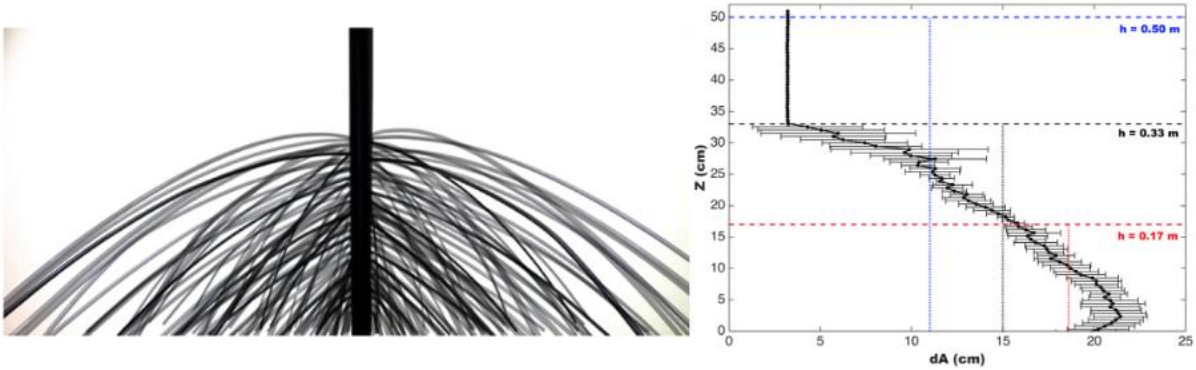


*Figure 2.13 Left: superposition of 8 pictures of the 1:6 scale root model at different angles. Right: calculated frontal area with variability due to the rotating angle represented by the error bars.*

### 2.4.2 Allometric equations

Multiple allometric equations have been developed for specific species of Rhizophora trees such as R *apiculata* , R *mucronata*, and R *stylosa*, and for R *sp.* in general (Aken et al., 2021; Clough & Scott, 1989). These equations can be developed to estimate the total above-ground biomass of the trees (Abdul-Hamid et al., 2022; Aken et al., 2021), or to account for biomass in specific parts of the tree such as the stilt roots, trunks, branches, and leaves (Clough & Scott, 1989; Ong et al., 1995, 2004). With the use of wood density information (e.g. Tobias et al., 2017), these equations can be used to estimate the volume of various tree components.

# 3. Methodology

## 3.1 Wave attenuation modelling and validation

The extended models of Dalrymple et al., (1984) by Mendez & Losada, (2004) and Suzuki et al., (2012) (Eq. 7 and 8) have been implemented in Python for the analyses.

Validation of the implemented models are done using published laboratory experiments by Vuik et al., (2016), van Wesenbeeck et al., (2022) and Wang et al., (2022). These studies focus on the wave attenuation effect of seagrasses, willow trees in storm conditions, and the root system of R *sp.* respectively. Vuik et al., (2016) and van Wesenbeeck et al., (2022) obtained $C_D$ values for the collected field data and experimental results by calibration in SWAN; Wang et al., (2022) obtained the $C_D$ by fitting Equation 4 to the experimental results.

The first two publications are used to validate the irregular wave model, while the last study is used to validate the regular wave model. These studies were validated for the following reasons. First, the studies by van Wesenbeeck et al., (2022) and Wang et al., (2022) are used to explore the sensitivity of the wave attenuation model to the choice of $C_D$ values (described in Chapter 3.2). Second, the implemented irregular wave model will be used to conduct further analysis with a hypothetical R *sp.* forest model (described in Chapter 3.3).

Validation of the model is done by comparing the calculated $k_t$ values (Eq. 12) to the reported values of the studies. The error is then calculated at the points for which data is available (Eq. 13).

$$k_t = \frac{H_x}{H_i} \quad \text{(Eq. 12)}$$

*where $H_x$ is the wave height at point x (points along the cross-shore direction) and $H_i$ is the initial wave height directly in front of the vegetated domain.*

$$error_x = k_{t,model,x} - k_{t,experiment,x} \quad \text{(Eq. 13)}$$

Specific details about the validation with Wang et al., (2022) and van Wesenbeeck et al., (2022) – both of which are experiments that are used for further analysis of the parameter $C_D$ – can be found in the Appendix (A1).

## 3.2 Analysis of errors in $k_t$ due to approximations in $C_D$

A brief analysis pertaining the bulk drag parameter, $C_D$, is performed using the inputs and results of van Wesenbeeck et al., (2022) and Wang et al., (2022). The first study looks at the transferability of calibrated CD values across vegetation models representing the same physical tree or tree model. The second analysis is conducted to quantify the range of errors when $C_D$ is approximated to 1. The former and latter study are conducted using Wang et al., (2022) and van Wesenbeeck et al., (2022) studies respectively.

The transferability of $C_D$ across vegetation models used to represent the same physical experiment is first done by producing a two-layered root-trunk model of the physical complex root model that Wang et al., 2022 used in their study. The diameters of the 2-layered model's root and trunk layers are calculated based on the total frontal areas of these respective layers of the physical model reported in the study. The final 2-layered model has the same submerged frontal area as the single-layered models that are used for calibration (Figure 3.1).

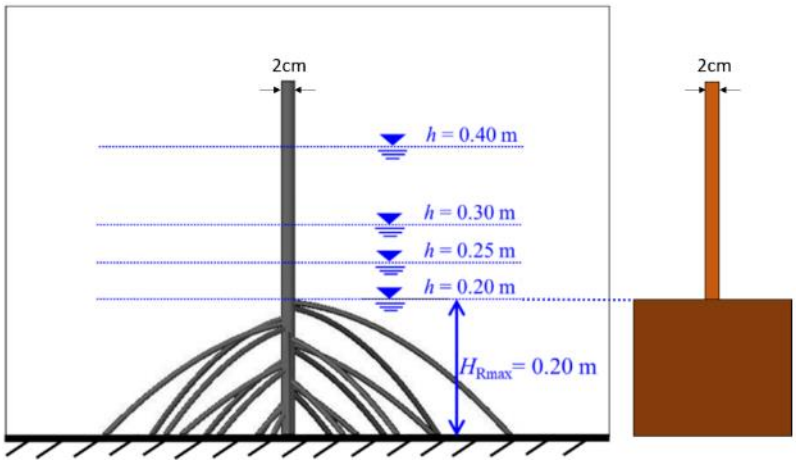


*Figure 3.1 Left: Sketch of the physical complex root model relative to the tested water levels (Wang et al., (2022). Right: Final two layered model that represents the physical complex root model*

Wave attenuation is then performed using the original single-layered model and the developed two-layered model. The $k_t$ values produced by the two models are compared with each other, and with the measurements of the flume experiments.

Next, the study of how errors would vary when $C_D = 1$ is conducted by comparing the results of $k_t$ when $C_D=C_{D,experiment}$ and $C_D=1$ are applied to the same physical conditions. The length of the physical experiment by van Wesenbeeck et al., (2022) was 40m. In this study, however, modelling were performed for a forest width of 2900m wide, the largest forest width considered in the hypothetical R *sp.* forest model (described in Chapter 3.3). This provides insights to how the errors due to fixing the $C_D$ at 1 would vary for the range of forest widths that is explored in the root sensitivity analysis and wave attenuation analysis for a R *sp.* forest (described in Chapter 3.3).

## 3.3 Analyses with hypothetical R *sp.* forest

Two main groups of analyses are conducted using hypothetical R *sp.* forest models. The first group of analyses focuses on understanding how different types of errors within the R *sp.* root model influence wave attenuation wave modelling results. The second group of analyses look the potential wave attenuation capacity of R *sp.* forests, including how different components of R *sp.* trees contribute to wave attenuation. This chapter will first provide an overview of the model set up, before describing in detail how the various root and tree models are developed. Finally, the approach to analysing the modelling results is described.

### 3.3.1 Overview of model set-up

The analyses pertaining to the R *sp.* complex roots and full tree models are conducted using one model set-up (Figure 3.2). This wave attenuation model starts where the hypothetical forest begins, and it is assumed that waves approach the forest at a perpendicular angle to the shoreline (Figure 3.2). The input variables of the wave attenuation model can be split into three groups: forest properties, hydrodynamic characteristics, and tree models. The input values were selected to provide a realistic range of conditions for the study. Table 3.1 presents the summary of the input forest and

hydrodynamic parameters for the sensitivity analysis of root models and contribution analysis of R *sp.* trees to wave attenuation.

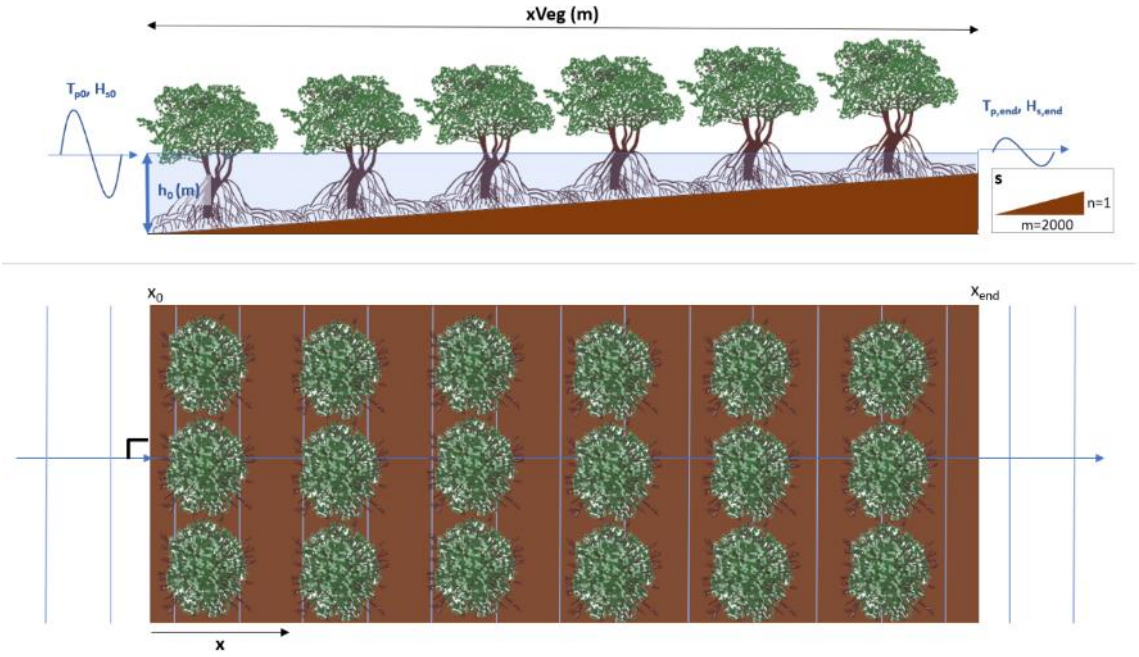


*Figure 3.2 schematic of model used for the sensitivity analyses. Top: cross-sectional view of model. Bottom: Bird's eye view of model.*

| Parameter type | Parameters | SA of root model | R *sp.* contribution analysis |
|---|---|---|---|
| Forest | xVeg (m) | 50, 125, 325, 950, 2900 | |
| | $N_v$ (trees/m2) | 0.06, 0.1, 0.25 | |
| | s | 1/2000 | |
| Hydrodynamic | $h_0$ (m) | 2, 3, 4, …, 10 | 6, 7, 8, …, 10 |
| | Wave steepness (%) | 1 to 3 | 3 |
| | $T_{p0}$ (s) | 8, 10, 12, 15, 17 | |

*Table 3.1 Summary of forest and hydrodynamic input parameters for sensitivity analyses of root model, and R sp. forest wave attenuation and contribution analysis*

### *Forest characteristic*

The input variables related to the forest properties are the cross-shore width of the forest (xVeg), slope of the forest ($s = \frac{n}{m}$) and vegetation density ($N_v$). The values of xVeg and *s* were selected based on global wetland transect data by van Zelst, (2018), which have been filtered to only include mangrove areas (Figure 3.3)(Bellinga, 2022). As the focus of this study is wave attenuation in storm surge conditions, only mangroves located outside 5° north and south of the equator are considered.

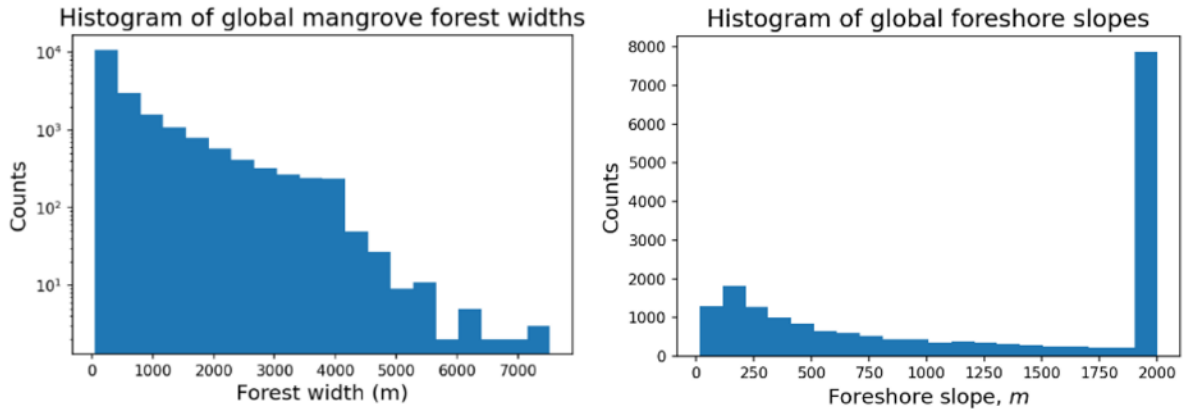


*Figure 3.3 Histograms of global mangrove forest widths and foreshore slope based on data be van Zelst, (2018)*

Five forest width values are selected as input for xVeg in the sensitivity analyses: they are the modal value, 25$^{th}$, 50$^{th}$, 75$^{th}$, and 90$^{th}$ percentile of the dataset. This corresponds to 50m, 125m, 325m, 950m, and 2900m.

The modal value of $m$=2000 ($s$=1/2000) is chosen as the only input for the analyses (Figure 3.3).

$N_v$ values of 0.06 trees/m$^2$, 0.10 trees/m$^2$, and 0.25trees/m$^2$ are chosen considering the DBH of the trees that would be modelled (Chapter 3.3.2), relationship between the diameter at breast height (DBH) and stem density shown in Figure 2.4, and expert opinion. It should be noted that other than the selection of $N_v$ input values, the inverse relationship between $N_v$ and DBH is not taken into account in this study. This means that the analyses (Chapter 3.3.3 and 3.3.4) will consider all combinations and permutations of DBH and $N_v$ instead of only having one $N_v$ per DBH.

### *Hydrodynamic parameters*

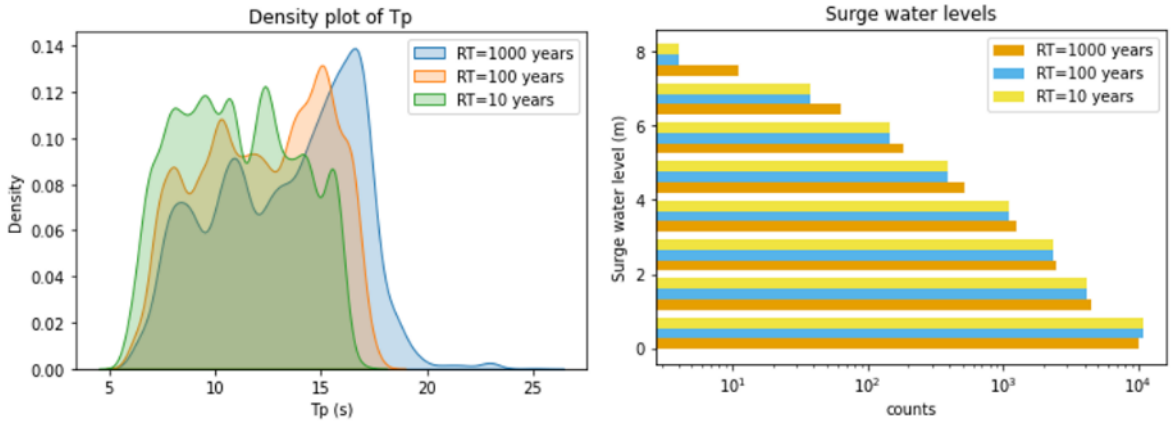


*Figure 3.4 Distribution of peak wave periods in mangrove areas for wave conditions of different return period*

The hydrodynamic input values were selected based on the filtered data set of van Zelst, (2018) from (Bellinga, 2022) (Figure 3.4). The peak wave period, $T_{p0}$, and surge water levels, $h_0$, of three return periods – 10, 100, and 1000 years – were considered in this study. Based on Figure 3.4, $T_{p0}$ of 8s, 10s, 12s, 15s, and 17s and $h_0$ of 2m to 8m were selected. In addition, it is known that ERA5 model – the model used to define the wave characteristic and update water level conditions in this set of data by van Zelst, (2018) – underestimate the effect of cyclones on storm surges. As such, the analyses will extend the range of $h_0$ to 10m; the input values for $h_0$ are 2m to 10m, with an interval of 1m. Putting the selected $T_{p0}$ and $h_0$ values together, two types of water conditions are considered in this study: shallow ($\frac{h}{\lambda} < \frac{1}{20}$, with $h$=water level and $\lambda$=wavelength) and intermediate ($\frac{1}{20} < \frac{h}{\lambda} < \frac{1}{2}$). The general

expressions for the dispersion equation (Eq. 14), horizontal velocity profile (Eq. 15) and group celerity (Eq. 16), which are applicable for both shallow and intermediate water conditions, are applied for this study.

$$\omega^2 = gk^2h \quad \text{(Eq. 14)}$$

*Where ω is the $\frac{2\pi}{T}$, where T is the wave period, g is the gravitational acceleration, k is the wave number, and h is water depth.*

$$u = \omega a \frac{\cosh k(z+h)}{\sinh kh} \sin(\omega t - kx) \quad \text{(Eq. 15)}$$

*Where u is the horizontal particle velocity, a is the wave amplitude, z is the vertical coordinate with upward as the positive direction and the water level as the origin, t is time, and x is the direction of propagation.*

$$c_g = \frac{1}{2}c(1 + \frac{2kh}{\sinh 2kh}) \quad \text{(Eq. 16)}$$

*Where $c_g$ is the group velocity, and $c = \frac{\lambda}{T}$ is the phase speed*

The maximum wave steepness considered in this study is 3%, and $H_{s0}$ is calculated based on the needs of the analyses. This is further elaborated in subsections 3.3.3 and 3.3.4.

### 3.3.2 Root and tree models

The roots and full-tree models of R *sp.* are built with a combination of information from literature review, field data, and expert opinion. This chapter will first describe how the models for the sensitivity analysis of the root layer are developed before presenting the methodology used to develop the full-tree and tree-component models that are applied in the R *sp.* forest analyses. Table 3.2 provides the general inputs used to develop the vegetation models. It should be noted that frontal area (FA) and frontal area per unit volume per vertical elevation (dFA) are used to describe the tree models instead of the average diameter of roots/branches multiplied density of branches ($b_vN_v$). This is because $b_vN_v$ assumes that the roots and branches are uniform in diameter, which is not the case.

| | $h_{tree}$ (m) | DBH (m) | Components |
|---|---|---|---|
| **Root Models** | - | 0.2 | Root-Trunk<br>Trunk only |
| **Tree Models** | 10.6 | 0.11 | Full tree<br>Root-Trunk<br>Canopy-Trunk<br>Trunk only |
| | 13.2 | 0.15 | |
| | 17.5 | 0.21 | |

*Table 3.2 Summary of the general inputs to the vegetation models. It should be noted that the values of htree and DBH for the tree models are fixed to each other i.e. one $h_{tree}$ has only one value of DBH.*

#### Root models for sensitivity analysis of the root layer

Maza et al., (2019) created scaled down models of R *sp.* trees using the equations proposed by Ohira et al., (2013). The root models used in this study are based on the calculated frontal area of these scaled down models (Maza et al., 2019) (Figure 2.13). Two sets of models were developed for sensitivity analyses (Table 3.3). The first set, Root-Layered, consists of four models of different resolutions: 1) Root-1L: the total frontal area of the root system is uniform over the entire height of the root layer, 2) Root-3L: the frontal area is distributed into three layers – where the dFA/dz = 0 within each layer, 3) Root-5L: the frontal area is distributed into five layers, and 4) Root-HR: the frontal area is distributed along the vertical as in Maza et al., (2019) (Figure 3.5). The second set, Root-FA, consists

of six models with the same resolution, but differing total root frontal area as Maza et al., (2019). The total frontal areas of these models are ±2%, ±5%, and ±10% of the original model (Figure 3.6). A trunk-only model (Root-TO), which omits the complex root system, is developed for this study (Figure 3.5).

| Application | Group name | Model names |
|---|---|---|
| Control | | Root-HR |
| Trunk-only | | Root-TO |
| SA of vertical resolution | Root-Layered | Root-1L, Root-3L, Root-5L |
| SA of total submerged frontal area | Root-FA | Root-2Neg, Root-5Neg, Root-10Neg, Root-2Pos, Root-5Pos, Root-10Pos |

*Table 3.3 Root models for the sensitivity analysis of root layer. These models have the same DBH of 0.2m.*

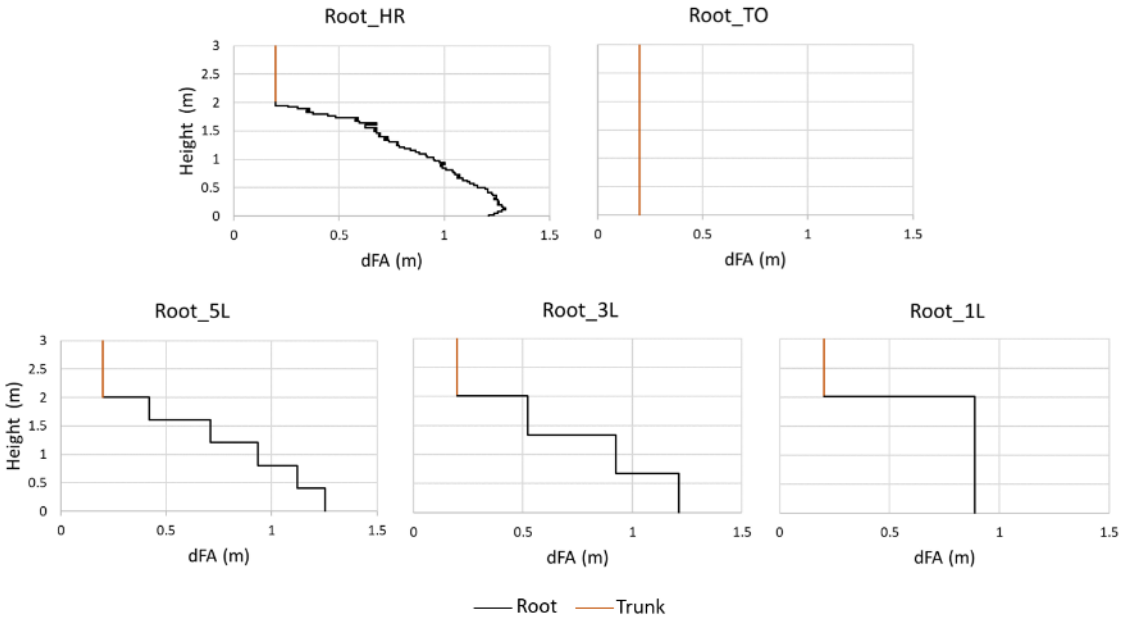


*Figure 3.5 Root models for studying the sensitivity of wave attenuation to the vertical resolution of dFA of root models. The trunk extends uniformly up until the water level, h, for which the analysis is carried out.*

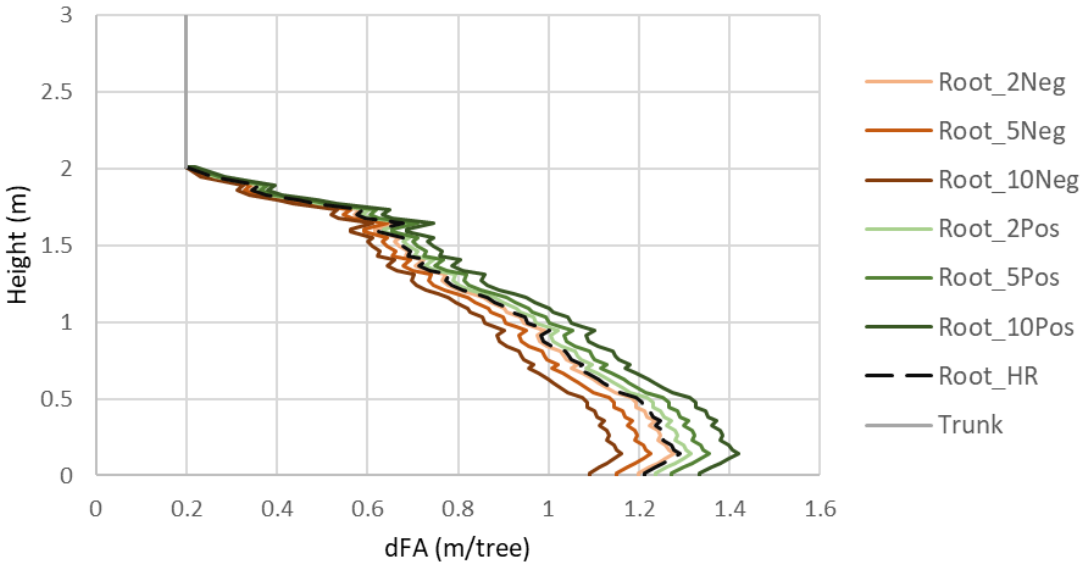


*Figure 3.6 Root models for studying the sensitivity of wave attenuation to the errors in submerged frontal area of the root layer. The trunk extends uniformly up until the water level, h, for which the analysis is carried out.*

*Full-tree models for wave attenuation and component analyses*

The approach to developing the full-tree models in this study can be grouped into three general steps. First, the height and DBH of the trees to be modelled have to be selected. Next, the high resolution root model by Maza et al., (2019) is scaled to the sizes of the tree models. Finally, models of the canopy are developed based on allometric equations and field data. The trunk is represented by a single cylinder of uniform diameter.

### General characteristics of the tree models

The height of the tree models are first decided based on global maximum mangrove distribution with respect to tropical cyclone occurrence by Simard et al., (2019) in Figure 2.3. Three heights were selected: 17.5m, 13.2m, and 10.6m (Table 3.2). A height of 17.5m selected because that is the maximum tree heights that are found between 10° north and south of the equator where there is a high frequency of cyclones in the region. The second value is chosen because Simard et al., (2019) reported that half of the world's forest have a maximum tree height of less than 13.2m. Finally, the value of 10.6m was chosen arbitrarily to study the influence of shorter trees that will still be emergent at the maximum $h_0$ (10m) water level considered in this study.

The diameters at breast height (DBH) are then calculated using the empirical relationship between DBH and tree height that has been collected from the field (A3) and literature (Figure 3.7). The DBH corresponding to the descending tree heights are 11.0cm, 14.9cm and 21.4cm (Table 3.2). The trunk is assumed to have a uniform diameter that equals to the DBH.

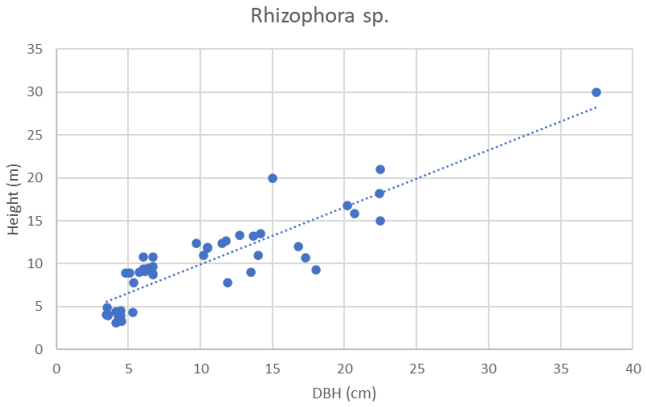


*Figure 3.7 Empirical relationship between DBH and tree heights in R sp. compiled from various sources (Clough et al., 1997; Cole et al., 1999; Gevana & Im, 2016; Lum, unpublished)*

### Root models

The original root model calculated by Maza et al., (2019) is scaled to the size of the tree models using the following procedure. First, the height from which of the highest root extend out from the trunk is calculated according to Equation 17 proposed by Ohira et al., (2013).

$$H_{R\_max} = 7.56(DBH) + 0.500 \quad \text{(Eq. 17)}$$

The ratio $\frac{H_{R_{max},model}}{H_{R_{max},0.2DBH}}$, where $H_{R_{max},0.2DBH}$ refers to the height from which the highest root extends from the trunk of the root model with DBH=0.2m developed by Maza et al., (2019), is calculated. The root models for the trees are obtained by scaling the height and frontal area per unit height (dFA) of the original root model with the calculated ratio.

### Canopy model

Two sets of canopy models were developed using different approaches. The first approach is based on allometric equations, while the second method relies on analysing an image of a full R *sp.* canopy.

The former approach applies the allometric relationship between DBH and above-ground biomass proposed by Clough & Scott, (1989) (Eq. 18), the wood density of R. *sp* as reported in (Tobias et al., 2017), and field estimations of average branch diameter of R. *sp* in Chek Jawa Wetland Reserve, Singapore (A4).

$$\log M_{branches} = -1.8953 + 2.6844 \log(DBH) \qquad \text{(Eq. 18)}$$

First, the canopy mass, $M_{branches}$ is calculated using Equation 18. The volume of branches, $V_{branches}$, is then estimated by $V_{branches} = \frac{M_{branches}}{\rho_{wood}}$, where $\rho_{wood}$ is the wood density. $\rho_{wood}$ of R *sp.* is reported to be approximately 0.840g/cm$^3$ (Tobias et al., 2017). Next, the number of branches is given by $N_{branches} = \frac{V_{branches}}{\pi\left(\frac{D_{branch}}{2}\right)^2 L}$, where $D_{branch}$ is the estimated branch diameter (Table 3.4), and L is an arbitrary length. Finally, the total frontal area of branches in the canopy is calculated by $FA_{branches} = N_{branches} * D_{branch} * L$. It should be noted that the value of L does not influence the final value of $FA_{branches}$ nor the shape of the canopy model.

Due to the plasticity of crown form R *sp.* (see Chapter 2.1.2), the height and shape of the tree model are decided arbitrarily. The frontal area of branches is distributed along the top half of the tree as an isosceles triangle (Figure 3.8A). The frontal area per unit height in the canopy is given by $dFA_{canopy} = dFA_{trunk} + dFA_{branches}$. As the analytical distribution of canopy FA is arbitrarily decided, a vertical resolution of 1m was chosen for the model for the sake of computation. The total FA of canopy was preserved in the process of reducing the resolution. As such, the final canopy model used for wave attenuation modelling is given by subplot B in Figure 3.8.

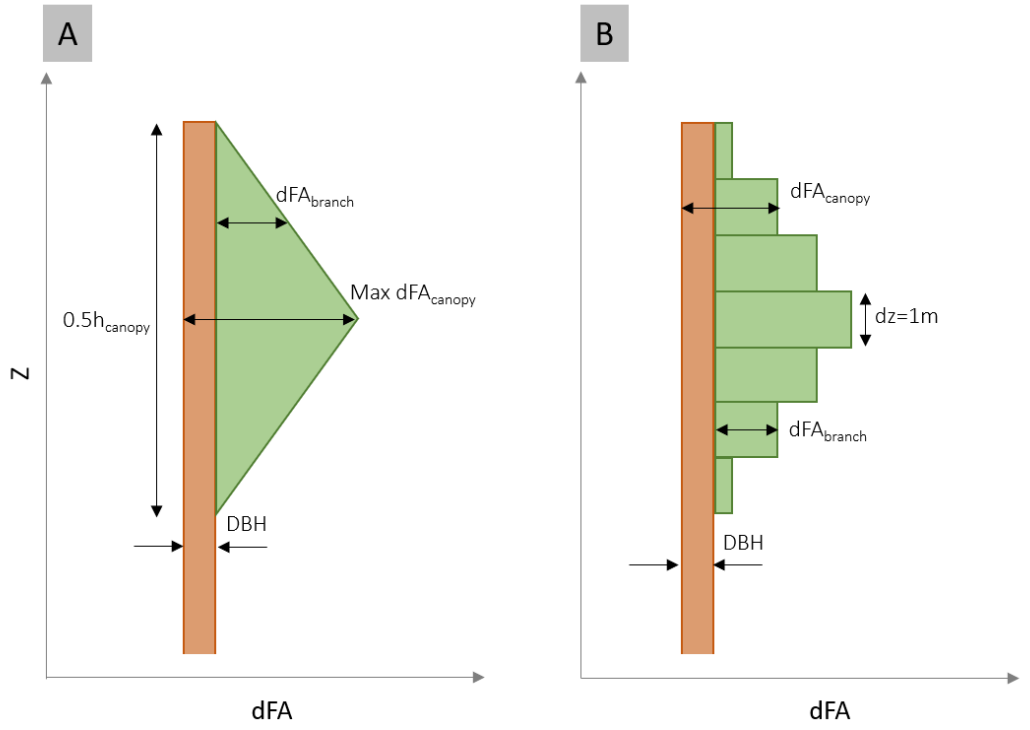


*Figure 3.8 A) Analytical model of canopy developed from allometric equations. B) Model of canopy with vertical resolution of one meter, which is used in the wave attenuation modelling process.*

Table 3.4 below summarises the values obtained for the analytical canopy model using the allometric approach.

| Height | DBH | $M_{branches}$ | $V_{branches}$ | $D_{branch}$ | L | $N_{branches}$ | $FA_{branches}$ | Max $dFA_{canopy}$ |
|---|---|---|---|---|---|---|---|---|
| 10.6m | 11.0cm | 8.0kg | 0.0095m$^3$ | 5cm | 3m | 1.62 | 0.243m$^2$ | 0.232m |
| 13.2m | 14.9cm | 18.0kg | 0.0213m$^3$ | 6cm | 3m | 2.51 | 0.456m$^2$ | 0.250m |
| 17.5m | 21.4cm | 47.3kg | 0.0563m$^3$ | 9cm | 3m | 2.95 | 0.796m$^2$ | 0.281m |

*Table 3.4 Summary of values of the canopy models obtained using the allometric approach*

The image-analysis approach begins with taking an undistorted photograph of a R *sp.* tree. This photo is then processed by hand to extract the silhouette of the tree roots, trunk, and thicker branches (Figure 3.9). Next, through raster analysis, the number of cells is calculated to obtain the required information for relating the DBH of the tree to frontal area of the canopy without its leaves. Figure 3.10 shows the vertical distribution of pixels along the vertical.

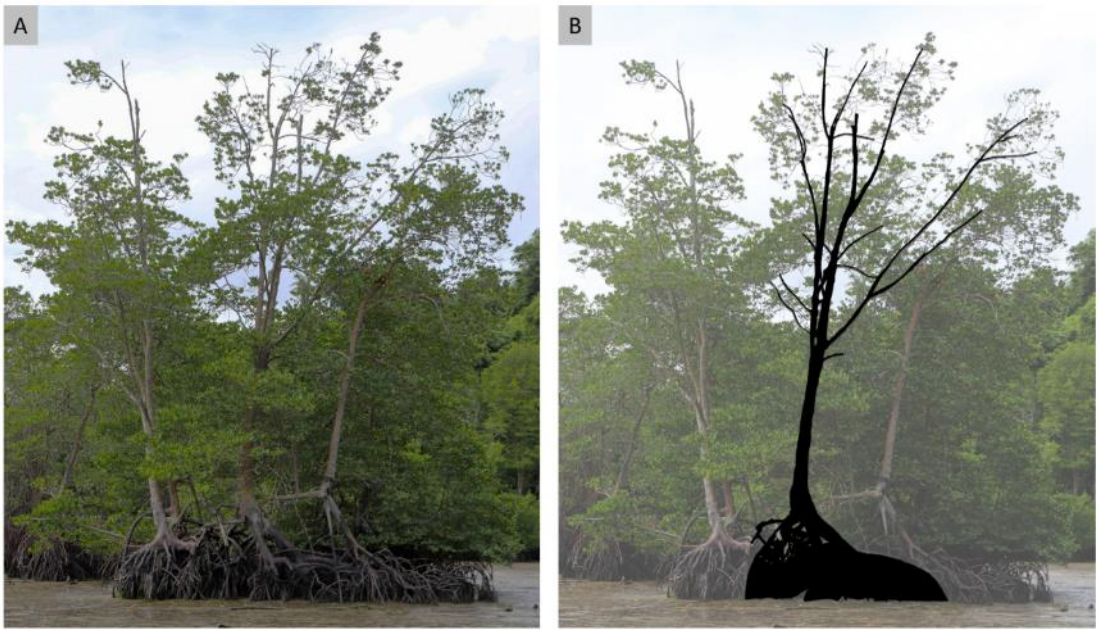


*Figure 3.9 A) Picture of R sp. taken at Check Jawa Wetlands, Singapore. B) Silhouette of the middle tree overlayed that is used for raster analysis*

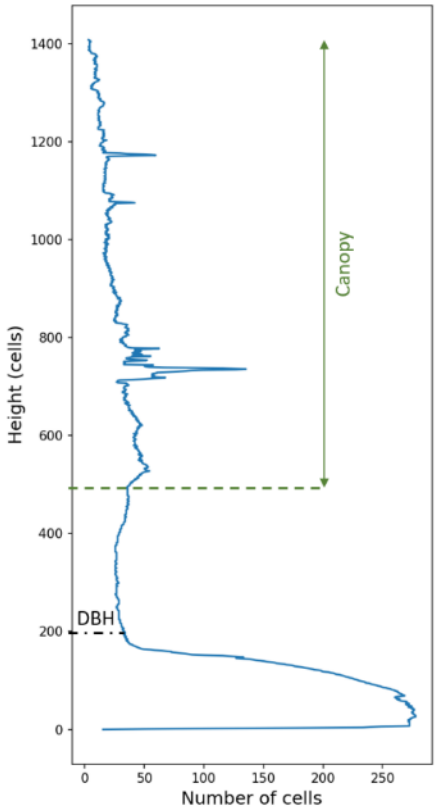


*Figure 3.10 Distribution of cells with height of silhouette of R sp. in Figure 3.7B*

The shape of the dFA(z) in the tree model is simplified to that shown in Figure 3.11. By summing the number of pixels and measuring the height of the canopy section, and measuring the DBH, the maximum dFA is calculated. Figure 3.10 shows where the canopy is defined to begin, and from where the value for DBH is obtained. The ratio of dFA to the DBH is then calculated to be 2.3. Subsequently, this value is applied to create the canopy models for trees of height and DBH as defined at the beginning of this chapter. As in the allometric approach, the canopy is assumed to start halfway down the height of the tree. However, unlike in the allometric approach where $dFA_{canopy}$ is obtained by adding the $dFA_{branch}$ and $dFA_{trunk}$, there is no separation between the frontal area of trunks and branches in this approach. This means that the smallest dFA, which occurs at the top of the canopy, is 0 (Figure 3.11A) instead of $dFA_{canopy}=dFA_{trunk}$ as in the allometric method (Figure 3.8A). It should be noted that this method assumes that the maximum width of the canopy, instead of the total FA, scales directly with the DBH. This causes the total FA to scale exponentially with DBH. The ratio of the length of the canopy to the total height of the tree was not considered in this model as this value is dependent on where the canopy begins, which is in turn influenced by the many factors that were discussed in Chapter 2.1.2. As in the case of the allometric approach, the vertical resolution of the model used for computation is 1m, and the total FA of the canopy was preserved in the process of reducing the resolution (Figure 3.11B).

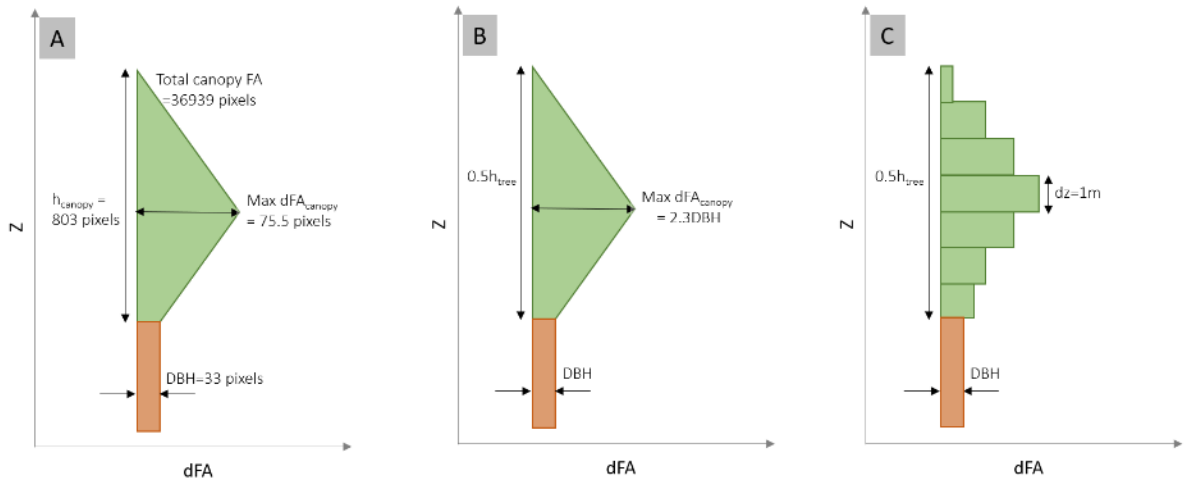


*Figure 3.11 A) Calculation of max $dFA_{canopy}$ based on information extracted from image 3.8 B) Parameters used to develop the canopy model for trees of various DBH and height. C) Canopy model with a resolution of 1m used for wave attenuation modelling*

## Final tree models

A total of 18 models were developed to study the total wave attenuation by full R *sp.* trees, and contributions of the different tree components to wave dampening in storm surge conditions (Table 3.5). The models are developed for trees of heights 10.6m, 13.2m, and 17.5m (Table 3.2). Four groups of models are made by combining the trunk models with the root and canopy models. The trunk-only models are represented by a single cylinder of uniform diameter that is equivalent to the tree's DBH.

| Application | Model group | Model names |
|---|---|---|
| Wave attenuation by R *sp.* forest | Full tree models | FT-Allo-106, FT-Allo-132, FT-Allo-175, FT-Pic-106, FT-Pic-132, FT-Pic-175 |
| Contribution analysis | No-root models | NR-Allo-106, NR-Allo-132, NR-Allo-175, NR-Pic-106, NR-Pic-132, NR-Pic-175 |
| | No-canopy models | NC-106, NC-132, NC-175 |
| | Trunk-only models | T-106, T-132, T-175 |

*Table 3.5 Tree models developed for wave attenuation and contribution analysis of R sp. tree*

Figure 3.13 presents the full-tree models. The no-root models consist of the canopy and trunk sections shown in Figure 3.12, with the root section replaced by extensions of the trunk. Similarly, the canopy sections of the no-root models are replaced by the trunk. Lastly, the trunk-only models are represented by a single cylinder of uniform diameter that is equivalent to the tree's DBH.

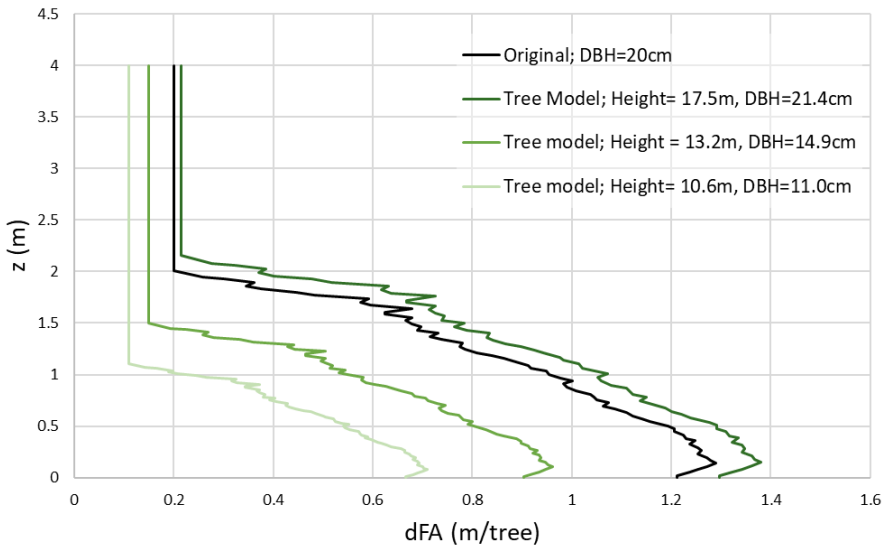


*Figure 3.12 Vertical distribution of frontal area of R sp. root models for trees of different DBH.*

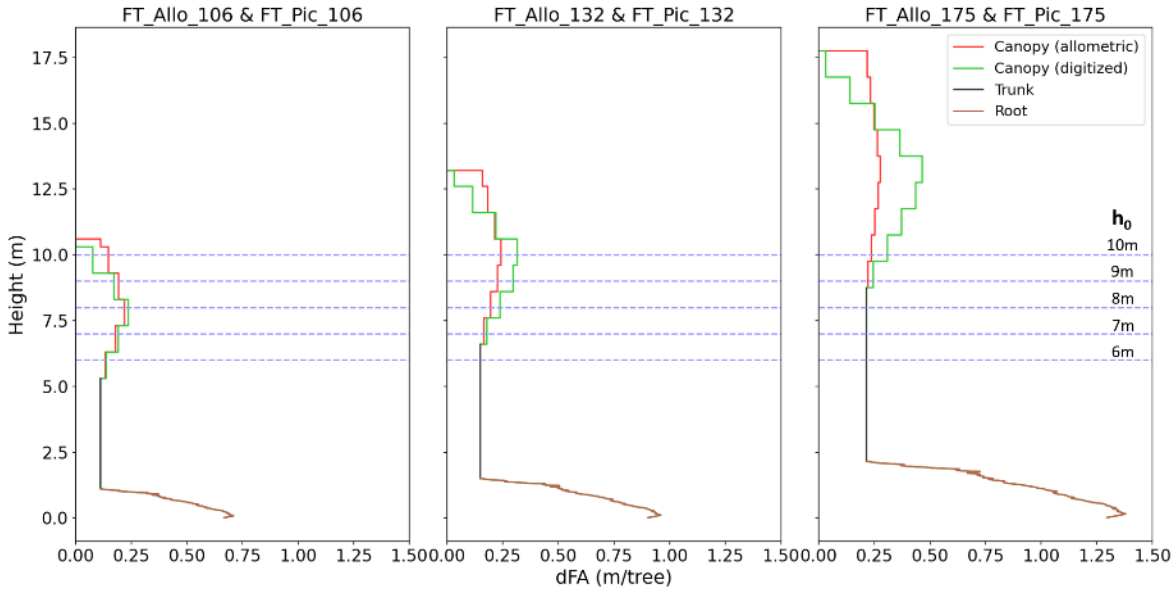


*Figure 3.13 Full tree models for the various defined tree heights and DBH, with the initial water levels, $h_0$, that were applied in the sensitivity analyses for comparison.*

### 3.3.3 Sensitivity analysis of root models

The sensitivity analysis of the root models is conducted with the root models developed in subsection 3.3.2 - *Root models*. This study focuses on analysing how the errors in $k_t$ vary with different input parameters and root models. The errors are defined in relation to the model by Maza et al., (2019). More specifically, three types of errors in the root model are analysed in this process (Eq. 19, 20, and 21). First, by comparing trunk-only models with the model of Maza et al., (2019), the errors that are produced as a result of omitting the complex root layer of an R *sp.* tree is studied. Next, the effect of the root model's vertical resolution on the generated errors are explored. Finally, this analysis looks at how errors in the total frontal area of the root layer would propagate into errors in $k_t$.

$$Error = k_{t,model} - k_{t,Root\_HR} \quad \text{(Eq. 19)}$$

$$Error_{abs} = |k_{t,model} - k_{t,Root\_HR}| \quad \text{(Eq. 20)}$$

$$Error_{rel} = \frac{|k_{t,model} - k_{t,Root_{HR}}|}{k_{t,Root\_HR}} \quad \text{(Eq. 21)}$$

*where $k_{t,model}$ and $k_{t,Root\_HR}$ are arrays of $k_t$ values along the cross-shore (x) direction of the wave attenuation model, produced by the model of interest and root model by Maza et al., (2019) respectively.*

The full range of $h_0$ and $N_v$ described in section 3.3.1, and four sets of wave conditions are applied to this analysis. The first three sets of wave conditions are defined by the $T_p$ values described in section 3.3.2 and have wave steepness of 1%, 2%, and 3%. These values are used to explore how wave attenuate with respect to changing wave heights. The fourth set of wave conditions were designed to study the effect of changing periods on wave attenuation, while holding wave height constant. The wave heights for each water level were calculated with the assumption that the wave steepness is 3%, and $T_p$ is 8s.

### 3.3.4 Wave attenuation by R *sp.* trees

In this section, wave attenuation is analysed in terms of wave height reduction, R (Eq 22).

$$R = \left(1 - \frac{H_x}{H_i}\right) \times 100\% = (1 - k_t) \times 100\% \quad \text{(Eq. 22)}$$

In the contribution analysis, where the contributions to wave attenuation by the root, trunk, and canopy were calculated, the contribution by each section is defined by Equations 23, 24, and 25.

$$C_{root} = R_{full\_tree} - R_{no\_roots} \quad \text{(Eq. 23)}$$

$$C_{canopy} = R_{full\_tree} - R_{no\_canopy} \quad \text{(Eq. 24)}$$

$$C_{trunk} = 1 - R_{no\_roots} - R_{no\_canopy} \quad \text{(Eq. 25)}$$

This study is conducted for $6m<h_0<10m$, with the same wave conditions and forest parameters that were used in the root model sensitivity analysis. The analysis aims to study how R *sp.* Forests affects wave height reduction and how the contribution by the different components of the tree changes with varying size of the tree (height and DBH), initial water levels and density of the forest.

# 4. Results

The results of the model validation process show that wave attenuation model for this study has been implemented well, with the magnitude of the errors well within reasonable ranges. A more detailed description of the results can be found in Appendix (A1). The following sections will present the results from the sensitivity analysis of the root layer (described in 3.3.3) and the wave attenuation and contribution analysis of the hypothetical R *sp.* forests (described in Chapter 3.3.4).

## 4.1 Sensitivity analysis of $C_D$

### 4.1.1 Validation with scaled down flume experiment with R *sp.* root models

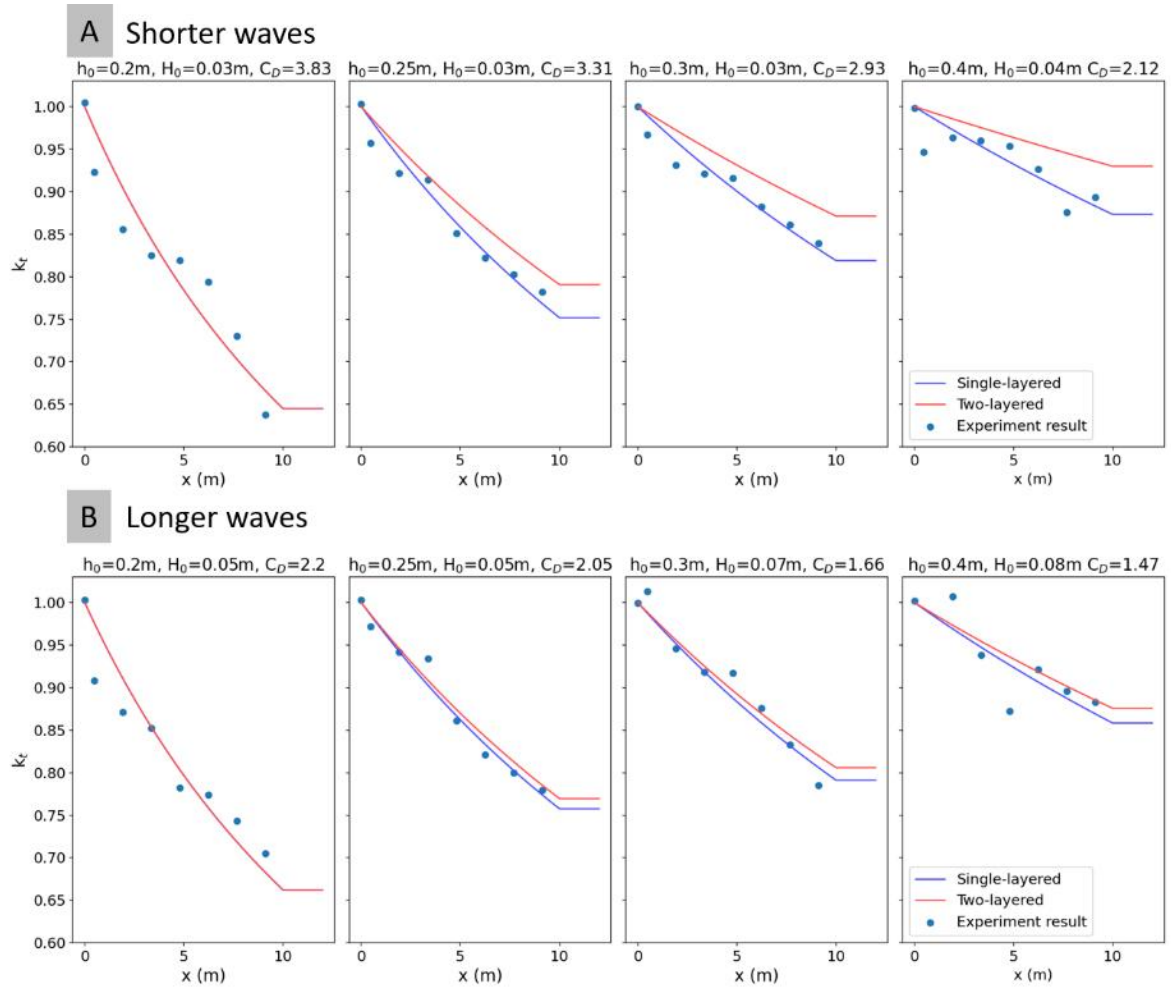


*Figure 4.1 Comparison of $k_t$ between the original (1-layered) model used for calibration in Wang et al., (2022) and 2-layered model when the reported $C_D$ values are used. A) Attenuation of shorter waves, where $T_0$ was fixed at 1s for these experiments. B) Attenuation of longer waves, where $T_0$ of the experiments are, from left to right, 1.4s, 1.6s, 1.8s, 1.8s.*

Two groups of four experiments from Wang et al., (2022) are used to study if the reported $C_D$ values, which were calibrated using a single-layered model, can be applied to a two-layered model with the same total submerged frontal area. The experiments were grouped according to the similarity of the wave period and wave height (Figure 4.1). It is found that with increasing water levels, the discrepancy between the single-layered and two-layered models increases (Figure 4.1: red and blue lines). The magnitude of the differences between the single-layered and two-layered models are observed to be greater for shorter waves (Figure 4.1B) than longer waves (Figure 4.1B).

### 4.1.2 Large scale flume experiment with willow trees

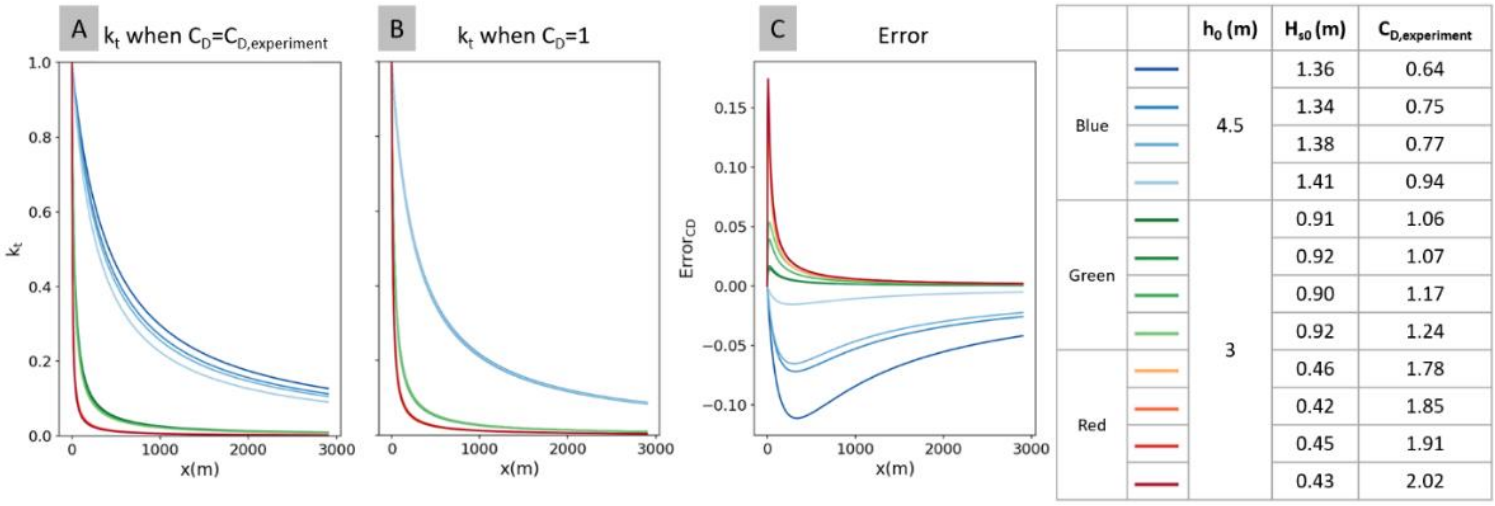


| | | $h_0$ (m) | $H_{s0}$ (m) | $C_{D,experiment}$ |
|---|---|---|---|---|
| Blue | | 4.5 | 1.36 | 0.64 |
| | | | 1.34 | 0.75 |
| | | | 1.38 | 0.77 |
| | | | 1.41 | 0.94 |
| Green | | 3 | 0.91 | 1.06 |
| | | | 0.92 | 1.07 |
| | | | 0.90 | 1.17 |
| | | | 0.92 | 1.24 |
| Red | | | 0.46 | 1.78 |
| | | | 0.42 | 1.85 |
| | | | 0.45 | 1.91 |
| | | | 0.43 | 2.02 |

*Figure 4.2 Comparison of $k_t$ values produced by models using $C_D$ values from van Wesenbeeck et al. (2022) i.e. $C_D$=$C_{D,experiment}$, and $C_D$=1. A) $k_t$ when $C_D$=$C_{D,experiment}$ is applied in the model. B) $k_t$ when $C_D$=1 is applied. C) The error: difference between $k_t$ values when $C_D$= $C_{D,experiment}$ and $C_D$= $C_D$=1 i.e. plot B minus plot A*

Figure 4.2 shows the wave transmission, $k_t$, and error when the reported $C_D$ values from van Wesenbeeck et al., (2022), $C_D$=$C_{D,experiment}$, and $C_D$=1 are applied in the wave attenuation model. The results of $k_t$ and error from this study can be separated into three groups based on the $C_{D,experiment}$ values: $C_{D,experiment}$ smaller than 1 (Figure 4.2, blue lines), $C_{D,experiment}$ larger than but close to 1 (Figure 4.2, green lines), and $C_{D,experiment}$ significantly greater than 1 ($C_{D,experiment}$>1.7) (Figure 4.2, red lines). From here on, these results will be referred to using the colours of their lines i.e. blue group, green group, and red group.

Overall, the magnitude of the errors in all three groups of results are observed to increase exponentially from x=0 and peak before x=350m (Figure 4.2C). The location of the maximum absolute error is observed to shift inland with lower $C_{D,experiment}$ and seaward with increasing $C_{D,experiment}$. Negative errors or underestimations of wave dampening are produced by the model of $C_D$=1 for the blue group experiments where $C_{D,experiment}$<1; positive errors or overestimations of wave attenuation are produced for the green and red group experiments where $C_{D,experiment}$ > 1. The maximum absolute error is 0.11 at x=338m, 0.05 at x=25m, and 0.17 at x=8m for the blue, green, and red group respectively. The errors are correspondingly produced by the model of $C_D$=1, when $C_{D,experiment}$=0.64, 1.24, 2.02. These errors in $k_t$ translate to absolute errors of $0.11H_{s0}$, $0.05H_{s0}$, and $0.17H_{s0}$ in terms of wave height prediction.

For experiments where $C_{D,experiment}$ > 1, the error decreases asymptotically towards zero after peaking (Figure 4.2C, red and green lines). The width between x=0 and the point where the plateau of the curve begins (i.e. when $Error_{CD}$≈1 after the peak error) is greater for larger $C_{D,experiment}$ values (Figure 4.2C, red and green lines). On the other hand, the gradients of errors for experiments where $C_{D,experiment}$ < 1 are observed to be gentler than that when $C_{D,experiment}$ > 1, and the errors do not reach zero within the range of the forest widths that is applied in this study (Figure 4.2C, blue lines). Within the blue group, the final error values at x=2900m are greater for smaller $C_{D,experiment}$.

## 4.2 Sensitivity analysis of the root layer

This section presents results of the sensitivity analyses of the wave attenuation model to the representation of frontal area in the root models. $C_D$ is kept constant at 1 for the entire analysis. Two groups of analyses pertaining to how the errors, absolute, and relative errors (Eq. 19, 20, 21 in Chapter

3.3.3) at the end of forests of vary widths (xVeg), vary with different parameters were conducted. First, the results of comparing a trunk-only model (Root-TO) and the complex-root model (Root-HR) is presented in chapter 4.2.1. In Chapter 4.2.2, the findings of the how wave attenuation modelling results are impacted by errors in the complex root model will be presented. In this section, the mathematical representation of the different types of errors – Error, $Error_{abs}$, and $Error_{rel}$ – are used, while "errors" refers to them in general.

### 4.2.1 Sensitivity of wave attenuation to the absence of the complex root in the vegetation model

*Variation of errors with $h_0$*

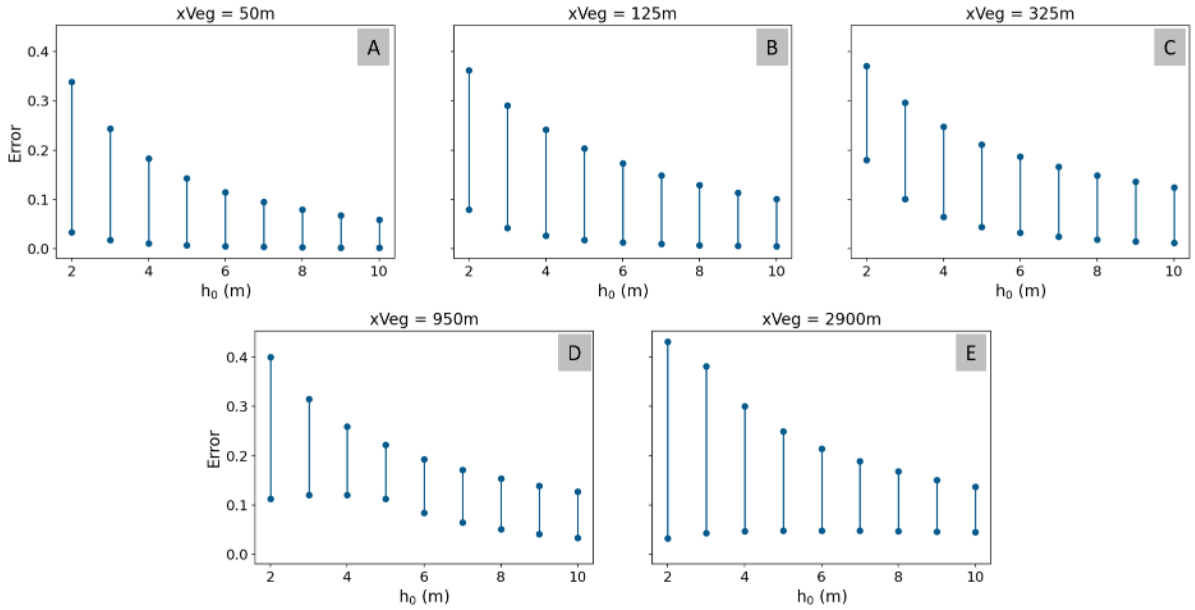


*Figure 4.3 The range of Errors that results from omitting the complex root of R sp. in the vegetation model for the entire range of parameters (Table 3.1) that were tested in this study*

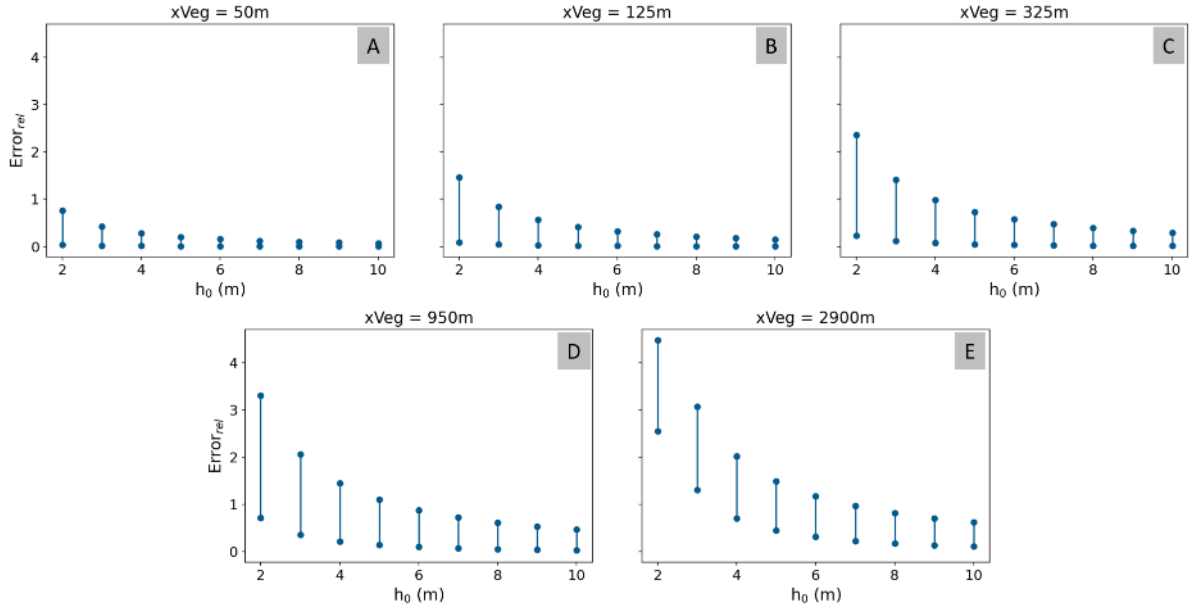


*Figure 4.4 The range of relative errors that results from omitting the complex root of R sp. in the vegetation model for the entire range of parameters (Table 3.1) that were tested in this study*

The analyses of the wave attenuation model to the root layer begins with exploring how the wave dissipation effect of the stilt roots vary with water levels. Figure 4.3 and Figure 4.4 provide an overview of the how the Error and $Error_{rel}$ vary with $h_0$ at the end of forests with different widths. Overall, the maximum Errors are observed to decrease with increasing water levels and forest widths. The minimum Errors, however, do not have such a consistent trend. Subplots D and E of Figure 4.3 show that the minimum Errors increase before decreasing again with the water levels. A comparison between the two subplots also show that the Errors for a forest of 950m width is greater than that for one with a width of 2900m. There is no consistent trend regarding the range of Errors observed. On the other hand, a consistent trend in the minimum, maximum, and range of $Error_{rel}$ can be observed in Figure 4.4. These values increase consistently with decreasing water levels and forest widths.

The maximum $Error_{rel}$ due to the absence of the root layer are produced when $N_v$=0.25, $T_{p0}$=17s, and wave steepness=3%. The corresponding input values that produce the minimum Errors are $N_v$=0.06tree/$m^2$, $T_{p0}$=8s, and wave steepness=1%. These observations hold true for the range of water levels and forest widths that are applied in this study.

At lower water levels ($h_0$=2m), the maximum Errors as a result of omitting the complex roots can be higher than 0.4 (Figure 4.3, subplot D and E), and the calculated $k_t$ can be 4 times larger than that of the actual value (Figure 4.4, subplot E). When these values are translated to actual wave heights, an Error of 0.4 would result in a predicted $H_s$ that is $0.4H_0$ greater than the $H_s$ that is calculated with a complex root model, and a $Error_{rel}$ of 4.0 gives a predicted $H_s$ that is five times greater than the root model.

At extremely high water levels ($h_0$=10m), the Error and $Error_{rel}$ can be as high as 0.14 and 0.62 respectively (Figure 4.3 and Figure 4.4, subplot E). These means that the trunk-only model can produce wave heights that are $0.14H_0$ larger, or 1.62 times the wave height predicted by the complex root model.

### *Variation of errors with $H_{s0}$ and $T_{p0}$*

An analysis on how the errors vary with the hydrodynamic parameters of initial wave height, $H_{s0}$, and wave period, $T_{p0}$, is also performed. Figure 4.5 and Figure 4.6 show how the Errors and $Error_{rel}$ vary with wave height. These values were obtained by holding the parameters of $N_v$ and $T_{p0}$ constant, while the magnitude of $H_{s0}$ is defined using the wave steepness – the steeper the wave, the greater the value of $H_{s0}$. On the other hand, Figure 4.7 and Figure 4.8 were derived by holding $H_{s0}$ constant for each water level (refer to Chapter 3.3.3).

In Figure 4.5, it is observed that Error increases with wave height in shorter forests for all $h_0$ (subplot A and B). For medium sized forests (subplot C and D), the opposite trend is observed for low $h_0$. The trend is then totally flipped in a large forest of 2900m width (subplot E). In contrast, the trends of the $Error_{rel}$ remain consistent across all forest widths, with taller waves producing greater $Error_{rel}$ (Figure 4.6). $Error_{rel}$ produced by different $H_{s0}$ are observed to converge at higher water levels (Figure 4.6).

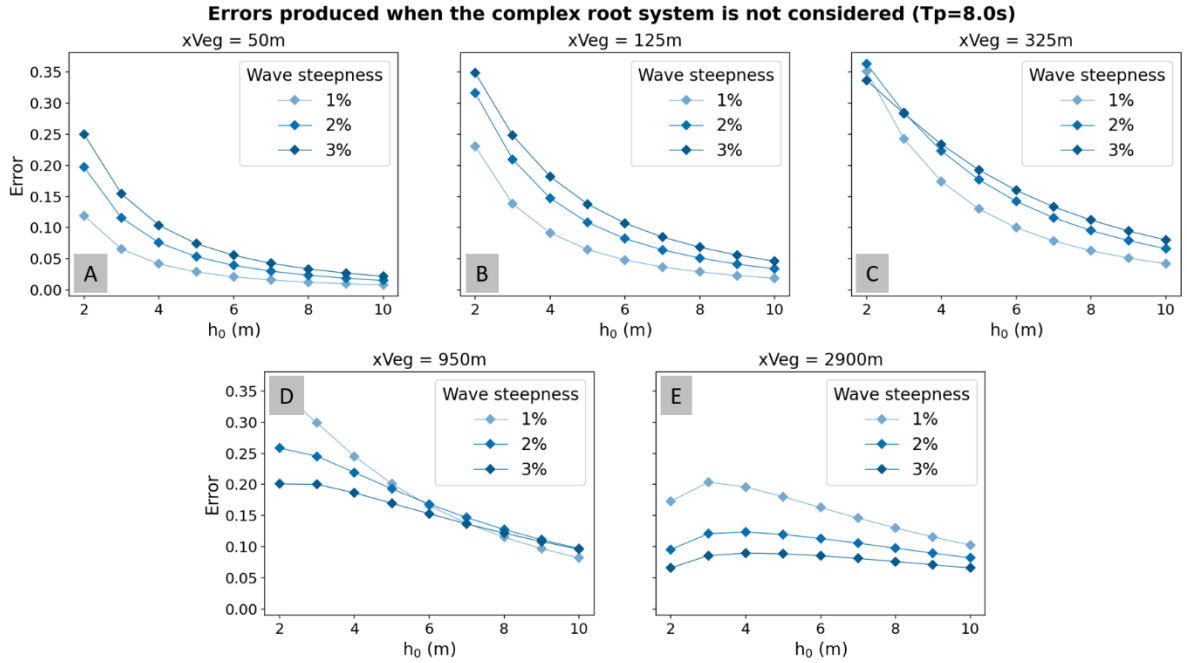


*Figure 4.5 Variation of Error generated by different root models against $h_0$ when $H_{s0}$ (wave steepness) is varied, while $T_{p0}$=8s and $N_v$=0.1tree/m2.*

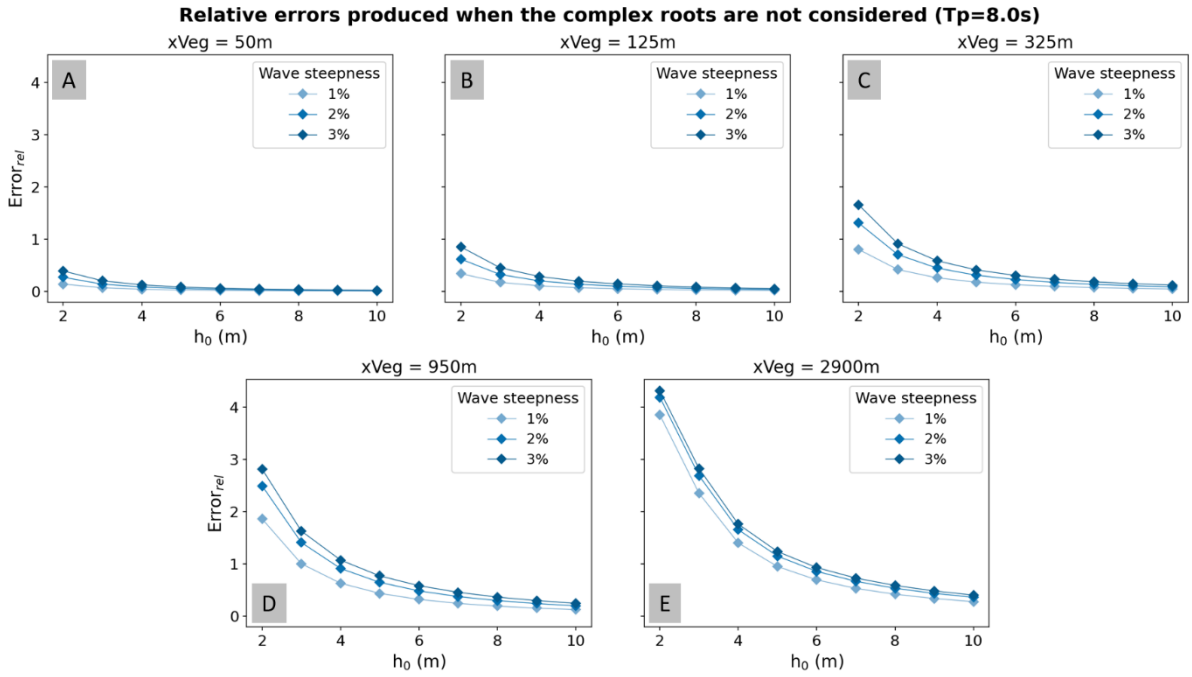


*Figure 4.6 Variation of $Error_{rel}$ generated by different root models against $h_0$ when $H_{s0}$ (wave steepness) is varied, while $T_{p0}$=8s and $N_v$=0.1tree/m2.*

Figure 4.7 show that Error increases with longer $T_{p0}$, with sensitivity increasing with $h_0$ and forest width (diverging lines). On the other hand, $T_{p0}$ has almost no effect on $Error_{rel}$, with only minimal divergence that can be observed for larger forests (Figure 4.8, subplot D and E). Error and $Error_{rel}$ due of missing root layer are less sensitive to $T_{p0}$ than wave height and water level.

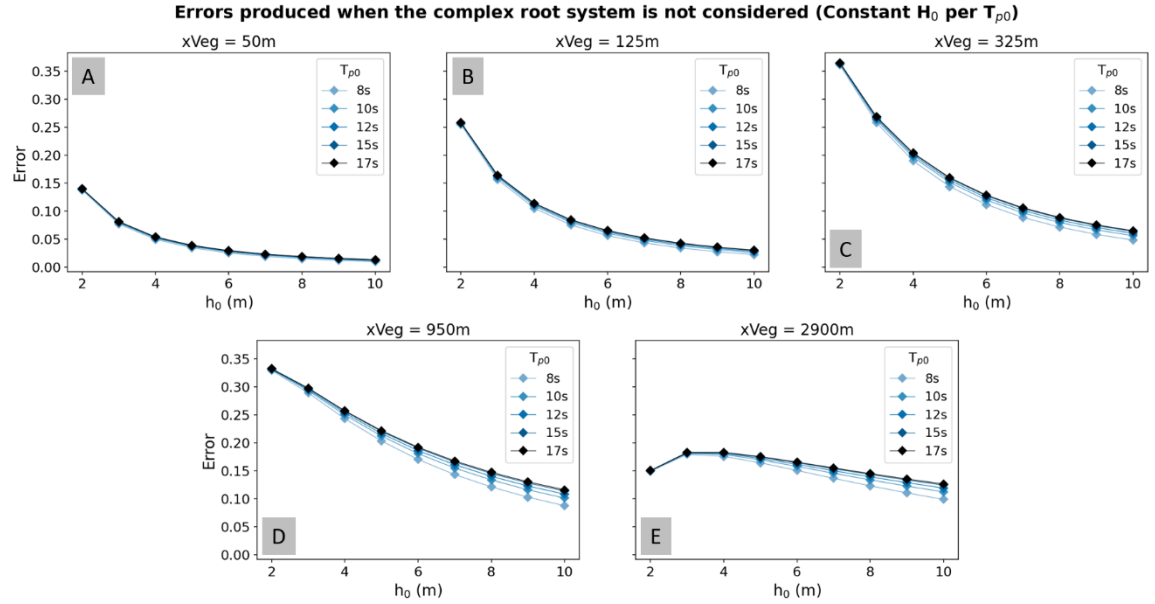


*Figure 4.7 Variation of Error generated by different root models against $h_0$ when $T_{p0}$ is varied, while $H_{s0}$ is kept constant per $T_{p0}$ per $h_0$, and $N_v$=0.1tree/m2.*

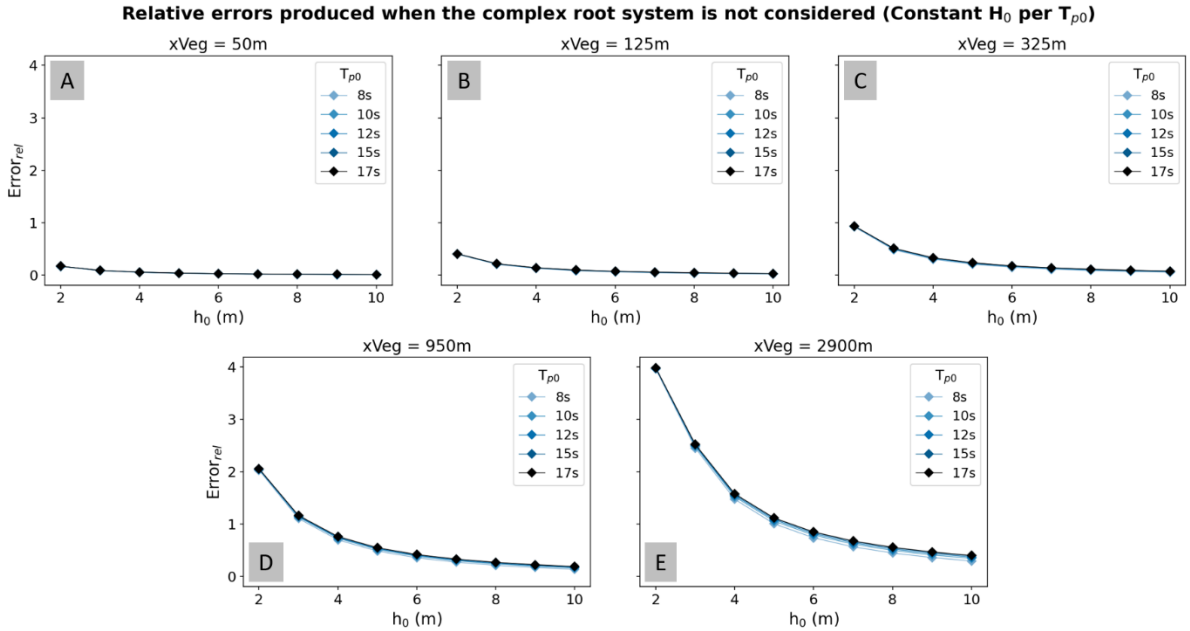


*Figure 4.8 Variation of $Error_{rel}$ generated by different root models against h0 when $T_{p0}$ is varied, while $H_{s0}$ is kept constant per $T_{p0}$ per $h_0$, and $N_v$=0.1tree/m2.*

### 4.2.2 Sensitivity of wave attenuation to errors in the complex root model

The sensitivity of wave attenuation to the choice of root models is studied by analysing the errors produced by the Root-Layered and Root-FA models (Table 3.3). The errors are defined relative to the results of Root-HR (Eq. 19, 20, 21).

The maximum and minimum $Error_{abs}$ and $Error_{rel}$ produced by various root models for the range of tested forest parameters and hydrodynamic conditions (Table 3.1) are shown in Table 4.1 and Table 4.2 below. Overall, model Root-1L and Root-2Neg produce the largest and smallest errors respectively.

An analysis of the input parameters that result in the maximum and minimum errors produced by each root model has also been done. The runs that produced the maximum errors have the following input parameters: $h_0$=2m, $T_{p0}$=8s, and wave steepness=1%. With the exception of model Root-5L, where $N_v$=0.1 tree/m$^2$ for the run that produced the maximum error, $N_v$=0.06 tree/m$^2$ for the rest of the models. On the other hand, the inputs corresponding to the minimum errors are given by $h_0$=10m, $T_{p0}$=17s, and wave steepness=3% for all models. The $N_v$ values of these runs with the Root-Layered and Root-FA models are 0.25 tree/m$^2$ and 0.06 tree/m$^2$ respectively.

| **$Error_{abs}$** | **Root-** | | | | | | | | |
|---|---|---|---|---|---|---|---|---|---|
| | **1L** | **3L** | **5L** | **2Neg** | **5Neg** | **10Neg** | **2Pos** | **5Pos** | **10Pos** |
| **Min ($10^{-2}$)** | 0.0055 | ≈0 | ≈0 | 0.092 | 0.46 | 0.93 | 0.19 | 0.46 | 0.92 |
| **Max ($10^{-2}$)** | 3.72 | 0.66 | 0.33 | 0.27 | 1.36 | 2.30 | 0.52 | 1.29 | 2.52 |

*Table 4.1 Summary of the minimum and maximum absolute errors produced by the Root-Layered and Root-FA models*

| **$Error_{rel}$** | **Root-** | | | | | | | | |
|---|---|---|---|---|---|---|---|---|---|
| | **1L** | **3L** | **5L** | **2Neg** | **5Neg** | **10Neg** | **2Pos** | **5Pos** | **10Pos** |
| **Min ($10^{-2}$)** | 0.038 | ≈0 | ≈0 | 0.13 | 0.65 | 1.30 | 0.26 | 0.64 | 1.28 |
| **Max ($10^{-2}$)** | 26.2 | 2.41 | 1.17 | 1.00 | 5.23 | 11.0 | 1.95 | 4.74 | 9.05 |

*Table 4.2 Summary of the minimum and maximum relative errors produced by the Root-Layered and Root-FA models*

#### *Variation of errors with $h_0$*

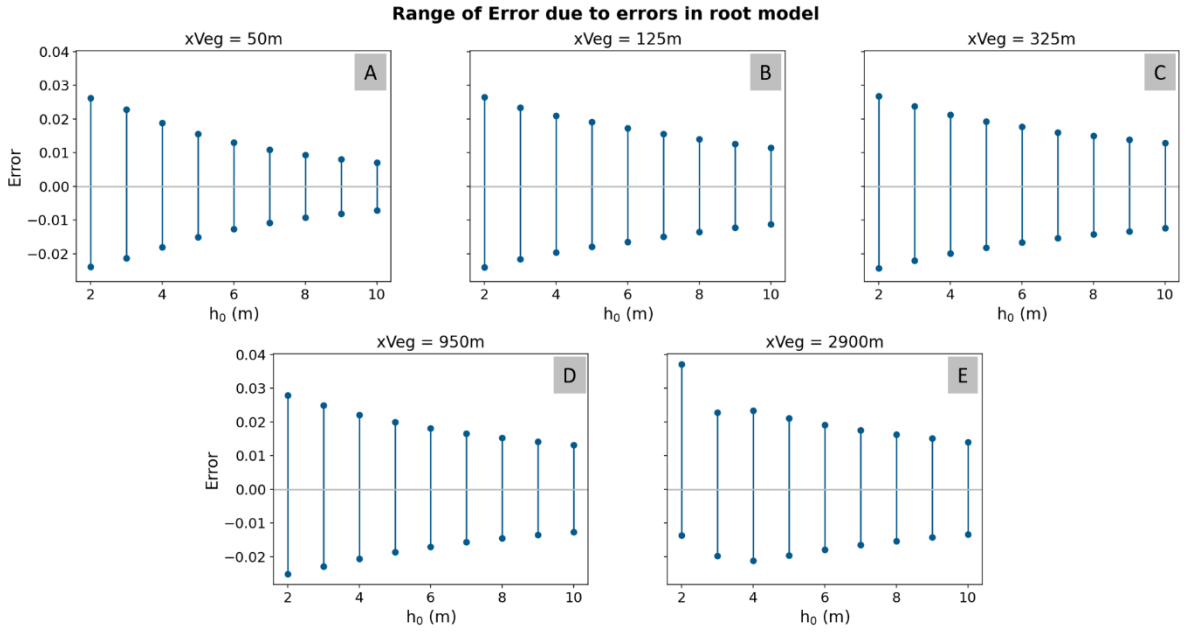


*Figure 4.9 The range of Errors produced by R sp. models with respect to water levels, at the end of forests of different widths, for the entire range of parameters (Table 3.1) that were tested in this study*

With the exception of the forest of width 2900m, the magnitude of Error produced by inaccuracies within the root model decreases with water level and increase with width of the forest (Figure 4.9). The maximum and minimum Error are produced by Root-10Neg and Root-10Pos respectively in these cases where 50m≤xVeg≤950m (Figure 4.9). As a whole, the Root-xNeg models (i.e. Root-2Neg, Root-5Neg, Root-10Neg) would result in positive errors while the Root-xPos i.e. Root-2Pos, Root-5Pos, Root-10Pos) models would result in negative errors. This is because the reduction (addition) in total frontal area in the root layer in Root-xNeg (Root-xPos) – relative to the control model, Root-HR – means that wave dampening is underpredicted (overpredicted). As such, the final $k_t$ produced by Root-xNeg (Root-xPos) is larger (smaller) than the results of Root-HR.

At 2900m from the shoreline, the maximum Error for $h_0$=2m is observed to be much higher than what the trend would predict, while the magnitude of the minimum Error at this point is smaller than expected (Figure 4.9, subplot E). The maximum Error is produced by Root-2L, while the minimum error is produced by Root-10Pos.

A further analysis is done to compare the how the errors produced by the different models compare. Figure 4.10 shows how the Error from individual models vary with distance for different waters levels, when $T_{p0}$=12s, $N_v$=0.1trees/m2, and wave steepness is 3%. Two main observations can be made from this. First, the errors produced by the Root-Layered and Root-FA models vary differently with distance. Second, at high water levels ($h_0$>4m), the errors generated by the Root-FA models are significantly larger than that by the Root-Layered models.

The Error of the Root-FA models have consistent pattern across all water levels (dashed lines in Figure 4.10). The magnitude of Error is observed to increase sharply at the beginning of the forest. A maximum is reached before the Error decrease for the rest of the distance. The slopes of the Error become gentler, and the peak Error reduces, as water level increases. On the other hand, the Error produced by Root-Layered models vary differently across $h_0$ (solid lines in Figure 4.10). At $h_0$=2m (Figure 4.10A), where the entire flow only passes through the 2.01m root layer, Error is mostly positive and wave attenuation is underestimated. The Error by all three models increase then decrease with gentler slopes compared to the Root-Layered models. At $h_0$=3m (Figure 4.10B), the Error generated by Root-3L and Root-5L are similar and are almost zero. Root-1L, however, slightly overpredict damping shorter distances. The magnitude of the Error increases moderately before decreasing over a gentle slope. At a point slightly after 2000m, a kink is observed and the gradient of the Error increases significantly (Figure 4.10B, blue solid line). From $h_0$≥4m, the Error by Model_3L and Model_5L are similar to that in $h_0$=3m, while the kink and increase in gradient that was observed when $h_0$=3m is not observed in Model_1L's Error (Figure 4.10C–F).

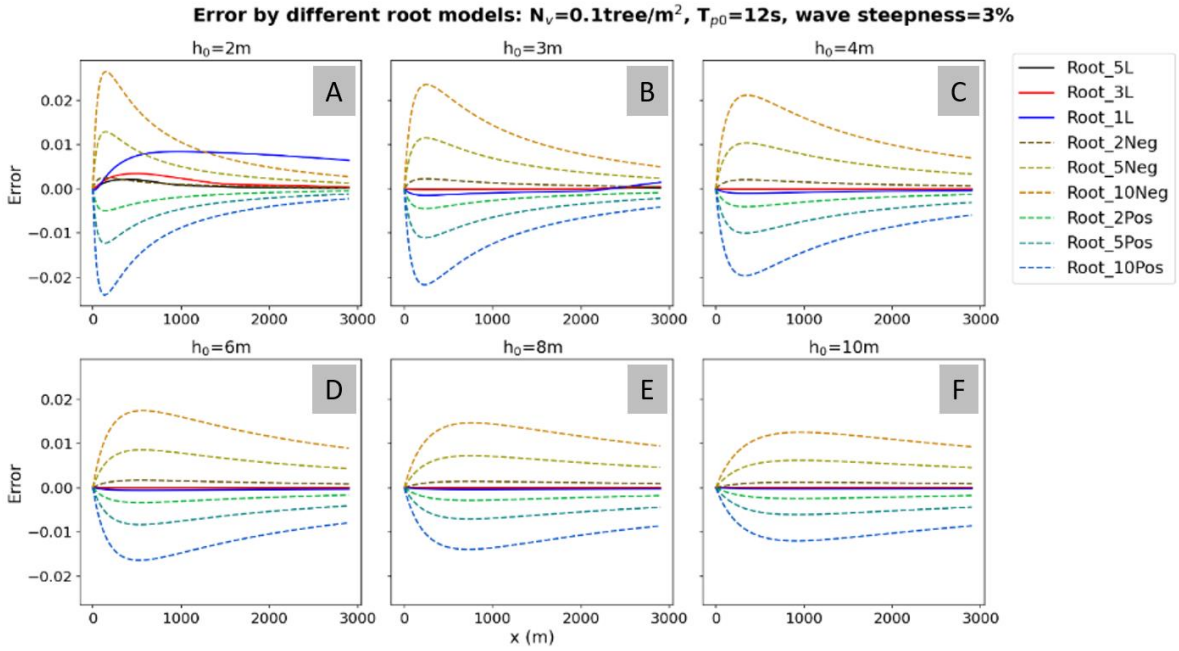


*Figure 4.10 Variation of Error produced by different root models with respect to distance for varying water levels.*

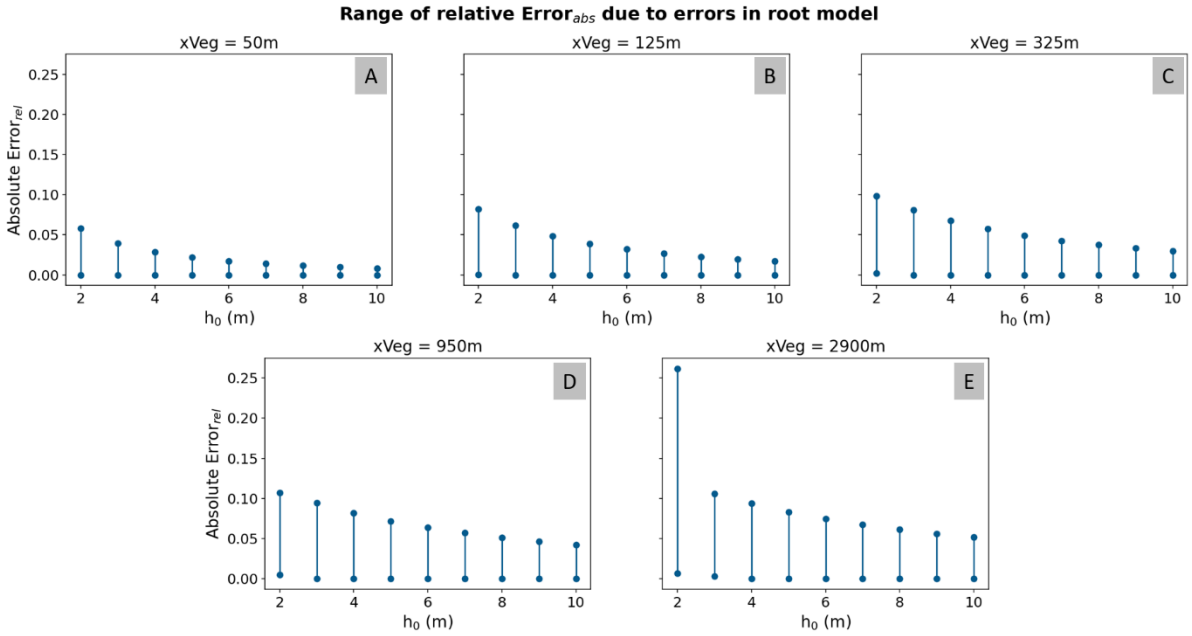


*Figure 4.11 The range of relative Error$_{abs}$ produced by R sp. models with respect to water levels, at the end of forests of different widths, for the entire range of parameters (Table 3.1) that were tested in this study*

As opposed to the trends seen in the Error, Error$_{rel}$ consistently decrease over increasing $h_0$ and increases over the width of the forest (Figure 4.11). The only anomaly is at x=2900m when $h_0$=2m where the maximum Error$_{rel}$ is much higher than what the trend would have predicted.

### *Variation of errors with $H_{s0}$ and $T_{p0}$*

Figure 4.12 and Figure 4.13 show how Error and Error$_{rel}$ vary with $h_0$ when wave height changes while the rest of the input parameters remain constant. Wave height is varied through the wave steepness parameter; steeper waves give larger $H_{s0}$. There are two main takeaways from these plots. First, Error decreases and relative Error$_{abs}$ increases with increasing wave heights (Figure 4.12 and Figure 4.13

respectively). Second, the errors are more sensitive to $h_0$ than variation in wave height. This conclusion was made by observing the relatively small the differences across the subplots of Figure 4.12 and Figure 4.13, compared to the differences in Error for different water levels.

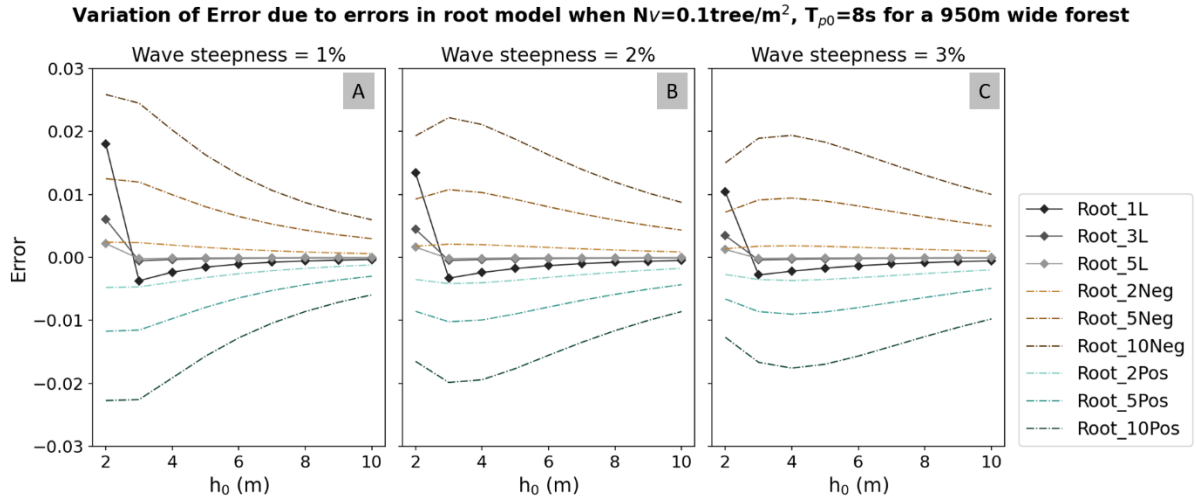


*Figure 4.12 Variation of Error generated by different root models against $h_0$ when wave height (wave steepness) is varied, while $N_v$=0.1tree/m² and $T_{p0}$=8s for a 950m wide forest.*

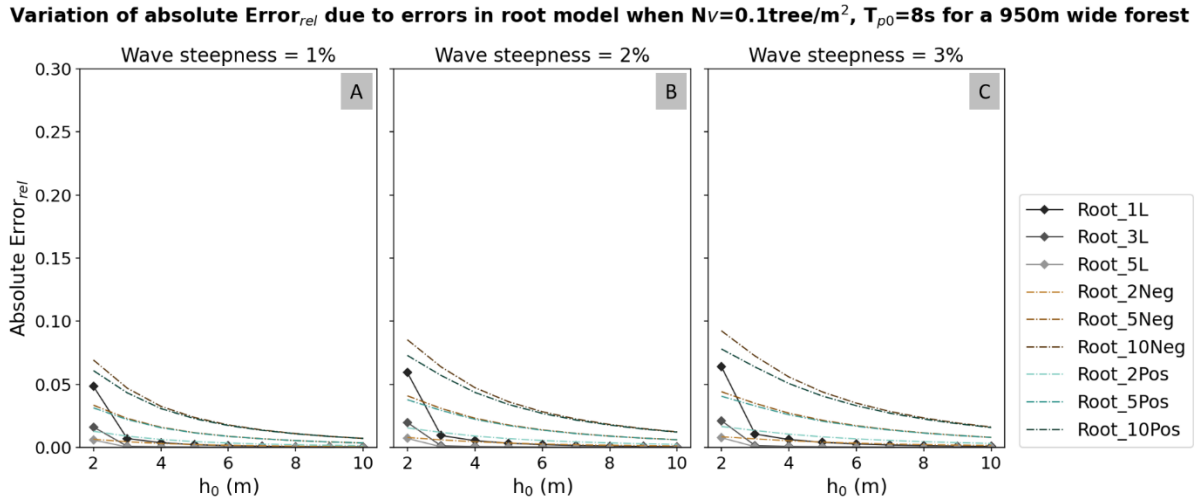


*Figure 4.13 Variation of absolute $Error_{rel}$ generated by different root models against $h_0$ when wave height (wave steepness) is varied, while $N_v$=0.1tree/m² and $T_{p0}$=8s for a 950m wide forest.*

An analysis of how errors varies with $T_{p0}$ is also performed. In Figure 4.14 and Figure 4.15, it can be observed that Error and absolute $Error_{rel}$ almost do not change with $T_{p0}$. The same is seen in forests of different widths (A2). As such, errors due to the inaccuracies in representation of the root layer is not sensitive to $T_{p0}$ for the range (Table 3.1) that is applied in the study.

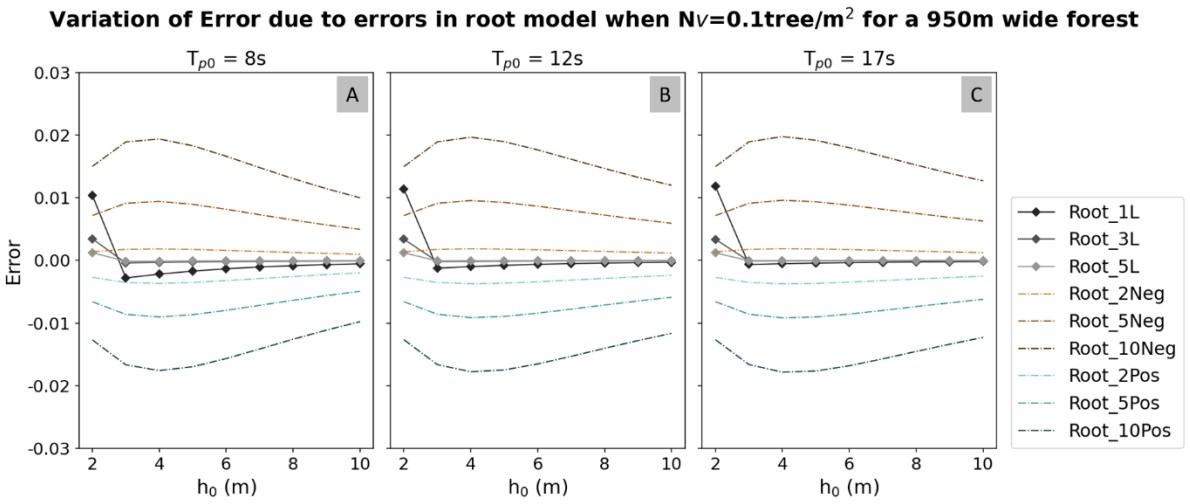


*Figure 4.14 Variation of Error generated by different root models against $h_0$ when $T_{p0}$ is varied, while $N_v$=0.1tree/m² and $T_{p0}$=8s for a 950m wide forest.*

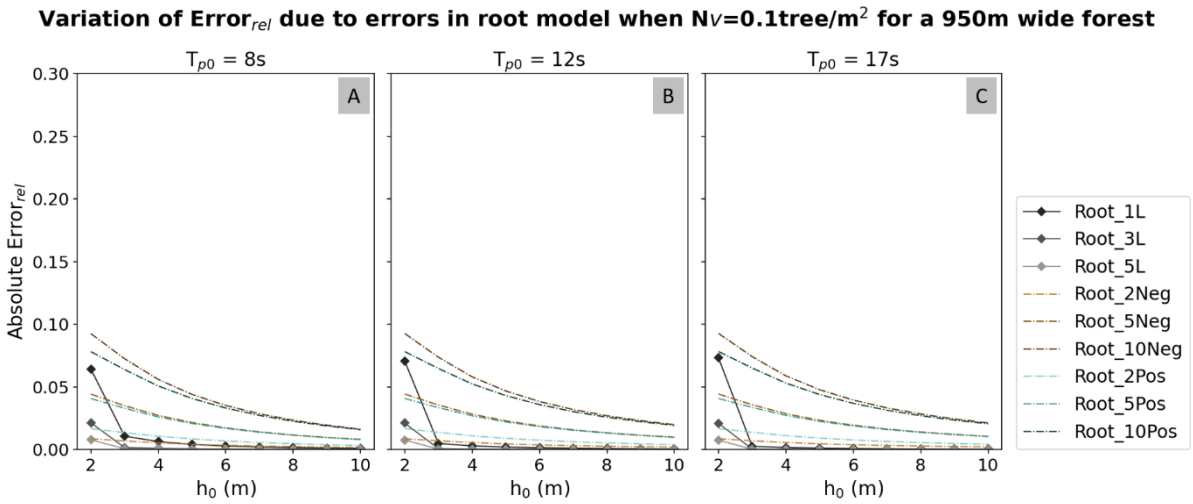


*Figure 4.15 Variation of absolute $Error_{rel}$ generated by different root models against $h_0$ when $T_{p0}$ is varied, while $N_v$=0.1tree/m2 and $T_{p0}$=8s for a 950m wide forest.*

## 4.3 Wave attenuation by R *sp.* trees

### 4.3.1 Wave attenuation by full tree models

The analysis of wave attenuation by R *sp.* forests is done with only two varying hydrodynamic parameters: $h_0$ and $T_{p0}$. The wave steepness is kept constant at 3% (Table 3.1). Figure 4.16 shows the range of wave height reduction by forests of different densities and widths for 6m<$h_0$<10m. It is observed that wave attenuation increases monotonically, with decreasing gradients, over the range of forests widths that have been studied. The maximum attenuation obtained for all forest densities and widths are produced by FT-Allo-175 and FT-Pic-175 in the following hydrodynamic conditions: $h_0$=6m and $T_{p0}$=17s. FT_Digi_106 gives the least wave attenuation when $h_0$=10m and $T_{p0}$ = 8s, while FT-Allo-106 produces the smallest amount of dampening when $h_0$≤9m and $T_{p0}$ = 8s

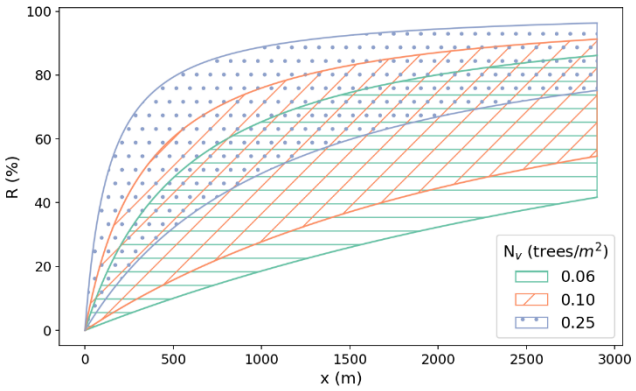


*Figure 4.16 Summary of wave attenuation by R sp. forest for varying densities and width. Reduction is calculated based on Equation 22 (subsection 3.3.4)*

The differences between the maximum and minimum wave height reduction by forests of varying densities are seen to increase then decrease over distance (Figure 4.17). The peak differences between the maximum (minimum) wave attenuation occur after distance of 1590m (209m) from the shoreline (Figure 4.17). Given the conditions that result in maximum wave attenuation i.e. $h_{tree}$=17.5m, $h_0$=6m, $T_{p0}$=17s, a forest of $N_v$=0.25trees/$m^2$ can result up to 34.6% and 22.7% more wave height reduction than $N_v$=0.06trees/$m^2$ and $N_v$=0.10trees/$m^2$ forests respectively (Figure 4.17, red lines). In wave conditions that lead to minimum wave attenuation i.e. forest with trees similar to FT_Digi_106, $h_0$=10m an $T_{p0}$=8s, a high density forest can reduce wave heights by a maximum 34.4% and 22.6% more than medium and low density forests respectively (Figure 4.17, blue lines).

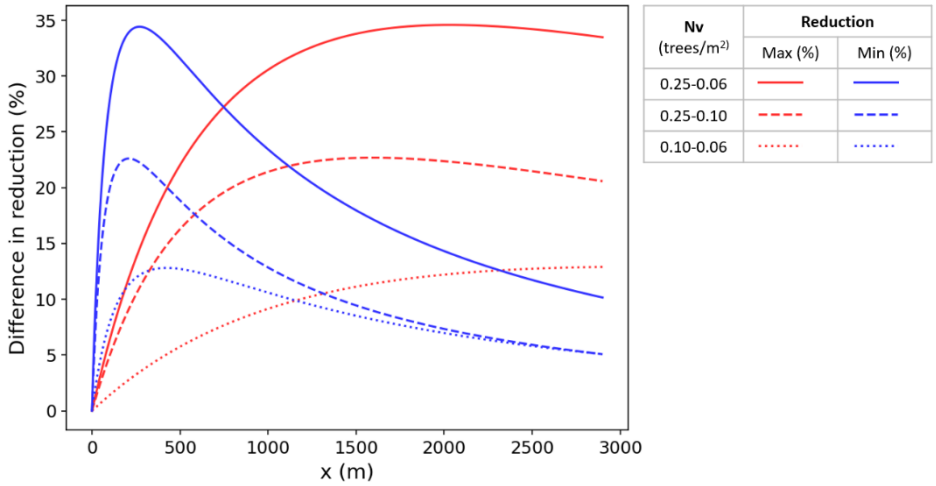


*Figure 4.17 Differences between the (maximums and minimums) wave height reduction by R sp. forests of different densities*

A further analysis is done to study the ranges of wave height reduction by forests of different densities in varying initial water depth, $h_0$. Figure 4.18 shows that for constant $T_{p0}$ and wave steepness, wave attenuation reduces with increasing $h_0$. The range of wave height reduction is also observed to decrease with increasing $h_0$ (Figure 4.18).

The tree models that correspond to the maximum and minimum wave attenuation at x=50m, 125m, 325m, 950m, and 2900m, are also identified. Holding $T_{p0}$ and wave steepness constant, FT-Allo-175 and FT-Pic-175 are found to produce the maximum wave attenuation for $6m \leq h_0 \leq 8m$ across all three forests densities. For $h_0 \geq 9m$, FT-Pic-175 gave the largest amount of wave reduction. This change is due to the difference in canopy frontal area between FT-Allo-175 and FT-Pic-175; the frontal area of FT-Pic-175 is larger than FT-Allo-175 between a height of 8.75m to 10m (Figure 3.13). The minimum wave attenuation for $6m \leq h_0 \leq 9m$ is produced by FT-Allo-106. For $h_0$ = 10m, FT-Pic-106 resulted in the least wave height reduction. Similarly, this change in models producing the minimum wave attenuation is due to the vertical distribution of frontal area in FT-Allo-106 and FT-Allo-106 between at a height of 9m and 10m ().

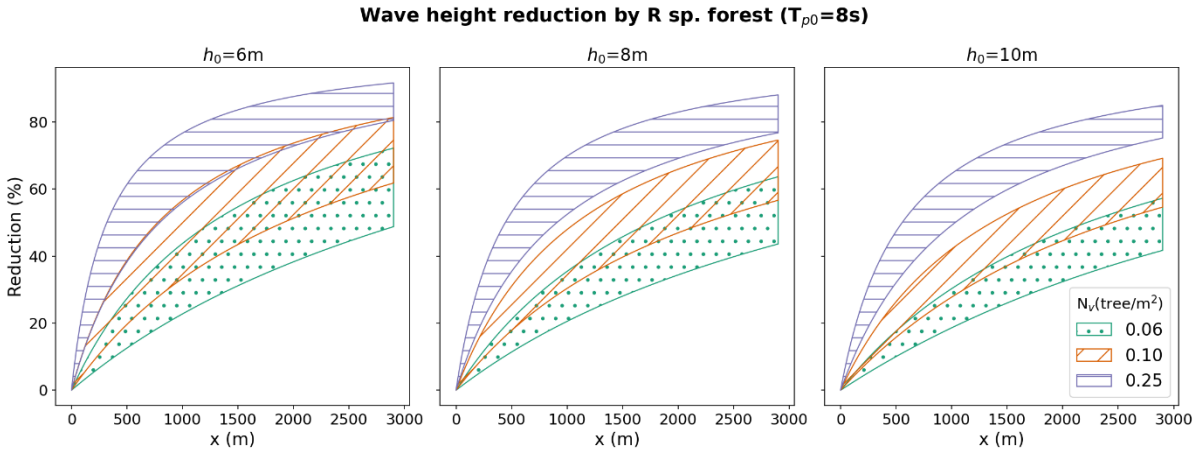


*Figure 4.18 Range of reduction for different water levels when $N_v$=0.1trees/m$^2$ and $T_{p0}$=8s*

Finally, an analysis is done to compare the amount of wave attenuation produced by the different full-tree models. This is done by keeping all other parameters, except $h_0$, constant. Wave attenuation by taller tree models is observed to be greater than shorter models across the range of $h_0$ that were

tested (Fig. 4.19). The difference in wave height reduction by trees of different heights decreases with increasing water depths.

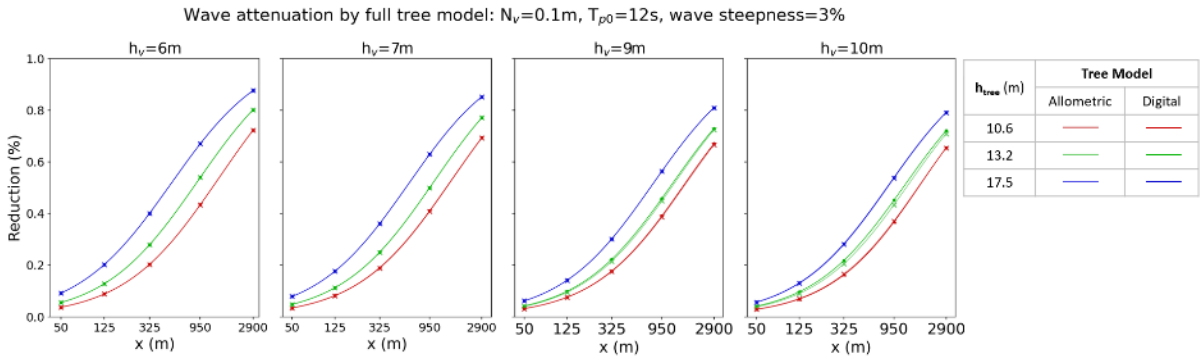


*Figure 4.19 Wave height reduction by R sp. forests of different heights for varying water levels.*

### 4.3.2 Wave attenuation by different components of a R *sp.* forest

The minimum and maximum contribution values by each tree layer are extracted for different forest widths and tree models (Figure 4.20). The results show that the trunks usually produce the most wave attenuation, followed by the roots, and then the canopy. The contribution by the trunks increases with the width of the forest, while the opposite occurs for the root and canopy layer.

Comparing across the same tree model of different heights, the fraction of wave attenuation by the canopy layer decreases as $h_{tree}$ increases, while it increases in the case of the root layer (Figure 4.20). The root layer of a 10.6m FT_Allo model is found to contribute up to 23% to 15% of the total wave height reduction for a 50m and 2900m wide forest respectively. These values decrease to 20% and 8% when $h_{tree}$=13.2, and 2% and almost 0% when $h_{tree}$=17.5m.

It is observed that when $h_{tree}$=10.6m, the canopy layer can contribute significantly more than the root layer to wave attenuation for both the FT_Allo and FT_Pic models (Figure 4.20). The maximum contribution to wave attenuation of the 13.2m FT_Pic model's canopy layer is more than its root layer, and that of the FT_Allo model. The differences between canopies' contributions are due to the differences in the total frontal area of, and distribution of frontal area within the canopy. When $h_{tree}$=10.6m, the maximum water level of 10m – which results in the highest contribution by the canopy layer – would pass through most of its canopy. Given the relatively small difference in submerged part of the canopy structure between the two models, the differences in contribution by the canopy layer is small for both models of 10.6m. However, when the tree models have a height of 13.2m, a surge of 10m would pass through only the bottom half of the canopy. FT_Pic has significantly more frontal area in the lower half of the canopy compared to FT_Allo. As such, the contribution of FT_Pic's canopy is much greater than FT_Allo. Lastly, when $h_{tree}$=17.5m, the flow only goes through a small portion of the canopy. The small difference in contribution by the canopies of the two models is due to the discrepancy in submerged frontal area between the height of 8.75m and 10m.

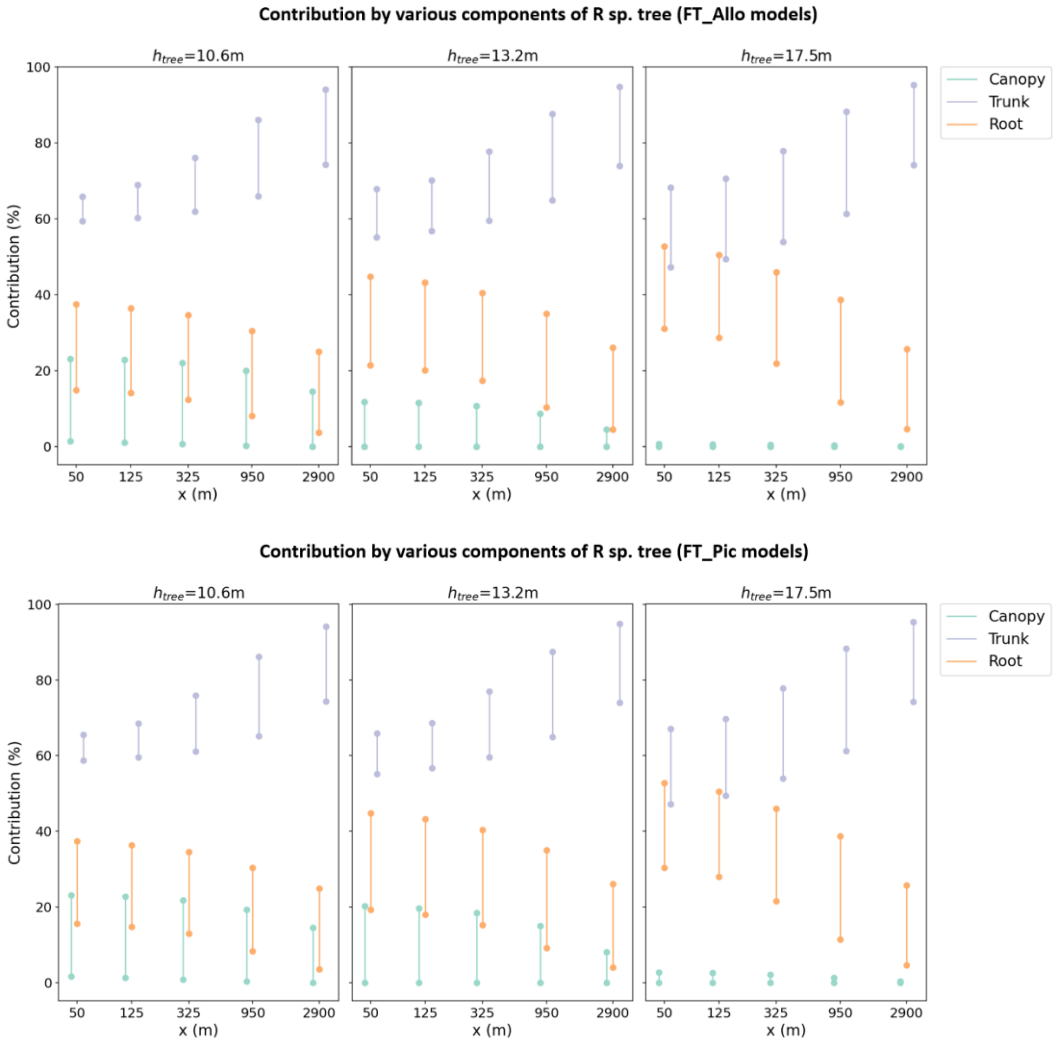


*Figure 4.20 Range of contribution to wave attenuation by different components of R sp. tree of varying heights. Top: Results produced by tree models with canopy developed using the allometric method (refer to Chapter 3.3.2). Bottom: Results produced by tree modesl with canopy developed using the image processing approach (refer to Chapter 3.3.2).*

A deeper analysis on how contribution by the three components vary with water level is presented in Figure 4.21. For a given tree model, the fraction of wave attenuation by the canopy and trunk components increase with water levels. The opposite trend is observed in the case of the root layer (Figure 4.21).

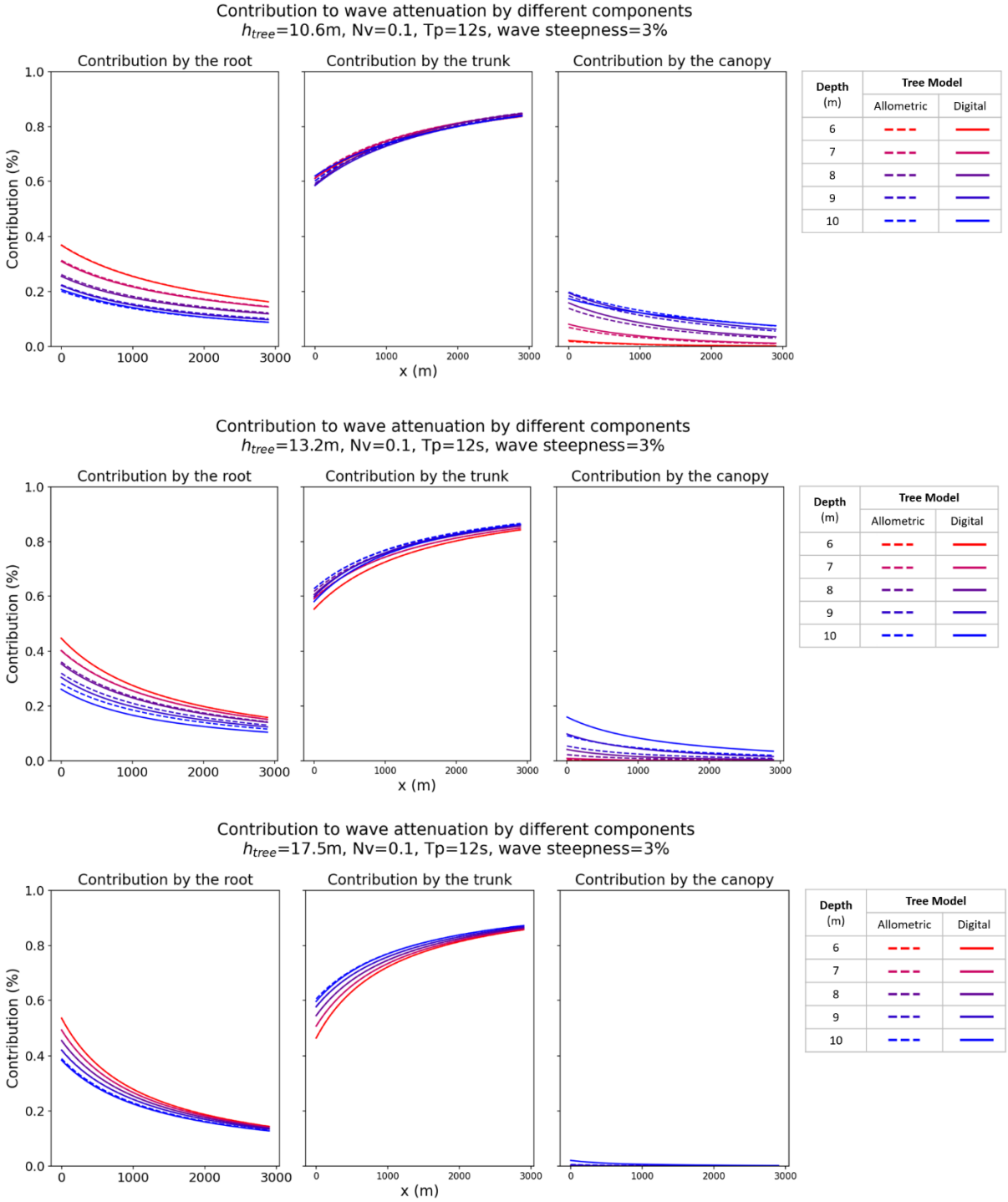


*Figure 4.21 Variability in contribution by different components of the R sp. trees of varying height when 6m < $h_0$ < 10m. Top: R sp. tree model of $h_{tree}$=10.6m, Middle: R sp. tree model of $h_{tree}$=13.2m, Bottom: R sp. tree model of $h_{tree}$=17.5m*

# 5. Discussion

## 5.1 The relevance of R *sp.* root models to wave attenuation modelling

The analysis of how errors and absolute errors, which are produced by omitting the complex root system, vary with water levels show that they reduce greatly with increasing water levels. However, even when this is so, the maximum error and absolute error for extremely high-water levels of 10m is still significant. For example, at $h_0$=10m with incoming waves of 17s and a steepness of 3%, the trunk-only model (Root-TO) would produce an Error and $Error_{rel}$ of 0.09 and 0.53 at the end of a 2900m forest of 0.1tree/$m^2$. This translates to a difference of 0.44m in wave height between the trunk-only and complex root model (Root-HR). For the same physical conditions, the Error produced by a narrower forest is smaller; forests of xVeg=50m and xVeg=125m produce errors in $k_t$ of 0.03 and 0.06 respectively. This translates to errors of 0.15m and 0.30m in wave height. It should also be noted that the root model used in this study only considers the primary roots. As such, the calculated errors are underestimated. As a whole, other than being sensitive to changes in $h_0$, the absolute $Error_{rel}$ are found to increase significantly with the width of the forests, and moderately with wave height. As such, it is expected that these values are larger for lower water depths, wider forests, and taller waves.

The effect of two types of errors within the root model – vertical resolution and error in total frontal area of the root layer – were also investigated in this study. Compared to the errors produced by the absence of the aerial roots, the errors in $k_t$ due to the errors in details within the root model is much less significant. The maximum Error that resulted from the omission of the model is larger than 0.4, while the maximum magnitude of the Error produced by errors in details of the root model is a magnitude smaller. Delving deeper, this study also found out that for water levels significantly higher than the root layer (which is this study is $h_0$>3m), the wave attenuation model is much more sensitive to the errors in frontal area than the errors due to the resolution of the vegetation model (Figure 4.12 and A2). Furthermore, it was observed that the errors produced by the model with a three-layered root layer (Root-3L) and five-layered root layer (Root-5L) are similar (Figure 4.12 and A2). These findings suggest that it is more important to collect information on the total frontal area of the root layer than it is to represent the vertical distribution of frontal area in the layer for high water levels. At lower water levels, when $h_0$<$h_{root}$, the wave attenuation model is observed to be significantly more sensitive to the resolution of the root model, especially for wider forests (xVeg>950m) (Figure 4.12 and A2).

## 5.2 Wave attenuation by R *sp.* forest

The ranges of reduction in wave height, $r_{Hs}$, (A3, Table 0.4) for xVeg>350m are comparable with the values of wave height reduction reported by Horstman et al., (2014) for the Rhizophora back forest in Trang province, Thailand. Field measurements by Horstman et al., (2014) – which were taken within the first few hundred meters from the shoreline – show that the back forest with R *sp.* of variable sizes and density between 0.006 to 0.15 trees/$m^2$ produce a general wave height reduction of 0.012$m^{-1}$. This value fit within the range of $r_{Hs}$ that is calculated for forests of widths less than 325m (A3, Table 0.4). It should be noted that the measurements in Horstman et al., (2014) were done for relatively low water levels (h<2m). There are no measurements of wave attenuation by mangroves to compare the results of the models for high water levels.

The R *sp.* models that are applied in this study do not account for drag by leaves. This decision was made based on the results by Van Wesenbeeck et al., (2022) where they reported that the leaves of the willow tree only contributed to less than 4% of the total wave attenuation. Assuming that the developed tree models represent the R *sp.* trees sufficiently well, the results of the study indicate that regardless of the water level, the taller and broader R *sp.* trees attenuate short waves better than

shorter and smaller trees. This indicates that the additional frontal area due to the shorter tree's canopy provide less drag than the additional frontal area the larger tree has in its root and trunk layer. This situation may not hold true when the intervals between the heights and DBH of the modelled trees are smaller. It should be noted that this analysis did not consider the inverse relationship between $N_v$ and DBH. Based on Chapter 2.1.2, it is unlikely for a dense forest to support trees with large DBH. As such, further analysis that accounts for this relationship should be done to better understand the capacity of mangrove forest to attenuate waves.

Next, the wave attenuation analysis is done assuming that $C_D$=1 for the entire tree. Based on the analysis in Chapter 4.1.2 with results from van Wesenbeeck et al., (2022), the error due to approximating $C_D$=1 should be relatively small in the R *sp.* forest wave attenuation and contribution analysis for water levels lower than the canopy and especially for xVeg>300m (Error<0.05) (Figure 4.2). This conclusion is made assuming that $C_D \geq 1$ for the root and trunk layers of R *sp.*. On the other hand, it is expected that the canopy has a smaller $C_D$ due to the flexibility of the branches. This mechanical property of the canopy has not been accounted for in this model. As such, the overall $C_D$ value for water levels that go through majority of the canopy would likely be less than 1. As such, the error due to approximating CD=1 could still be significant for large xVeg (Figure 4.2).

The study by van Wesenbeeck et al., (2022) was selected for this analysis because of its scale. The calibration of $C_D$ inherently bridges the assumptions made in the wave attenuation model and physical measurements. This means that the parameter depends on complex physics, such as skin friction, pressure differences, turbulence etc. (van Wesenbeeck et al., 2022), and some of these effects may not be replicated in scaled-down laboratory experiments. In this analysis, the only relevant parameter to the error analysis that is varied is $C_D$ – $N_V$ (0.16trees/$m^2$) and the vertical distribution of frontal area of the vegetation model (Figure 2.11) are held constant. It should, however, be noted that these two input parameters will also influence how errors vary with cross-shore distance, x, given the same hydrodynamic conditions. For example, if $C_{D,experiment}$>1, a denser forest and broader trees (i.e. larger dFA or diameter) would result in larger maximum error that occur closer to the shoreline (i.e. at smaller x).

## 5.3 $C_D$, velocity profile, and distribution of frontal area

The results of comparing the single layered model – which Wang et al., (2022) used in their calibration of the $C_D$ values – and the introduced two-layered model show that $C_D$ values are specific to the vegetation model that is applied in the wave attenuation model. This is illustrated by the variability in differences between predicted $k_t$ values produced by the calibrated single-layered vegetation model and the two-layered model, with water depth, when the same $C_D$ was applied (Chapter 4.1.1) (Figure 5.1). At a low water level of 0.2m, where the flow only goes through the root layer, the vertical distribution of submerged frontal areas of both models are the same. As such, with the same $C_D$ values, the two-layered model produced the same result as the single-layered model. With increasing water levels, the vertical distribution of frontal area becomes increasingly different between the two vegetation models. As such, the $C_D$ value calibrated on the single-layered model becomes less suitable for the two layered model. Additionally, the $k_t$ produced by the two-layered model is observed to increase monotonically in the positive direction relative to the single-layered model (Figure 4.1).

This means that at higher water levels, damping is underestimated, and the reported $C_D$ values – which are calibrated on the single-layered model – are smaller than what would be obtained should the parameter be calibrated with the two-layered model. This is due to the interaction between the hypothetical vertical velocity profile assumed in linear wave theory and the distribution of the model's frontal area over the water column. The Dalrymple formular (Eq. 2) can be expressed as given by

Equation 26 and 27 below. The term to the left of the integral in Equation 26, where the vegetation parameters are included, are constant for each point along the cross-shore direction and within the vertical layers. $|u|^3$ follows a logarithmic shape, with the minimum horizontal velocity starting at the bottom, and the highest at the top (Figure 5.1). As such, the frontal area of the vegetation model near the top of the water column has a greater "weight" compared to the lower portions. The root section of the two-layered model is significantly larger than its trunk. Therefore, for the same physical experiments (i.e. same physical vegetation model and hydrodynamic conditions), if a height-averaged $C_D$ value is calibrated for the vegetation model, the calibrated $C_D$ for a two-layered model of a R *sp.* root would be greater than a single layered model.

$$\varepsilon_{v,vertical} = \frac{\sum_{i=0}^{n} \rho C_{D,i} b_{v,i} N_i \Delta z_i}{2T} \int_0^T |u|^3 dt \qquad \text{(Eq. 26)}$$

$$\int_0^T |u|^3 dt = |\omega a \frac{\cosh k(d+z)}{\sinh kd}|^3 \int_0^T |\sin(\omega t - kx)|^3 dt \qquad \text{(Eq. 27)}$$

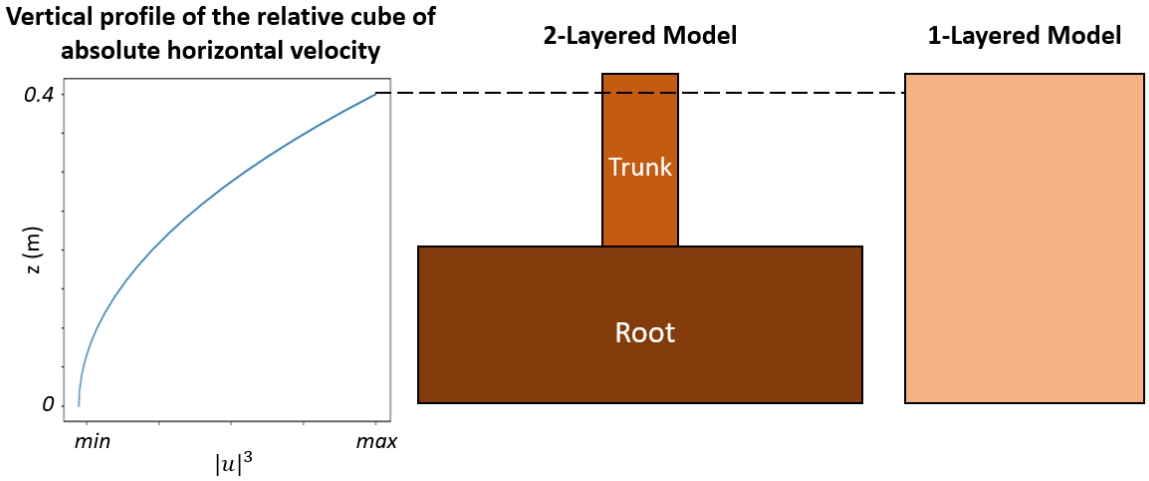


*Figure 5.1 Vertical profile of $|u|^3$ compared with a 2-layered and single layered model with the same total submerged frontal area*

The large differences in the Error variation with water level by the Root-Layered models observed in Chapter 4.1.2 are due to two reasons: 1) the interaction between the vertical velocity profile and the vertical distribution of frontal area of the root models, and 2) the difference in total submerged frontal areas for the low water level models ($h_0$=2m, 3m). First, when a low-resolution model is used to represent the root layer in low water conditions, the error in vertical distribution of frontal area is "magnified" compared to that in high water levels. This is because at low water levels, the relative gradient of $|u|^3$ at the root level is greater than that in high water levels (Figure 5.2 and Figure 5.3). Second, at $h_0$=2m, the total submerged area of Root-1L, Root-3L, and Root-5L at the start of the forest are respectively 1%, 0.6%, and 0.5% smaller than that of Root-HR. These errors in submerged frontal area increase with distance due to the slope of the forest (1/2000). The slope of the forest also results in such errors when $h_0$=3m; the water depth for x>1976m is lower than the height of the root layer.

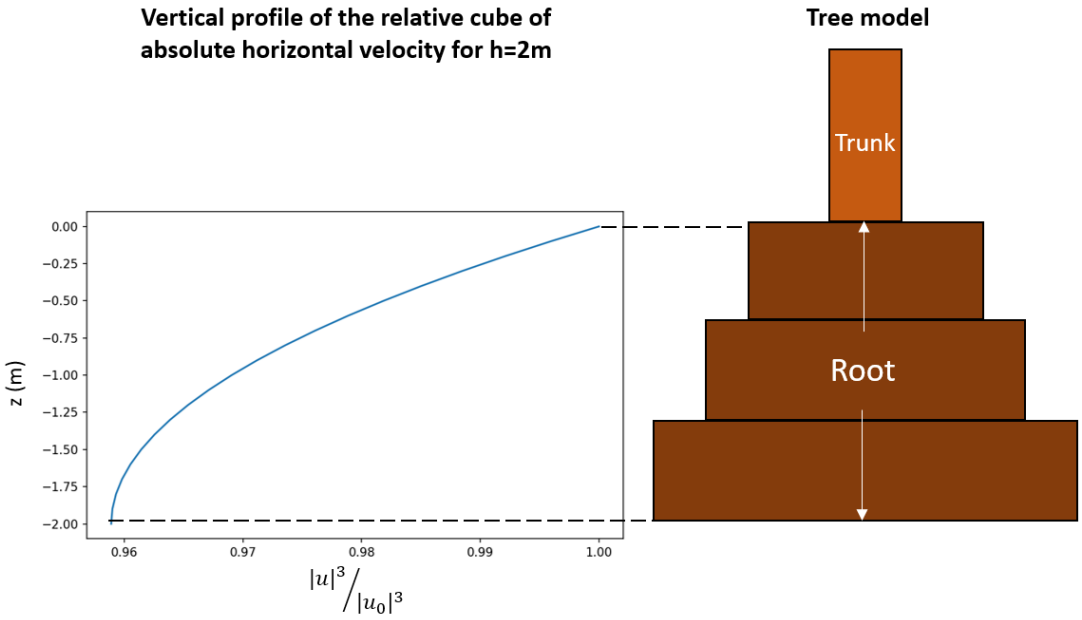


*Figure 5.2 Cube of the absolute velocity profile for h=2m compared to tree model*

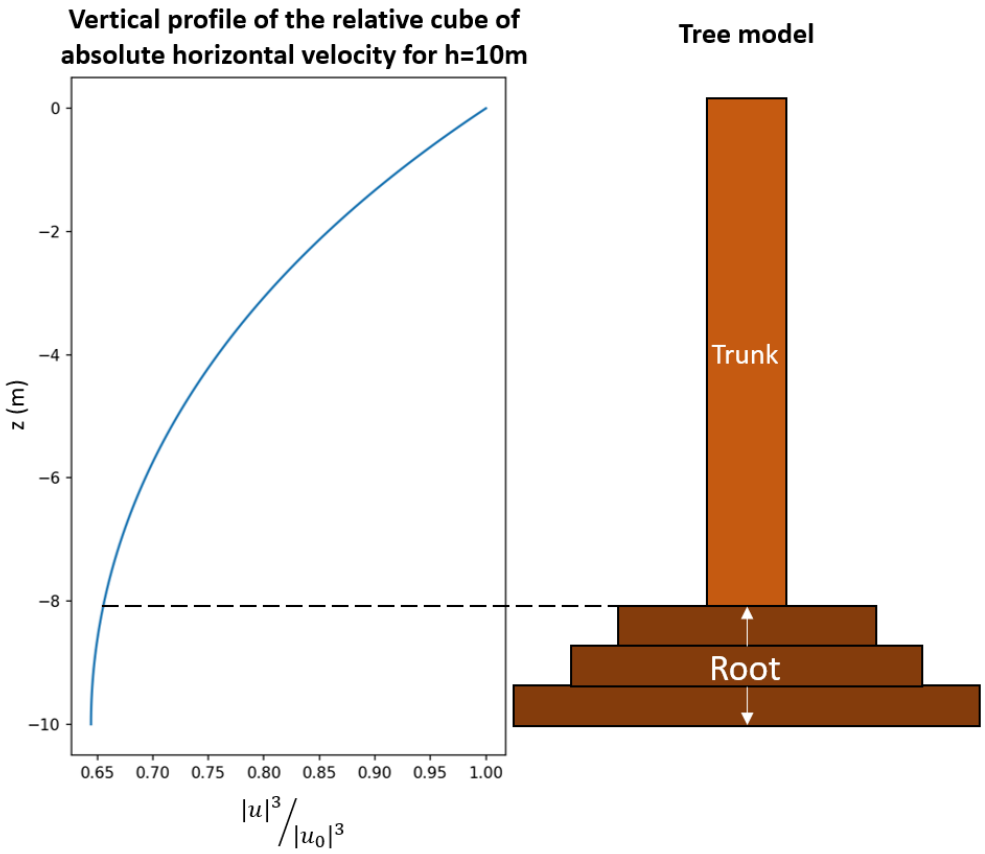


*Figure 5.3 Cube of the absolute velocity profile for h=10m compared to tree model*

## 5.4 Expectation vs the results of the developed tree models

An initial hypothesis prior to developing the canopy model is that models produced using the allometric method would overestimate the frontal area of an R *sp.* tree, while those created based on analysing the picture of an R *sp.* tree would underestimate the frontal area. The reason for this is because the allometric method does not account for the position of the branches around the tree, and it assumes that the branches as all arranged such that they result in maximum dissipation of the incoming waves. On the other hand, the image-processing method can only extract the 2D projection of the branches from the angle the image was taken, and hence, it neglects the fact that branches within the canopy may overlap in space. The expected outcomes of the canopy models, however, is not observed in the final models (Figure 3.13). There are two reasons that can possibly explain for this.

First, the allometric equation – which relates the DBH of the tree to the biomass of the branches in the canopy – that is used in this study, was developed based on the measurements taken in a closed canopy forest (0.08 trees/$m^2$). On the other hand, the R *sp.* tree sample for which its picture was analysed grew in an open mudflat with access to plenty of sunlight. The depth at which the canopy of a mangrove tree begins, and hence the total frontal area of the canopy, depends on the tree's access to light. As such, the frontal area of the canopies of trees found in different environment can be significantly different.

Second, the approach taken to scale the frontal area of the canopy to the DBH of the tree in the models developed from image analysis may not be representative of the relationship between the DBH and canopy area in real trees. This could lead to an overestimation of the frontal area especially in the taller tree models. The relationship between the projected area of the canopy and DBH may be explored further by analysing more images of R *sp.* from different environments. This, however, could be challenging when studying closed forests with tall trees as it is important to obtain an undistorted image where the main branches of the trees are visible.

Aside from the models of the canopy that has been developed in this study, it should also be noted that it could be valuable to study the trunk layer in greater detail too. R *sp.* have extreme plasticity in their morphology that is dependent on their physical environments and past experiences (Tomlinson, 1986). In the field, especially in a natural mangrove forest, it is not uncommon to spot trees with two main trunks (e.g. Figure 5.4). Given that the trunk layer contributes the most to wave attenuation, further studies on such occurrences may be beneficial to understanding of wave attenuation by this species of mangroves. A possible approach to do such studies would be counting the occurrences of such trees within mangrove forests. If these trees account for a significant portion of the forest, the relationship between the DBH (of each trunk), height of the trees, and area of the canopy should be compared with the single-trunk trees. The additional frontal areas contributed by the "extra" trunks (and canopy) can then be added to the model.

*Figure 5.4 R sp. tree from Chek Jawa Wetland Reserve with two main trunks.*

Finally, it should be noted that the root model by Ohira et al., (2013) and Maza et al., (2019) that is adapted for this study only considers the primary roots. Therefore, there the total frontal area of the root layer in this study is likely an underestimation.

# 6. Conclusion

**Is short wave attenuation sensitive to the root system at high water levels? Above what water levels are the effects of wave attenuation by the root system negligible?**

The sensitivity analyses of the root model show that the root layer does contribute quite significantly to wave attenuation even for water levels as high as 10m. Even as wave attenuation becomes less sensitive to the root layer with increasing water levels, the magnitude of the error and relative error in $k_t$ due to omitting the complex root layer can be as high as 0.14 and 0.62. The magnitude of the errors generally increases with the forest width, while relative error is larger for higher waves (i.e. larger $H_{s0}$).

**How sensitive is modelled short-wave attenuation to the complexity of the schematized root system?**

At low water levels, when the flow goes through the root layer, the resolution of the root model has relatively significant effects the results of the wave attenuation model. A maximum Error in $k_t$ of 0.037 is produced by the single cylinder model when $h_0$=2m at x=2900m. Comparatively, the errors of the three-layered (Root-3L) and five-layered (Root-5L) models were significantly smaller at Error=0.002, and Error=0.001 respectively at this location. For such water levels, the errors due to model resolution may be greater than the errors due to inaccuracies in the total frontal area of the complex roots, especially at larger cross-shore widths.

At high water levels, when $h_0$ is significantly higher than the height of the root layer, the accuracy of the total frontal area of the root layer is more important than the resolution of the root model. At $h_0$>6m, the errors due to the resolution of the root model is almost 0, while comparatively significant errors can produced due to errors in the total frontal area of the root layer.

**How much uncertainty does the choice of $C_D$ contribute to the results of wave attenuation?**

The errors in predicted $k_t$ when $C_D$ is approximated to 1 can be as high as 0.17 in short willow forests with moderate tree densities ($N_v$=0.16tree/m$^2$). This error decreases for forests with greater cross-shore widths. In an R *sp.* forest of similar density, the maximum error could be slightly higher assuming that the total submerged frontal area of a R *sp.* tree of the same height would be larger than that for the willow trees. The variation of error with cross-shore distances also differ for cases where the actual $C_D$<1 and $C_D$>1. When the true $C_D$ is more than one, the error is observed to approach zero for x>1500m. On the other hand, the magnitude of the error does not attenuate to zero when the true $C_D$ is less than one for forests widths as large as 2900m. Similar behavior in error can be expected in R *sp.* forests of similar densities (as the willow forest).

Through the analysis with Wang et al., (2022), it is found that the $C_D$ values calibrated on a specific vegetation model is not transferable to another model with a different vertical resolution, even if they are representing the same vegetation. The magnitude of error due to applying a mismatched pair of $C_D$ and vegetation model for full-scale forest has not been studied, but preliminary analysis show that such error is expected to increase with increasing water levels (relative to the heights of the vegetation model layers).

**How much do canopies contribute to wave attenuation during storm surges?**

The amount of contribution by canopies to wave attenuation depends much on the relative height of the storm surge to that of the tree. It is found that canopies of R *sp.* can contribute more to wave attenuation than the aerial roots for certain conditions. For the range of tree heights and water levels tested in this study, it was found that the canopy can contribute as much as 23% to wave attenuation

($h_{tree}$=10.6m, $h_0$=10m). This value can change significantly depending on the frontal area and distribution of the frontal area of the canopy in the vegetation model. The maximum contribution to wave attenuation by canopies is generally expected to increase with decreasing tree height and start height of the canopy, so long as the trees are emergent from the water i.e. $h_{tree}>h_0$.

# 7. Recommendations

This section consists of three parts. The first part addresses the problem of the transferability of $C_D$, the second looks at future data collection and modelling of the R *sp.* root system, and the last focuses on the need to produce more information surrounding the canopy.

## Choice of $C_D$ values

Based on the analysis of $C_D$ with the studies by van Wesenbeeck et al., (2022) and Wang et al., (2022), it is recommended for the choice of $C_D$ values to be informed by the aim of the study.

First, based on the analysis with Wang et al., (2022), it is found that the $C_D$ values calibrated for a specific vegetation model is not transferable to another model that represents the same plant. Furthermore, the problem of the transferability of $C_D$ values across experiments is also a known problem within this field; empirical formulas of $C_D$ that are derived in one experiment does not agree with the results in another. A possible step to make $C_D$ more transferable could be for future studies to consider the idea of vertically distributed $C_D$. This suggestion is made based on the proposed empirical relationship between $C_D$ and the KC and Reynold's number (Burger, 2005; Mendez & Losada, 2004; van Wesenbeeck et al., 2022). The KC number varies with velocity and the diameter of the vegetation, and hence, along the vertical of the water column. Today, it is still common for studies to calibrate one $C_D$ per experiment regardless of the number of layers present in the physical and numerical model. This, however, would mean that the calibrated $C_D$ would be only applicable for the parameters it was calculated for. The calibration of multiple $C_D$ per experiment and then deriving empirical formulas based on these results would, hopefully, allow greater generalisation of the parameter. $C_D$ can be understood as the bridge that connects the complex physical conditions in the real world to the simplified analytical model proposed by Dalrymple et al., (1984). For example, should the vegetation model be well represented in the analytical model, the calibrated $C_D$ for the different layers would describe the discrepancies between the theoretical velocity profile based on linear wave theory, and the actual one. In this case of R *sp.*, assuming that the flow reaches part of the canopy, there should be three calibrated $C_D$ values – one for the root layer, one for the trunk, and one for the submerged portion of the canopy.

Second, based on chapter 4.1.2 and 5.2, if the objective of a particular study is to estimate the amount of wave attenuation at the end of a thick and dense forest such that the surge does not flow through majority of the canopy, then $C_D$ can be approximated to 1. Assuming that the R *sp.* trees in the forest of interest have similar or greater submerged frontal area compared to the willows in van Wesenbeeck et al., (2022), and that the R *sp.* forest has similar or greater tree density than the willow forest where $N_v$=0.16 trees/m$^2$, then the predicted $k_t$ values when $C_D$=1 would decrease with x for x>350m (Figure 4.2). If Error<0.1 is acceptable for the study, then it should be alright to approximate $C_D$ = 1 for x>350m.

Finally, if the forest of interest is relatively sparse and thin (i.e. small xVeg), and a higher level of accuracy in $k_t$ prediction is required, then creating a vegetation model and calibrating the $C_D$ with measurements would be the most ideal solution. However, field measurements and large scale flume experiments (as in van Wesenbeeck et al., (2022)) are expensive, time consuming, and not always a viable option. In such cases – acknowledging the other uncertainties due to various other factors such as the scale and hydrodynamic conditions of the experiments/field measurements – it is recommended to consider applying a tree model for which the $C_D$ was calibrated on, and the empirical formular of $C_D$ derived from the set of experiments. For example, if the empirical formular for $C_D$ proposed by Wang et al., (2022), then a single-cylinder model should be used to represent the vegetation in the wave attenuation model – since they calibrated the $C_D$ values and derived the empirical formular assuming a single-cylinder model.

### Modelling R *sp.* root level for high water levels

The results of the sensitivity analysis of the root layer shows that even at extremely high water levels, the complex roots of R *sp.* still contribute significantly to wave attenuation. This means that the vegetation model used to study wave height reduction by R *sp.* at high water levels have to account for these roots. These root models, however, do not need to be highly detailed at such high water levels. Chapter 4.2.2 has shown that the results of the wave attenuation model are slightly sensitive to the errors in total root frontal area, while it is not sensitive to the vertical resolution of the root model – the errors produced by a three- and five-layered model is almost the same and they are negligible. This means that if there is a need to obtain high accuracy wave attenuation results, more effort should be used to accurately measure the frontal area of the R *sp.* roots than to model the vertical distribution of the frontal area in detail.

### Canopy modelling

The contribution analysis of the different tree layers (Chapter 4.3.2) has shown that at high water levels, the canopy can contribute up to 23% of wave attenuation. It also shows that, given certain conditions, the canopy can contribute more to wave attenuation than the root layer (Figure 4.20). This value can increase depending on the height of the tree and the relative height of the water level to the tree. As of now, there is little information that can be directly used for modelling the canopy of R *sp.* (and other species of mangroves). Prior to this study, known models of mangrove canopies are generally based on assumptions – such as having a maximum frontal area per unit volume and using a factor to scale this maximum value to different trees – which have not been validated with real-world measurements. Given that the canopy can contribute to wave attenuation as much as, if not more than the root layer, there should be more effort invested to characterise this layer.

The vertical distribution of frontal area of the canopy can significantly influence the results of contribution and wave attenuation (refer to Chapter 4.3.2). The characterization of mangrove canopies is important to develop accurate models of the canopy and this process can be challenging, especially in the case of R *sp.*. There are many reasons for this. One of which is the inaccessibility of this layer. The canopy of R sp. can be as high as 30m, as such, physically measuring the branches can be difficult in the field. In addition, given how tall these trees can be, obtaining an undistorted image of the entire tree requires technical expertise. Next, the canopies of mangroves (and R *sp.*) can be extremely dense. This makes it almost impossible to extract any information of the branches from pictures alone. Finally, the crown shape of mangroves – specifically R *sp.* – can come in all sorts of forms. This is not just limited to the range at which the canopy starts (discussed in Chapter 2.1.2), but also the shape of the crown. The variety of forms and shapes of the canopy makes it tricky to characterize this layer. Given the challenges in characterizing the canopy of mangroves, which morphology can be influenced by many environmental factors, it would be beneficial to have more collaborations with mangrove ecologists to work on developing canopy models. There is much knowledge in the field of ecology that would be extremely helpful in this process.

# Bibliography


Abdul-Hamid, H., Mohamad-Ismail, F.-N., Mohamed, J., Samdin, Z., Abiri, R., Tuan-Ibrahim, T.-M., Mohammad, L.-S., Jalil, A.-M., & Naji, H.-R. (2022). Allometric Equation for Aboveground Biomass Estimation of Mixed Mature Mangrove Forest. *Forests*, *13*(2), 325. https://doi.org/10.3390/f13020325

Aken, I. A., Marjolaine, O.-G., Emmanuel, O. A., Nwutih, A. G., & Jean-Bernard, M. (2021). Local Allometric Equations for Estimating Above-Ground Biomass (AGB) of Mangroves (Rhizophora spp. And Avicennia germinans) from the Komo, Mondah and Rio Mouni Estuaries in Gabon. *European Scientific Journal ESJ*, *17*(34). https://doi.org/10.19044/esj.2021.v17n34p172

Alongi, D. M. (2008). Mangrove forests: Resilience, protection from tsunamis, and responses to global climate change. *Estuarine, Coastal and Shelf Science*, *76*(1), 1–13. https://doi.org/10.1016/j.ecss.2007.08.024

Augustin, L. N., Irish, J. L., & Lynett, P. (2009). Laboratory and numerical studies of wave damping by emergent and near-emergent wetland vegetation. *Coastal Engineering*, *56*(3), 332–340. https://doi.org/10.1016/j.coastaleng.2008.09.004

Bellinga, W. J. (2022). *Non-stationary multivariate extreme events in mangrove environments* [TU Delft]. https://repository.tudelft.nl/islandora/object/uuid%3A169d8d39-c499-467c-87c4-0fadb170a568

Borsje, B. W., van Wesenbeeck, B. K., Dekker, F., Paalvast, P., Bouma, T. J., van Katwijk, M. M., & de Vries, M. B. (2011). How ecological engineering can serve in coastal protection. *Ecological Engineering*, *37*(2), 113–122. https://doi.org/10.1016/j.ecoleng.2010.11.027

Bosboom, J., & Stive, M. (2021). *Coastal Dynamics*. https://doi.org/10.5074/T.2021.001

Brinkman, R. M. (2006). *Wave attenuation in mangrove forests: An investigation through field and theoretical studies*.

Burger, B. (2005). *Wave Attenuation in Mangrove Forests* [TU Delft]. https://repository.tudelft.nl/islandora/object/uuid:0e4c6450-fe5d-4693-9ca9-58da343448b7/datastream/OBJ/download

Cahoon, D. R., Hensel, P., Rybczyk, J., McKee, K. L., Proffitt, C. E., & Perez, B. C. (2003). Mass Tree Mortality Leads to Mangrove Peat Collapse at Bay Islands, Honduras after Hurricane Mitch. *Journal of Ecology*, *91*(6), 1093–1105.

Cao, H., Feng, W., Hu, Z., Suzuki, T., & Stive, M. J. F. (2015). Numerical modeling of vegetation-induced dissipation using an extended mild-slope equation. *Ocean Engineering*, *110*, 258–269. https://doi.org/10.1016/j.oceaneng.2015.09.057

Clough, B. F., Ong, J.-E., & Gong, W. (1997). Estimating leaf area index and photosynthetic production in canopies of the mangrove Rhizophora apiculata. *Marine Ecology Progress Series*, *159*, 285–292. https://doi.org/10.3354/meps159285

Clough, B. F., & Scott, K. (1989). Allometric relationships for estimating above-ground biomass in six mangrove species. *Forest Ecology and Management*, *27*(2), 117–127. https://doi.org/10.1016/0378-1127(89)90034-0

Cole, T. G., Ewel, K. C., & Devoe, N. N. (1999). Structure of mangrove trees and forests in Micronesia. *Forest Ecology and Management*, *117*(1–3), 95–109. https://doi.org/10.1016/S0378-1127(98)00474-5

Daba, D. E., & Soromessa, T. (2019). The accuracy of species-specific allometric equations for estimating aboveground biomass in tropical moist montane forests: Case study of Albizia

grandibracteata and Trichilia dregeana. *Carbon Balance and Management*, *14*(1), 18. https://doi.org/10.1186/s13021-019-0134-8

Dalrymple, R. A., Kirby, J. T., & Hwang, P. A. (1984). Wave Diffraction Due to Areas of Energy Dissipation. *Journal of Waterway, Port, Coastal, and Ocean Engineering*, *110*(1), 67–79. https://doi.org/10.1061/(ASCE)0733-950X(1984)110:1(67)

Dasgupta, S., Islam, Md. S., Huq, M., Khan, Z. H., & Hasib, Md. R. (2017). *Mangroves as Protection from Storm Surges in Bangladesh*. The World Bank. https://doi.org/10.1596/1813-9450-8251

Doyle, T. W., Krauss, K. W., & Wells, C. J. (2009). Landscape analysis and pattern of hurricane impact and circulation on mangrove forests of the Everglades. *Wetlands*, *29*(1), 44–53. https://doi.org/10.1672/07-233.1

Furukawa, K., & Wolanski, E. (1996). Sedimentation in Mangrove Forests. *Mangroves and Salt Marshes*, *1*(1), 3–10. https://doi.org/10.1023/A:1025973426404

Gevana, D. T., & Im, S. (2016). *Allometric models for Rhizophora stylosa griff. In dense monoculture plantation in the Philippines*. 16.

Gijsman, R., Horstman, E. M., van der Wal, D., Friess, D. A., Swales, A., & Wijnberg, K. M. (2021). Nature-Based Engineering: A Review on Reducing Coastal Flood Risk With Mangroves. *Frontiers in Marine Science*, *8*, 702412. https://doi.org/10.3389/fmars.2021.702412

Hasselmann, K., Collins, J. I. ,,. (1968). *Spectral dissipation of finite-depth gravity waves due to turbulent bottom friction*. /z-wcorg/.

He, F., Chen, J., & Jiang, C. (2019). Surface wave attenuation by vegetation with the stem, root and canopy. *Coastal Engineering*, *152*, 103509. https://doi.org/10.1016/j.coastaleng.2019.103509

Horstman, E. M., Dohmen-Janssen, C. M., Narra, P. M. F., van den Berg, N. J. F., Siemerink, M., & Hulscher, S. J. M. H. (2014). Wave attenuation in mangroves: A quantitative approach to field observations. *Coastal Engineering*, *94*, 47–62. https://doi.org/10.1016/j.coastaleng.2014.08.005

Huang, Z., Yao, Y., Sim, S. Y., & Yao, Y. (2011). Interaction of solitary waves with emergent, rigid vegetation. *Ocean Engineering*, *38*(10), 1080–1088. https://doi.org/10.1016/j.oceaneng.2011.03.003

Iimura, K., & Tanaka, N. (2012). Numerical simulation estimating effects of tree density distribution in coastal forest on tsunami mitigation. *Ocean Engineering*, *54*, 223–232. https://doi.org/10.1016/j.oceaneng.2012.07.025

Jacobsen, N. G., Bakker, W., Uijttewaal, W. S. J., & Uittenbogaard, R. (2019). Experimental investigation of the wave-induced motion of and force distribution along a flexible stem. *Journal of Fluid Mechanics*, *880*, 1036–1069. https://doi.org/10.1017/jfm.2019.739

Janssen, M. (2016). *Flood hazard reduction by mangroves*. TU Delft.

Kalloe, S. A., Hofland, B., Antolínez, J. A. A., & van Wesenbeeck, B. K. (2022). Quantifying Frontal-Surface Area of Woody Vegetation: A Crucial Parameter for Wave Attenuation. *Frontiers in Marine Science*, *0*. https://doi.org/10.3389/fmars.2022.820846

Karambas, T., Koftis, T., & Prinos, P. (2016). Modeling of Nonlinear Wave Attenuation due to Vegetation. *Journal of Coastal Research*, *32*(1), 142–152. http://dx.doi.org/10.2112/JCOASTRES-D-14-00044.1

Kelty, K., Tomiczek, T., Cox, D. T., Lomonaco, P., & Mitchell, W. (2022). Prototype-Scale Physical Model of Wave Attenuation Through a Mangrove Forest of Moderate Cross-Shore Thickness:

LiDAR-Based Characterization and Reynolds Scaling for Engineering With Nature. *Frontiers in Marine Science*, *8*. https://www.frontiersin.org/article/10.3389/fmars.2021.780946

Keulegan, G. H., & Carpenter, L. H. (1958). Forces on cylinders and plates in an oscillating fluid. *Journal of Research of the National Bureau of Standards*, *60*(5), 423. https://doi.org/10.6028/jres.060.043

Kirezci, E., Young, I. R., Ranasinghe, R., Muis, S., Nicholls, R. J., Lincke, D., & Hinkel, J. (2020). Projections of global-scale extreme sea levels and resulting episodic coastal flooding over the 21st Century. *Scientific Reports*, *10*(1), 11629. https://doi.org/10.1038/s41598-020-67736-6

Kobayashi, N., Raichle, A. W., & Asano, T. (1993). Wave Attenuation by Vegetation. *Journal of Waterway, Port, Coastal, and Ocean Engineering*, *119*(1), 30–48. https://doi.org/10.1061/(ASCE)0733-950X(1993)119:1(30)

Krauss, K. W., Doyle, T. W., Doyle, T. J., Swarzenski, C. M., From, A. S., Day, R. H., & Conner, W. H. (2009). Water level observations in mangrove swamps during two hurricanes in Florida. *Wetlands*, *29*(1), 142–149. https://doi.org/10.1672/07-232.1

Krauss, K. W., Lovelock, C. E., McKee, K. L., López-Hoffman, L., Ewe, S. M. L., & Sousa, W. P. (2008). Environmental drivers in mangrove establishment and early development: A review. *Aquatic Botany*, *89*(2), 105–127. https://doi.org/10.1016/j.aquabot.2007.12.014

Krauss, K. W., & Osland, M. J. (2019). Tropical cyclones and the organization of mangrove forests: A review. *Annals of Botany*, mcz161. https://doi.org/10.1093/aob/mcz161

Kulp, S. A., & Strauss, B. H. (2019). New elevation data triple estimates of global vulnerability to sea-level rise and coastal flooding. *Nature Communications*, *10*(1), 4844. https://doi.org/10.1038/s41467-019-12808-z

Li, C. W., & Yan, K. (2007). *Numerical Investigation of Wave–Current–Vegetation Interaction*. https://ascelibrary-org.recursos.biblioteca.upc.edu/doi/full/10.1061/%28ASCE%290733-9429%282007%29133%3A7%28794%29

Li, S., Meng, X., Ge, Z., & Zhang, L. (2015). Evaluation of the threat from sea-level rise to the mangrove ecosystems in Tieshangang Bay, southern China. *Ocean & Coastal Management*, *109*, 1–8. https://doi.org/10.1016/j.ocecoaman.2015.02.006

Liu, P. L.-F., Chang, C.-W., Mei, C. C., Lomonaco, P., Martin, F. L., & Maza, M. (2015). Periodic water waves through an aquatic forest. *Coastal Engineering*, *96*, 100–117. https://doi.org/10.1016/j.coastaleng.2014.11.002

Losada, I. J., Maza, M., & Lara, J. L. (2016). A new formulation for vegetation-induced damping under combined waves and currents. *Coastal Engineering*, *107*, 1–13. https://doi.org/10.1016/j.coastaleng.2015.09.011

Lowe, J. A., Gregory, J. M., & Flather, R. A. (2001). Changes in the occurrence of storm surges around the United Kingdom under a future climate scenario using a dynamic storm surge model driven by the Hadley Centre climate models. *Climate Dynamics*, *18*(3–4), 179–188. https://doi.org/10.1007/s003820100163

Ma, G., Kirby, J. T., Su, S.-F., Figlus, J., & Shi, F. (2013). Numerical study of turbulence and wave damping induced by vegetation canopies. *Coastal Engineering*, *80*, 68–78. https://doi.org/10.1016/j.coastaleng.2013.05.007

Marois, D. E., & Mitsch, W. J. (2015). Coastal protection from tsunamis and cyclones provided by mangrove wetlands – a review. *International Journal of Biodiversity Science, Ecosystem Services & Management*, *11*(1), 71–83. https://doi.org/10.1080/21513732.2014.997292

Maza, M., Lara, J. L., & Losada, I. J. (2013). A coupled model of submerged vegetation under oscillatory flow using Navier–Stokes equations. *Coastal Engineering*, *80*, 16–34. https://doi.org/10.1016/j.coastaleng.2013.04.009

Maza, M., Lara, J. L., & Losada, I. J. (2016). Solitary wave attenuation by vegetation patches. *Advances in Water Resources*, *98*, 159–172. https://doi.org/10.1016/j.advwatres.2016.10.021

Maza, M., Lara, J. L., & Losada, I. J. (2019). Experimental analysis of wave attenuation and drag forces in a realistic fringe Rhizophora mangrove forest. *Advances in Water Resources*, *131*, 103376. https://doi.org/10.1016/j.advwatres.2019.07.006

Mazda, Y., Magi, M., Ikeda, Y., Kurokawa, T., & Asano, T. (2006). Wave reduction in a mangrove forest dominated by Sonneratia sp. *Wetlands Ecology and Management*, *14*(4), 365–378. https://doi.org/10.1007/s11273-005-5388-0

Mazda, Y., Wolanski, E., King, B., Sase, A., Ohtsuka, D., & Magi, M. (1997). *Drag force due to vegetation in mangrove swamps*. 7.

Mclvor, A., Möller, I., Spencer, T., & Spalding, M. (2012). *Reduction of Wind and Swell Waves by Mangroves*. https://www.conservationgateway.org/ConservationPractices/Marine/crr/library/Documents/wind-and-swell-wave-reduction-by-mangroves.pdf

Mclvor, A., Spencer, T., Möller, I., & Spalding, M. (2012). *Storm surge reduction by mangroves*. https://repository.tudelft.nl/islandora/object/uuid%3A79fe752e-ce52-4bf6-a45c-2847bead07ab

Mei, C. C., Chan, I.-C., Liu, P. L.-F., Huang, Z., & Zhang, W. (2011). Long waves through emergent coastal vegetation. *Journal of Fluid Mechanics*, *687*, 461–491. https://doi.org/10.1017/jfm.2011.373

Mendez, F. J., & Losada, I. J. (2004). An empirical model to estimate the propagation of random breaking and nonbreaking waves over vegetation fields. *Coastal Engineering*, *51*(2), 103–118. https://doi.org/10.1016/j.coastaleng.2003.11.003

Mogensen, L. A., Rogers, K., & nueva, E. a sitio externo E. enlace se abrirá en una ventana. (2018). Validation and Comparison of a Model of the Effect of Sea-Level Rise on Coastal Wetlands. *Scientific Reports (Nature Publisher Group)*, *8*, 1–14. http://dx.doi.org/10.1038/s41598-018-19695-2

Möller, I., Spencer, T., French, J. R., Leggett, D. J., & Dixon, M. (1999). Wave Transformation Over Salt Marshes: A Field and Numerical Modelling Study from North Norfolk, England. *Estuarine, Coastal and Shelf Science*, *49*(3), 411–426. https://doi.org/10.1006/ecss.1999.0509

Montgomery, J. M., Bryan, K., Horstman, E., & Mullarney, J. (2018). Attenuation of Tides and Surges by Mangroves: Contrasting Case Studies from New Zealand. *Water*, *10*(9), 1119. https://doi.org/10.3390/w10091119

Montgomery, J. M., Bryan, K. R., Mullarney, J. C., & Horstman, E. M. (2019). Attenuation of Storm Surges by Coastal Mangroves. *Geophysical Research Letters*, *46*(5), 2680–2689. https://doi.org/10.1029/2018GL081636

Morison, J. R., Johnson, J. W., & Schaaf, S. A. (1950). The Force Exerted by Surface Waves on Piles. *Journal of Petroleum Technology*, *2*(05), 149–154. https://doi.org/10.2118/950149-G

Narayan, S. (2009). *The Effectiveness of Mangroves in Attenuating Cyclone- induced Waves*.

Neumann, B., Vafeidis, A. T., Zimmermann, J., & Nicholls, R. J. (2015). Future Coastal Population Growth and Exposure to Sea-Level Rise and Coastal Flooding—A Global Assessment. *PLOS ONE*, *10*(3), e0118571. https://doi.org/10.1371/journal.pone.0118571

Ng, P. K. L., & Sivasothi, N. (2001). *Guide to the Mangroves of Singapore*. http://mangrove.nus.edu.sg/guidebooks/text/1015a.htm

Ohira, W., Honda, K., Nagai, M., & Ratanasuwan, A. (2013). Mangrove stilt root morphology modeling for estimating hydraulic drag in tsunami inundation simulation. *Trees*, *27*(1), 141–148. https://doi.org/10.1007/s00468-012-0782-8

Ong, J.-E., Gong, W. K., & Clough, B. F. (1995). Structure and Productivity of a 20-Year-Old Stand of Rhizophora apiculata Bl. Mangrove Forest. *Journal of Biogeography*, *22*(2/3), 417. https://doi.org/10.2307/2845938

Ong, J.-E., Gong, W. K., & Wong, C. H. (2004). Allometry and partitioning of the mangrove, Rhizophora apiculata. *Forest Ecology and Management*, *188*(1–3), 395–408. https://doi.org/10.1016/j.foreco.2003.08.002

Ozeren, Y., Wren, D. G., & Wu, W. (2014). Experimental Investigation of Wave Attenuation through Model and Live Vegetation. *Journal of Waterway, Port, Coastal, and Ocean Engineering*, *140*(5), 04014019. https://doi.org/10.1061/(ASCE)WW.1943-5460.0000251

Paling, E. I., Kobryn, H. T., & Humphreys, G. (2008). Assessing the extent of mangrove change caused by Cyclone Vance in the eastern Exmouth Gulf, northwestern Australia. *Estuarine, Coastal and Shelf Science*, *77*(4), 603–613. https://doi.org/10.1016/j.ecss.2007.10.019

Piou, C., Feller, I. C., Berger, U., & Chi, F. (2006). Zonation Patterns of Belizean Offshore Mangrove Forests 41 Years After a Catastrophic Hurricane1. *Biotropica*, *38*(3), 365–374. https://doi.org/10.1111/j.1744-7429.2006.00156.x

Quang Bao, T. (2011). Effect of mangrove forest structures on wave attenuation in coastal Vietnam. *Oceanologia*, *53*(3), 807–818. https://doi.org/10.5697/oc.53-3.807

Quartel, S., Kroon, A., Augustinus, P. G. E. F., Van Santen, P., & Tri, N. H. (2007). Wave attenuation in coastal mangroves in the Red River Delta, Vietnam. *Journal of Asian Earth Sciences*, *29*(4), 576–584. https://doi.org/10.1016/j.jseaes.2006.05.008

Rovai, A. S., Twilley, R. R., Castañeda-Moya, E., Midway, S. R., Friess, D. A., Trettin, C. C., Bukoski, J. J., Stovall, A. E. L., Pagliosa, P. R., Fonseca, A. L., Mackenzie, R. A., Aslan, A., Sasmito, S. D., Sillanpää, M., Cole, T. G., Purbopuspito, J., Warren, M. W., Murdiyarso, D., Mofu, W., … Riul, P. (2021). Macroecological patterns of forest structure and allometric scaling in mangrove forests. *Global Ecology and Biogeography*, *30*(5), 1000–1013. https://doi.org/10.1111/geb.13268

S. V., S., Vethamony, P., Bhaskaran, P. K., Pednekar, P., Jishad, M., & James, R. A. (2019). Attenuation of Wave Energy Due to Mangrove Vegetation off Mumbai, India. *Energies*, *12*(22), 4286. https://doi.org/10.3390/en12224286

Simard, M., Fatoyinbo, L., Smetanka, C., Rivera-Monroy, V. H., Castañeda-Moya, E., Thomas, N., & Van der Stocken, T. (2019). Mangrove canopy height globally related to precipitation, temperature and cyclone frequency. *Nature Geoscience*, *12*(1), 40–45. https://doi.org/10.1038/s41561-018-0279-1

Srikanth, S., Lum, S. K. Y., & Chen, Z. (2016). Mangrove root: Adaptations and ecological importance. *Trees*, *30*(2), 451–465. https://doi.org/10.1007/s00468-015-1233-0

Steinke, T. D., & Ward, C. J. (1989). Some effects of the cyclones Domoina and Imboa on mangrove communities in the St Lucia Estuary. *South African Journal of Botany*, *55*(3), 340–348. https://doi.org/10.1016/S0254-6299(16)31186-3

Suzuki, T., Hu, Z., Kumada, K., Phan, L. K., & Zijlema, M. (2019). Non-hydrostatic modeling of drag, inertia and porous effects in wave propagation over dense vegetation fields. *Coastal Engineering*, *149*, 49–64. https://doi.org/10.1016/j.coastaleng.2019.03.011

Suzuki, T., Zijlema, M., Burger, B., Meijer, M. C., & Narayan, S. (2012). Wave dissipation by vegetation with layer schematization in SWAN. *Coastal Engineering*, *59*(1), 64–71. https://doi.org/10.1016/j.coastaleng.2011.07.006

Swales, A., Bentley Sr, S. J., & Lovelock, C. E. (2015). Mangrove-forest evolution in a sediment-rich estuarine system: Opportunists or agents of geomorphic change? *Earth Surface Processes and Landforms*, *40*(12), 1672–1687. https://doi.org/10.1002/esp.3759

Tanaka, N., Sasaki, Y., Mowjood, M. I. M., Jinadasa, K. B. S. N., & Homchuen, S. (2007). Coastal vegetation structures and their functions in tsunami protection: Experience of the recent Indian Ocean tsunami. *Landscape and Ecological Engineering*, *3*(1), 33–45. https://doi.org/10.1007/s11355-006-0013-9

Tang, J., Shen, S., & Wang, H. (2015). Numerical model for coastal wave propagation through mild slope zone in the presence of rigid vegetation. *Coastal Engineering*, *97*, 53–59. https://doi.org/10.1016/j.coastaleng.2014.12.006

The Ocean Portal Team. (2018). *Mangroves | Smithsonian Ocean*. https://ocean.si.edu/ocean-life/plants-algae/mangroves

Tobias, A., Malabrigo, Umali, A. G. A., Galang, M. A., Rolly C. Urriza, Replan, E. L., & Dida, J. J. V. (2017). *Mangrove Forest Inventory and Estimation of Carbon Storage and Sedimentation in Pagbilao*. https://doi.org/10.13140/RG.2.2.15851.03364

Tomlinson, P. B. (1986). *The botany of mangroves / P.B. Tomlinson.* Cambridge University Press.

van Wesenbeeck, B. K., Wolters, G., Antolínez, J. A. A., Kalloe, S. A., Hofland, B., de Boer, W. P., Çete, C., & Bouma, T. J. (2022). Wave attenuation through forests under extreme conditions. *Scientific Reports*, *12*(1), 1884. https://doi.org/10.1038/s41598-022-05753-3

van Zelst, V. T. M. (2018). *Global flood hazard reduction by foreshore vegetation*.

van Zelst, V. T. M., Dijkstra, J. T., van Wesenbeeck, B. K., Eilander, D., Morris, E. P., Winsemius, H. C., Ward, P. J., & de Vries, M. B. (2021). Cutting the costs of coastal protection by integrating vegetation in flood defences. *Nature Communications*, *12*(1), 6533. https://doi.org/10.1038/s41467-021-26887-4

Villamayor, B. M. R., Rollon, R. N., Samson, M. S., Albano, G. M. G., & Primavera, J. H. (2016). Impact of Haiyan on Philippine mangroves: Implications to the fate of the widespread monospecific Rhizophora plantations against strong typhoons. *Ocean & Coastal Management*, *132*, 1–14. https://doi.org/10.1016/j.ocecoaman.2016.07.011

Vogt, J., Skóra, A., Feller, I. C., Piou, C., Coldren, G., & Berger, U. (2012). Investigating the role of impoundment and forest structure on the resistance and resilience of mangrove forests to hurricanes. *Aquatic Botany*, *97*(1), 24–29. https://doi.org/10.1016/j.aquabot.2011.10.006

Vo-Luong, P., & Massel, S. (2008). Energy dissipation in non-uniform mangrove forests of arbitrary depth. *Journal of Marine Systems*, *74*(1–2), 603–622. https://doi.org/10.1016/j.jmarsys.2008.05.004

Vuik, V., Jonkman, S. N., Borsje, B. W., & Suzuki, T. (2016). Nature-based flood protection: The efficiency of vegetated foreshores for reducing wave loads on coastal dikes. *Coastal Engineering*, *116*, 42–56. https://doi.org/10.1016/j.coastaleng.2016.06.001

Wang, Y., Yin, Z., & Liu, Y. (2022). Experimental investigation of wave attenuation and bulk drag coefficient in mangrove forest with complex root morphology. *Applied Ocean Research*, *118*, 102974. https://doi.org/10.1016/j.apor.2021.102974

Wells, N. (1997). The Atmosphere and Ocean: A physical introduction. 2nd Edition. *Undefined*. https://www.semanticscholar.org/paper/The-Atmosphere-and-Ocean%3A-a-physical-introduction.-Wells/8a206f7b3fb359c04f45d5c0fd07ff44bfb63a63

Xu, H., Zhang, K., Shen, J., & Li, Y. (2010). Storm surge simulation along the U.S. East and Gulf Coasts using a multi-scale numerical model approach. *Ocean Dynamics*, *60*(6), 1597–1619. https://doi.org/10.1007/s10236-010-0321-3

Yang, Z., Tang, J., & Shen, Y. (2018). Numerical study for vegetation effects on coastal wave propagation by using nonlinear Boussinesq model. *Applied Ocean Research*, *70*, 32–40. https://doi.org/10.1016/j.apor.2017.09.001

Zhang, K., Liu, H., Li, Y., Xu, H., Shen, J., Rhome, J., & Smith, T. J. (2012). The role of mangroves in attenuating storm surges. *Estuarine, Coastal and Shelf Science*, *102–103*, 11–23. https://doi.org/10.1016/j.ecss.2012.02.021

Zhang, X. (2014). *An investigation on the root system of mangroves and its influence on crrent flow*. National University of Singapore.

Zhang, Y., Yang, Y., Yang, K., Tan, X., Sun, X., Leng, B., Zhou, C., & Zhu, B. (2020). Non-linear wave attenuation quantification model improves the estimation of wave attenuation efficiency of mangroves. *Estuarine, Coastal and Shelf Science*, *245*, 106927. https://doi.org/10.1016/j.ecss.2020.106927

# Appendix

## A1.1 Validation with scaled down flume experiment with R. *sp* root models

Validation for the regular-wave model is performed with the results from Wang et al., (2022), where the complex root models of R. *sp* were studied. The performance of the model is evaluated by comparing $k_t$ values for nine points – WG2 to WG10 – along the flume (Fig. 2.9).

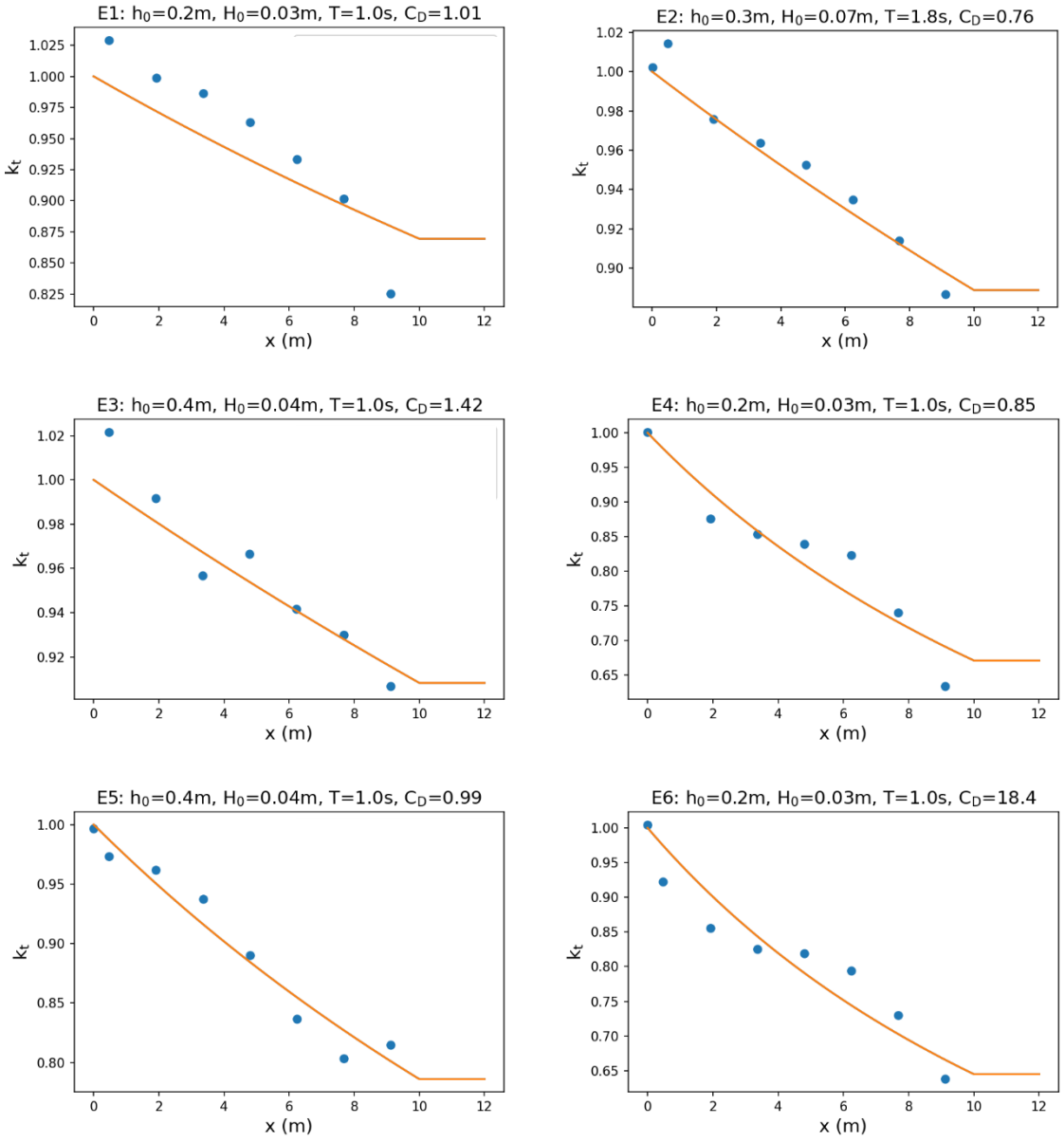

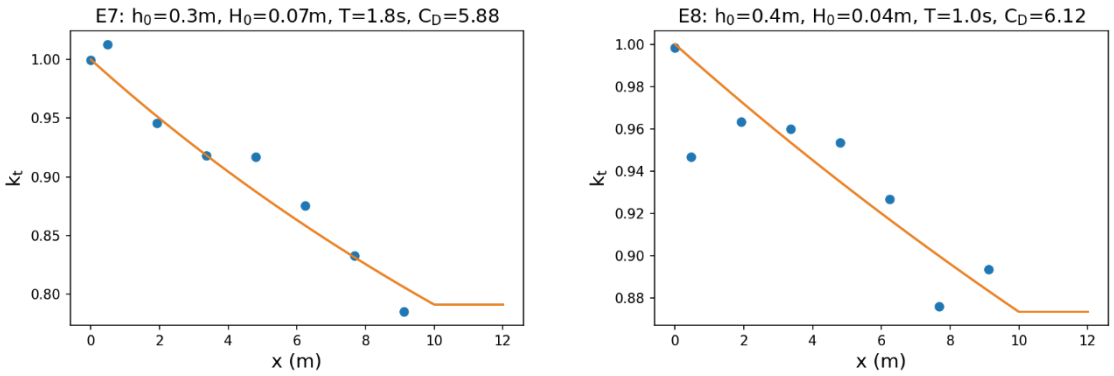


*Figure 0.1 Plots of experiment measurements and wave attenuation model results. Blue dots: Measurements of experiments (E1-E8) with different hydroynamic conditions. Orange line: Obtained modelling results when a single-cylinder model is used for wave attenuation modeeling.*

| | E1 | E2 | E3 | E4 | E5 | E6 | E7 | E8 |
|---|---|---|---|---|---|---|---|---|
| **RMS ($10^{-2}$)** | 1.23 | 0.329 | 0.489 | 1.37 | 0.544 | 1.26 | 0.597 | 0.728 |
| **Error ($10^{-2}$)** | -1.39 | -0.407 | -0.473 | -0.024 | 0.0992 | 0.455 | -0.568 | 0.462 |

*Table 0.1 Sum of error and root mean square error of the modelling results when validated against Wang et al., (2022) experiments (E1-E8) (refer to Fig. 0.1)*

## A1.2 Validation with large scale flume experiment with willow trees

The model developed for studying irregular waves is validated with the flume experiment results by van Wesenbeeck et al., (2022). The inputs into model are summarized in Table 0.2 below. Specific experiments were intentionally omitted from this validation process as there were run-ups that were measured in the respective control experiments. These run-ups are caused by processes within the flumes which the implemented model is unable to account for. The distribution of frontal area of the model tree used in this validation exercise is based on the model of willow trees that was developed by Kalloe et al., (2022) for this specific experiment (Fig. 2.11).

The performance of the model is evaluated by comparing $k_{t,end}$, the $k_t$ value at the end of the willow "forest" (Fig. 2.10). In order to isolate the effect of the flume on wave attenuation, $k_{t,end}$ of the experiment is given by equation x below.

$$k_{t,end} = \frac{H_{s,end,control} - H_{s,end,willows}}{H_{s,i,willow}} \quad (28)$$

*Where $H_{s,end}$ is the significant wave height at the radar wave gauge behind the forest, and $H_{s,i}$ is the significant wave height at the radar wave gauge in front of the forest.*

| | Vegetation | | | | Hydrodynamic condition | | |
|---|---|---|---|---|---|---|---|
| **Test Index** | **Nv (trees/m)** | **Dv** | **Cd (trunk)** | **Cd (canopy)** | **h (m)** | **Hs (m)** | **Tp (s)** |
| 1 | 0.16 | Figure x | 1.2 | 1.85 | 3 | 0.42 | 0.44 |
| 2 | | | | 1.07 | 3 | 0.92 | 0.95 |
| 3 | | | | 1.91 | 3 | 0.45 | 0.45 |
| 7 | | | | 2.02 | 3 | 0.43 | 0.43 |
| 8 | | | | 1.17 | 3 | 0.90 | 0.93 |
| 9 | | | | 1.78 | 3 | 0.46 | 0.43 |
| 10 | | | | 1.24 | 3 | 0.92 | 0.97 |
| 11 | | | | 0.77 | 4.5 | 1.38 | 1.40 |
| 12 | | | | 0.94 | 4.5 | 1.41 | 1.44 |

*Table 0.2 Conditions in which the model is validated for, against experimental results of van Wesenbeeck et al., (2022). Trunk is defined for the area from z=0m to z=1m; the canopy is defined for z>1m.*

The model's $k_t$ values at the end of the willow forest compares well with experiments where h=3m van Wesenbeeck et al., (2022), with absolute error values of $k_t$ ranging between 0.008 to 0.077 (Table 0.3). Significant deviation between the model and experimental results, however, are observed for experiments where h=4.5m.

| Test Index | h (m) | $\Delta H_{s,control}$ | Error |
|---|---|---|---|
| 1 | 3 | 0.027 | 0.057 |
| 2 | 3 | 0.012 | -0.07 |
| 3 | 3 | 0.012 | 0.077 |
| 7 | 3 | 0.027 | 0.008 |
| 9 | 3 | 0.012 | 0.005 |

*Table 0.3 Validation results with van Wesenbeeck et al., (2022)*

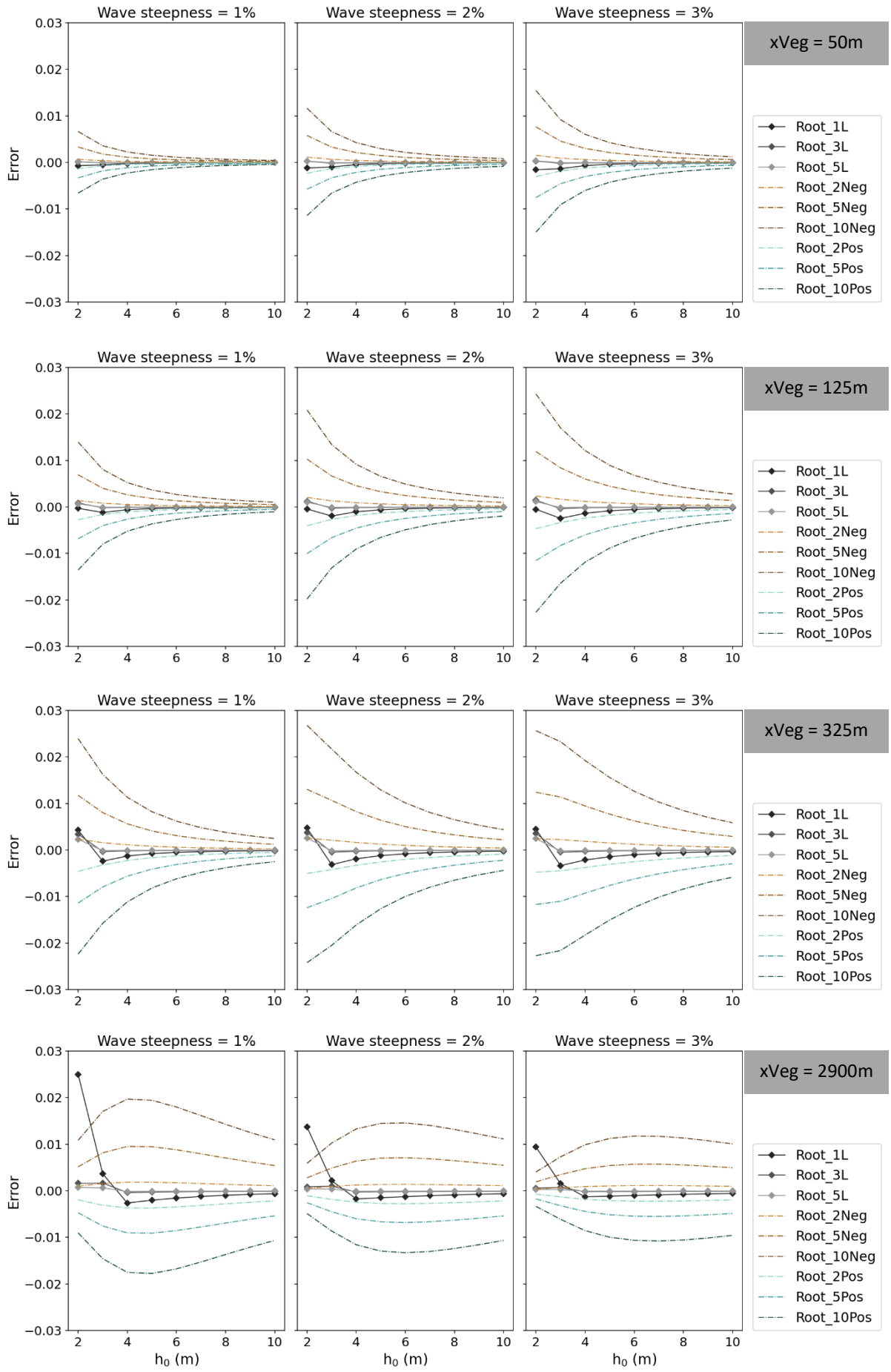


*Figure 0.2 Variation of Error with water depth at the end of R sp. forest of various widths for varying wave heights, when Nv=0.1 and Tp0=8s. Results for xVeg = 950m have been presented in Figure 4.12.*

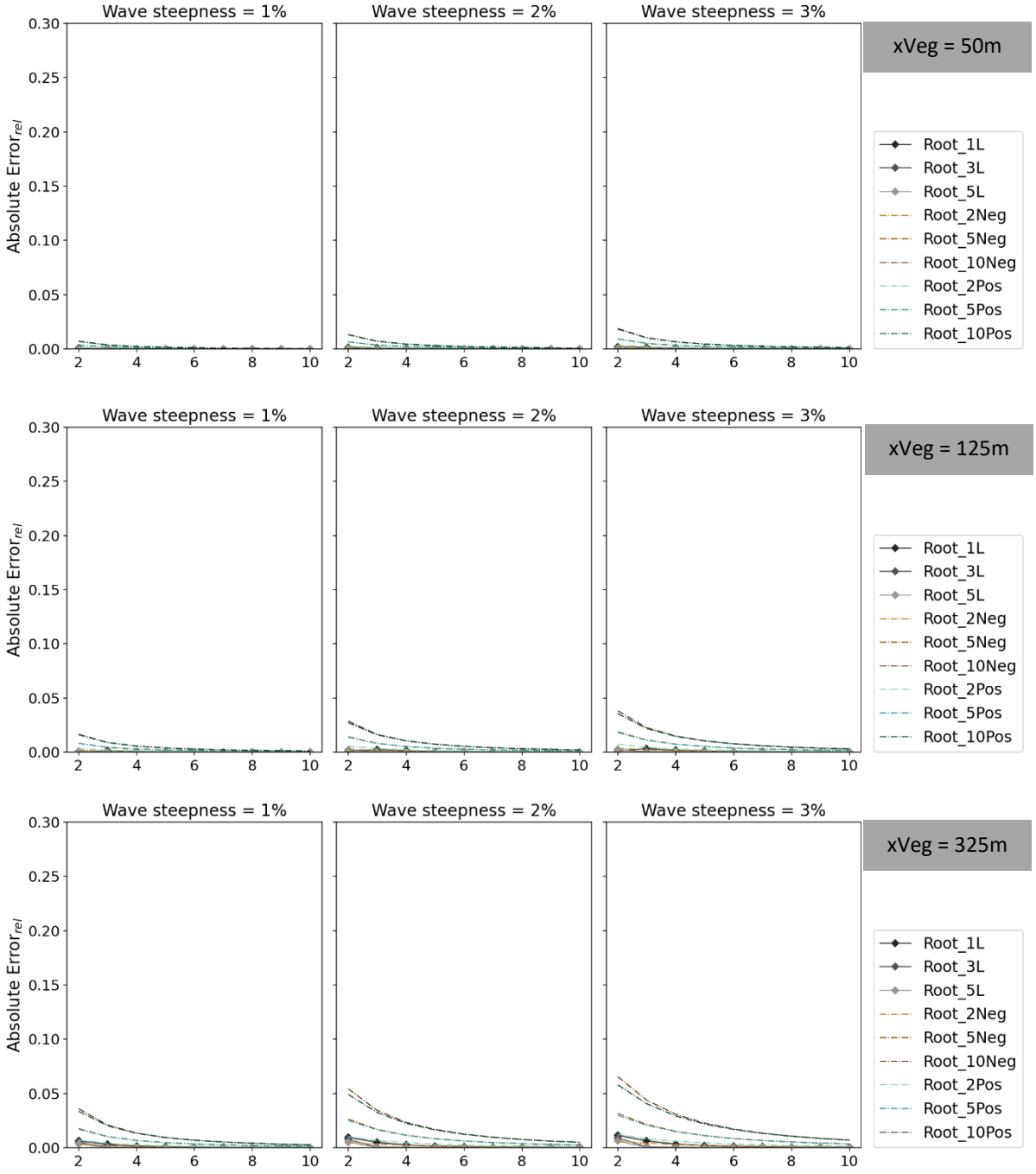
Wave steepness = 1%
Wave steepness = 2%
Wave steepness = 3%
xVeg = 50m
xVeg = 125m
xVeg = 325m
Absolute Error$_{rel}$
0.00
0.05
0.10
0.15
0.20
0.25
0.30
2
4
6
8
10
Root_1L
Root_3L
Root_5L
Root_2Neg
Root_5Neg
Root_10Neg
Root_2Pos
Root_5Pos
Root_10Pos

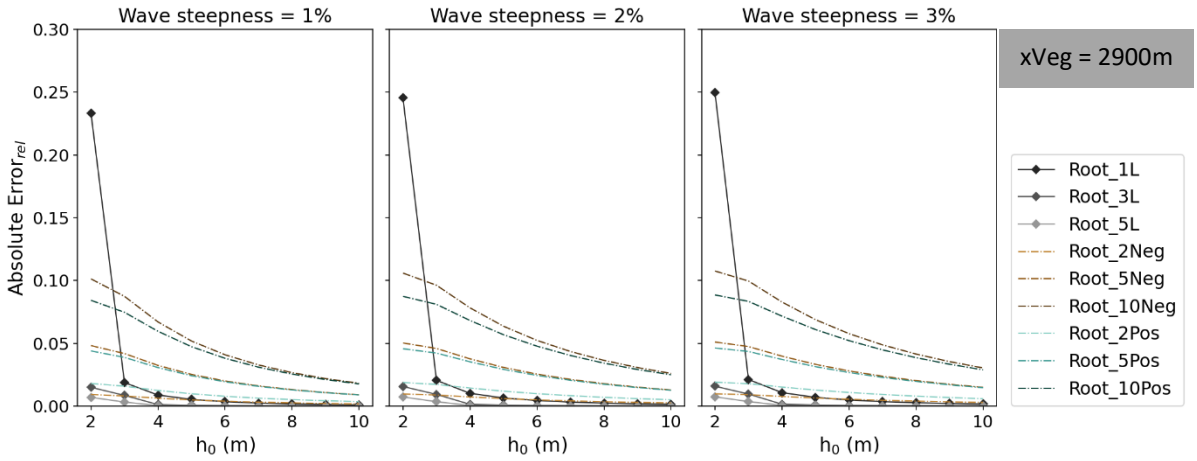


*Figure 0.3 Variation of absolute Error$_{rel}$ with water depth at the end of R sp. forest of various widths for varying wave heights, when Nv=0.1 and Tp0=8s. Results for xVeg = 950m have been presented in Figure 4.13.*

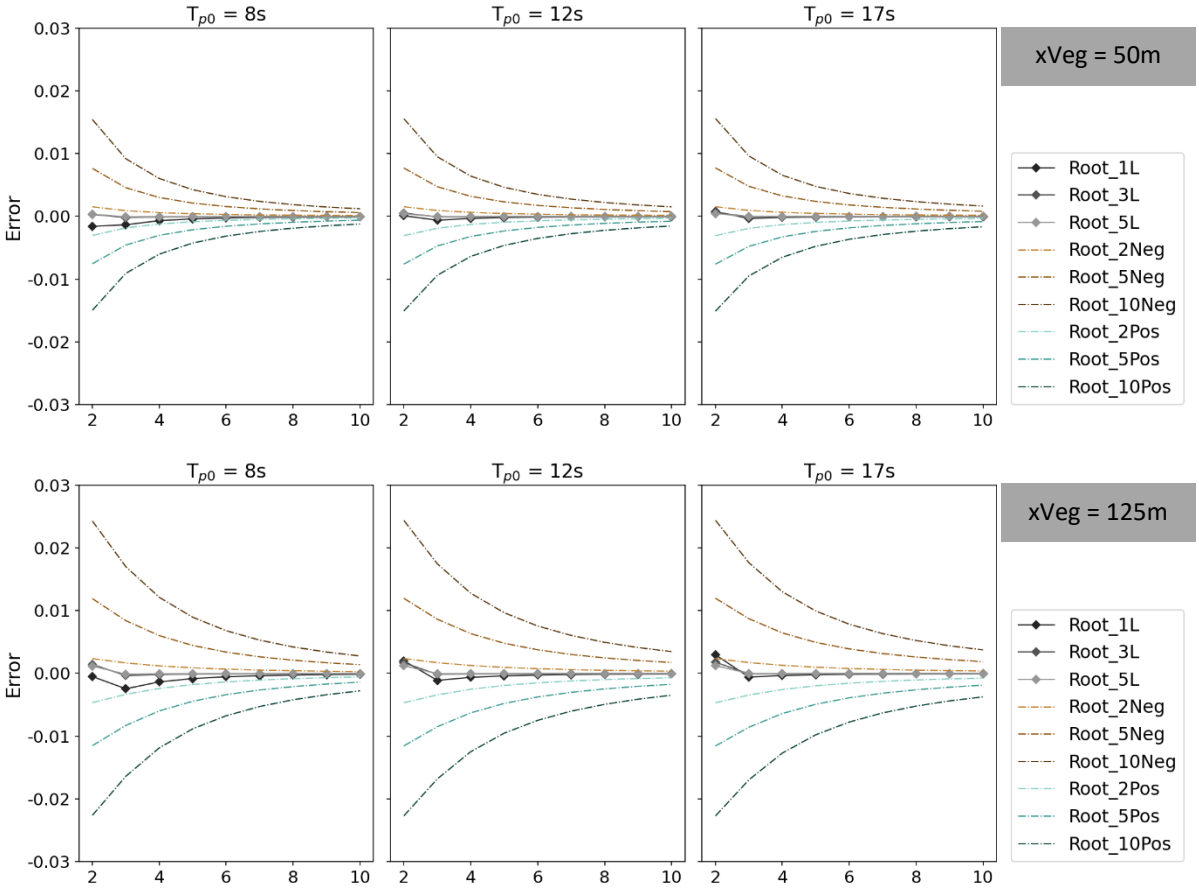

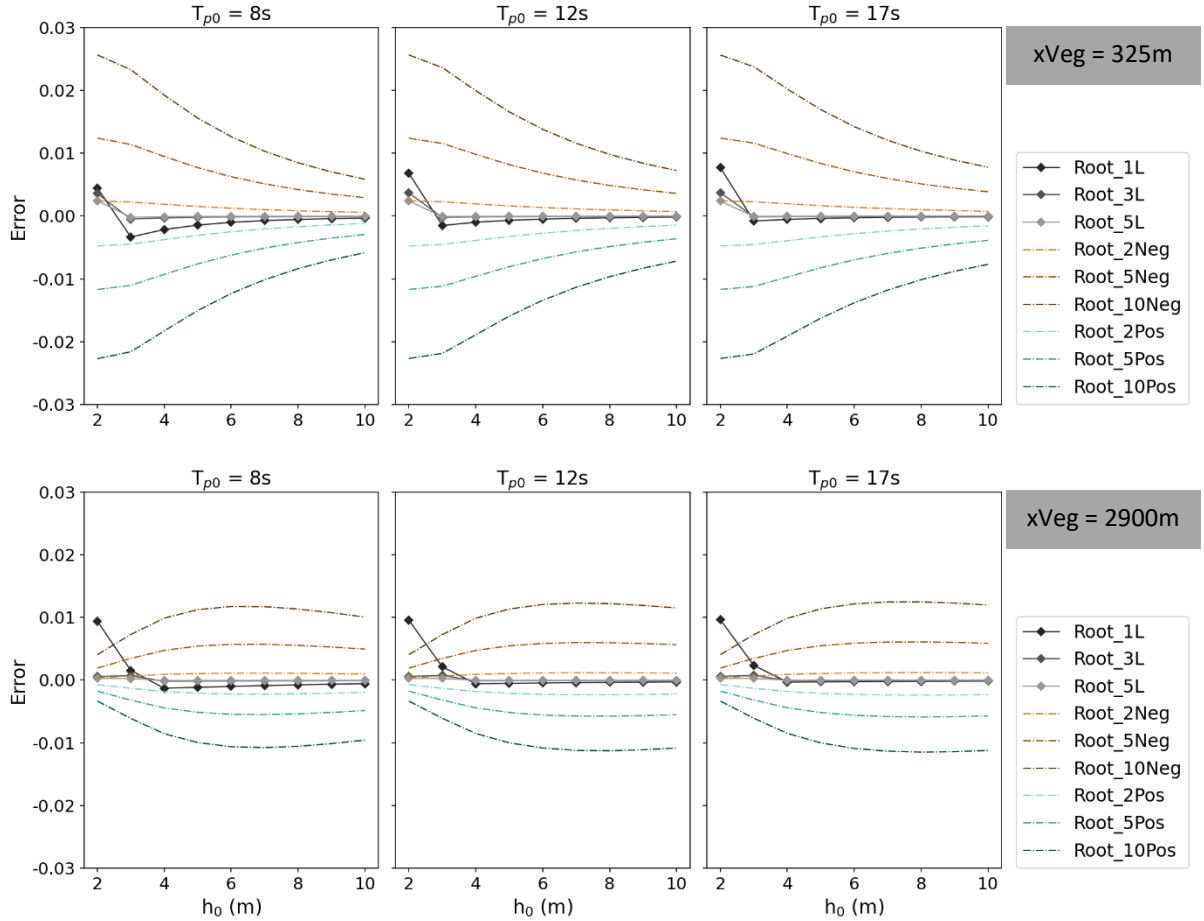


*Figure 0.4 Variation of Error with water depth at the end of R sp. forest of various widths for varying $T_{p0}$, when Nv=0.1 and Hs0 is constant for each water level. Results for xVeg = 950m have been presented in Figure 4.14.*

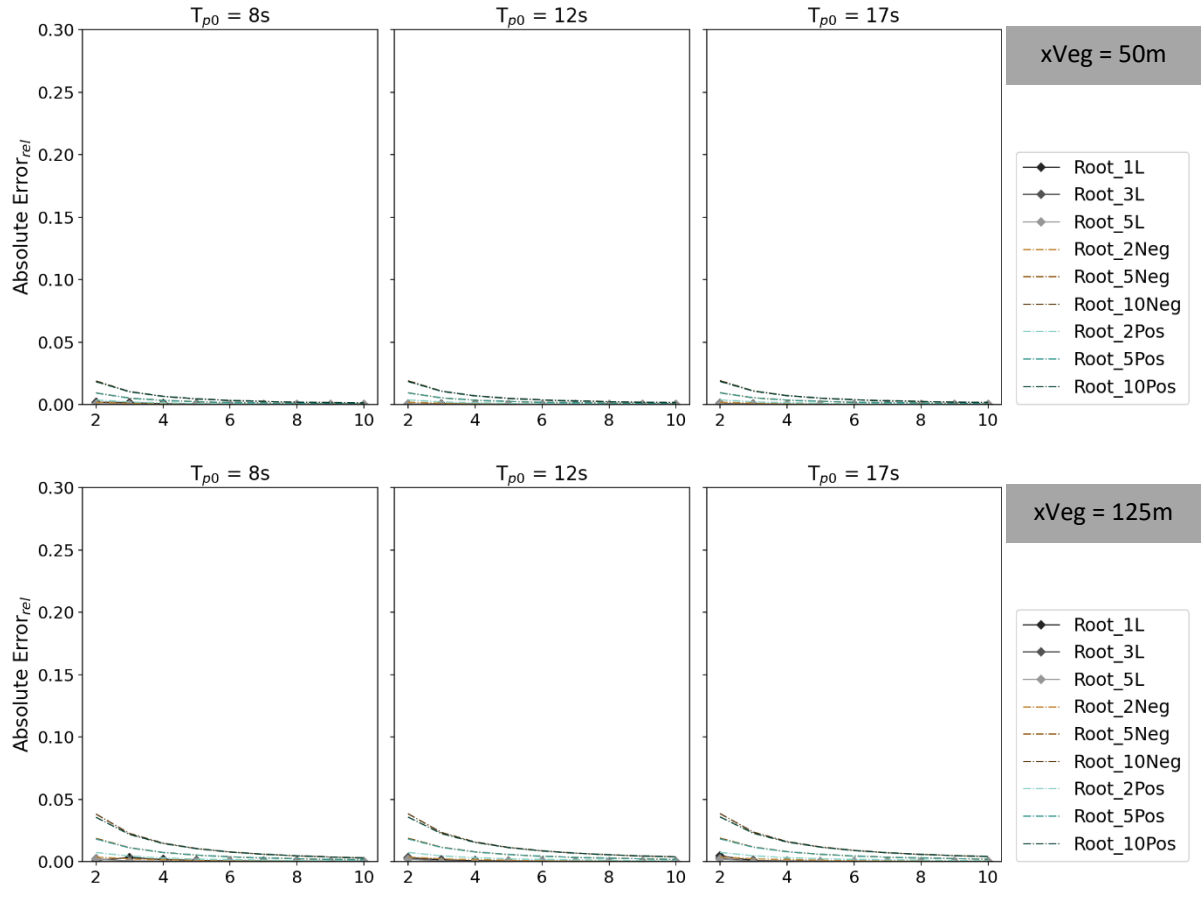

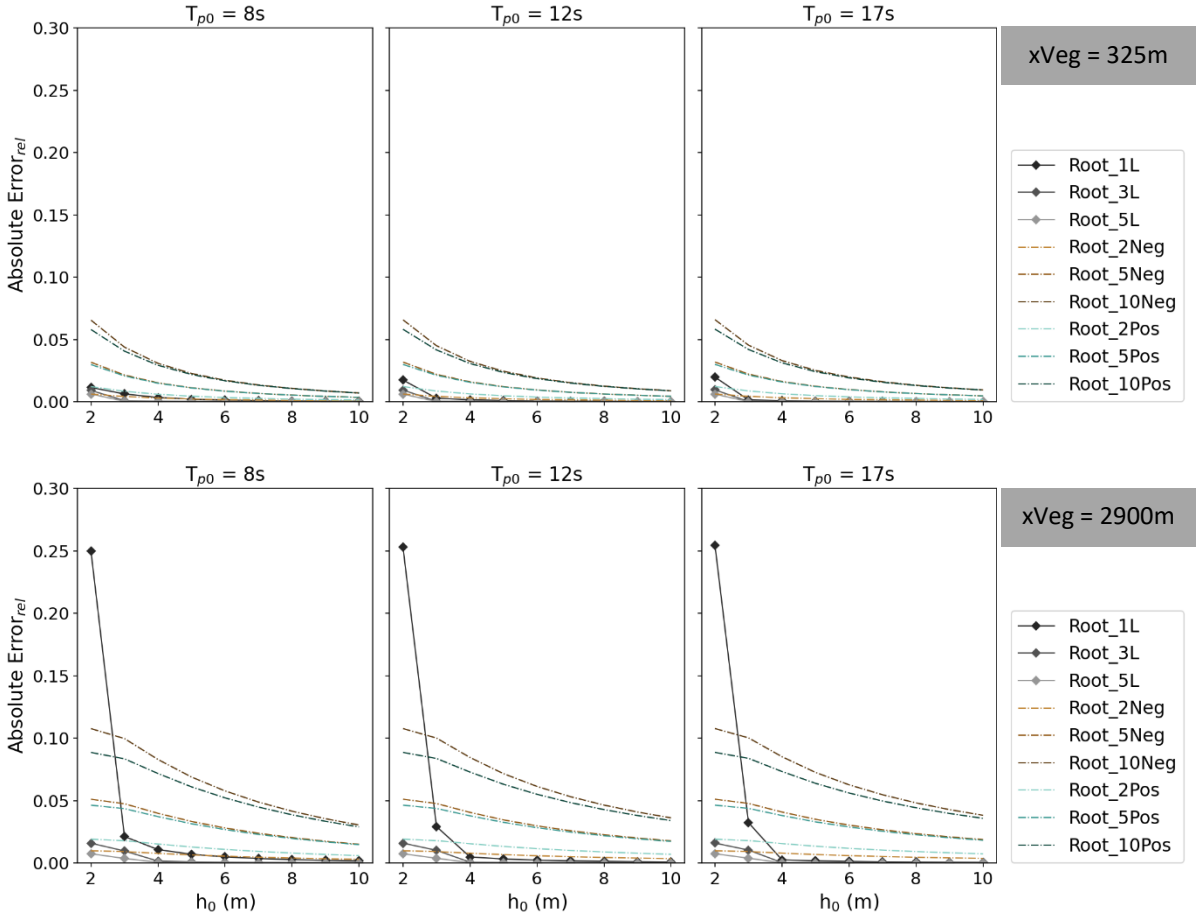


*Figure 0.5 Variation of absolute Error$_{rel}$ with water depth at the end of R sp. forest of various widths for varying Tp0, when Nv=0.1 and Hs0 is constant for each water level. Results for xVeg = 950m have been presented in Figure 4.15.*

## A3 Maximum and minimum $r_{Hs}$ values for difference forest widths

The wave height reduction per unit length, $r_{hs}$, for the reduction values obtained in Chapter 4.3.1 have been calculated for comparison with results from Horstman et al., (2014) . The equation for $r_{Hs}$ given in Horstman et al., (2014) as in Equation 29.

$$r_{Hs} = \frac{H_x - H_i}{\Delta x \cdot H_i} = \frac{1}{\Delta x}(1 - k_t) \quad \text{(Eq. 29)}$$

*Where $H_x$ is the wave height at point x along the cross-shore direction, $H_i$ is the initial wave height, $\Delta x$ is the distance between the shoreline and x.*

| **xVeg (m)** | **50** | **125** | **325** | **950** | **2900** |
|---|---|---|---|---|---|
| **Min $r_{Hs}$ ($m^{-1}$)** | 0.0022 | 0.0021 | 0.0021 | 0.0019 | 0.0014 |
| **Max $r_{Hs}$ ($m^{-1}$)** | 0.0545 | 0.0388 | 0.0219 | 0.0093 | 0.0033 |

*Table 0.4 Range of rHs values for forests of varying widths that are obtained in the R sp. wave attenuation analysis (Chapter 4.3.1)*

## A4 Tree measurements from Chek Jawa Wetland Reserve, Singapore

| Tree sample | Height (m) | DBH (cm) | Branch diameter (cm) | Est. number of branches |
|---|---|---|---|---|
| 1 | 19 | 23 | 6 - 10 | 10-16 |
| 2 | 22.5 | 26.2 | 6 - 11.5 | 18-19 |
| 3 | 8 | - | 4 | - |

*Table 0.5 Table of field measurements from Chek Jawa Wetland Reserve, Singapore*